AD-A119 200 OHIO STATE UNIV COLUMBUS ELECTROSCIENCE LAB F/G 9/5
PATTERN OPTIMIZATION OF WING-MOUNTED ARRAY ANTENNAS AT UHF.(U)
JAN 76 R J MARHEFKA, W D BURNSIDE N00123-74-C-1580
UNCLASSIFIED ESL-3884-1 NL

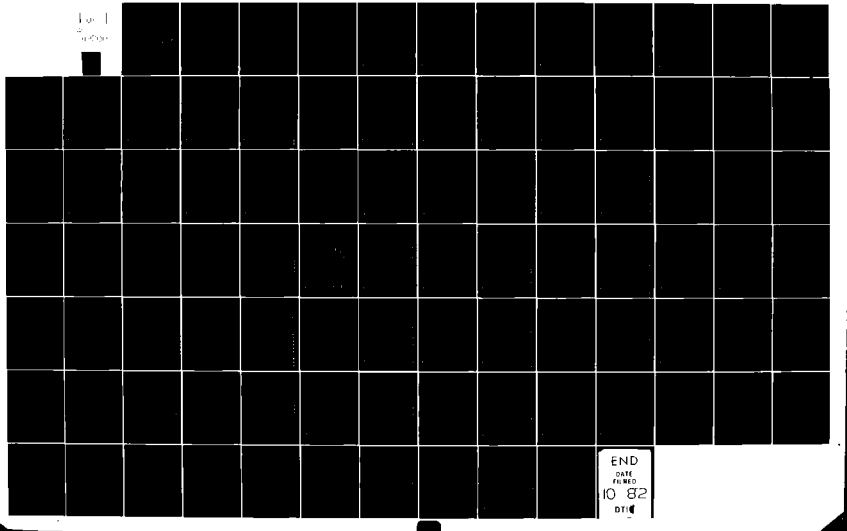

END
DATE FILMED
10 82
DTIC

(2)

# PATTERN OPTIMIZATION OF WING-MOUNTED ARRAY ANTENNAS AT UHF

R. J. Marhefka and W. D. Burnside



The Ohio State University

ElectroScience Laboratory

Department of Electrical Engineering
Columbus, Ohio 43212



FINAL REPORT 3884-1

January 1976



Naval Regional Procurement Office
Long Beach, California 90801

## NOTICES

When Government drawings, specifications, or other data are used for any purpose other than in connection with a definitely related Government procurement operation, the United States Government thereby incurs no responsibility nor any obligation whatsoever, and the fact that the Government may have formulated, furnished, or in any way supplied the said drawings, specifications, or other data, is not to be regarded by implication or otherwise as in any manner licensing the holder or any other person or corporation, or conveying any rights or permission to manufacture, use, or sell any patented invention that may in any way be related thereto.

SECURITY CLASSIFICATION OF THIS PAGE (When Data Entered)

| REPORT DOCUMENTATION PAGE | | READ INSTRUCTIONS BEFORE COMPLETING FORM |
|---|---|---|
| 1. REPORT NUMBER | 2. GOVT ACCESSION NO. AD-A119 200 | 3. RECIPIENT'S CATALOG NUMBER |
| 4. TITLE (and Subtitle) PATTERN OPTIMIZATION OF WING-MOUNTED ARRAY ANTENNAS AT UHF | | 5. TYPE OF REPORT & PERIOD COVERED Final Report 3/1/74 - 10/31/75 |
| | | 6. PERFORMING ORG. REPORT NUMBER ESL 3884-1 |
| 7. AUTHOR(s) R. J. Marhefka and W. D. Burnside | | 8. CONTRACT OR GRANT NUMBER(s) N00123-74-C-1580 |
| 9. PERFORMING ORGANIZATION NAME AND ADDRESS The Ohio State University ElectroScience Laboratory, Department of Electrical Engineering Columbus, Ohio 43212 | | 10. PROGRAM ELEMENT, PROJECT, TASK AREA & WORK UNIT NUMBERS 60530-74-C-1580 |
| 11. CONTROLLING OFFICE NAME AND ADDRESS Naval Regional Procurement Office Long Beach, California 90801 | | 12. REPORT DATE January 1976 |
| | | 13. NUMBER OF PAGES 87 |
| 14. MONITORING AGENCY NAME & ADDRESS (if different from Controlling Office) | | 15. SECURITY CLASS. (of this report) Unclassified |
| | | 15a. DECLASSIFICATION/DOWNGRADING SCHEDULE |

16. DISTRIBUTION STATEMENT (of this Report)

DISTRIBUTION STATEMENT A
Approved for public release;
Distribution Unlimited

17. DISTRIBUTION STATEMENT (of the abstract entered in Block 20, if different from Report)

18. SUPPLEMENTARY NOTES

19. KEY WORDS (Continue on reverse side if necessary and identify by block number)

radiation patterns
wing-mounted airborne antennas
volumetric patterns
Geometrical Theory of Diffraction
F-4 antenna design

20. ABSTRACT (Continue on reverse side if necessary and identify by block number)

A systematic design procedure for high frequency wing-mounted antenna systems by means of a digital computer has been undertaken in this report. In particular, the design of an antenna system to give full hemispherical coverage in the aft region of an aircraft for quadrant detection at UHF has been of concern. The principal objective of this study has been to determine the number and placement of elements and their excitation for arrays on the surfaces of

cont'd

DD FORM 1 JAN 73 1473 EDITION OF 1 NOV 65 IS OBSOLETE

UNCLASSIFIED
SECURITY CLASSIFICATION OF THIS PAGE (When Data Entered)

the wings for a specified pattern. The constraints that are imposed are the frequency, element type, aircraft, stores and sector of coverage. Classical array techniques are used to find the array parameters. The placement of the array on the wings are determined with numerical aircraft models developed using the Geometrical Theory of Diffraction. Measurements of a single slot element on an F-4 aircraft were taken to compare with the calculated results. Although the results are not directly comparable because the measurements are in the near-field and calculations are in the far-field, the results are encouraging. A method to present the volumetric pattern for an antenna mounted on an aircraft has been used to aid the system designer in viewing the performance of the antenna system in all space. The method is based on displaying different directive gain levels by different colors on a two-dimensional graph.

CONTENTS

# I. INTRODUCTION

The aircraft antenna designer must not only concern himself with the development of an antenna element for a particular application, but he must also be concerned with the performance of the antenna system in the presence of the aircraft structure. As the available real estate for antennas becomes increasingly more difficult to find, wing locations have become increasingly desirable for many applications. A systematic design procedure for high frequency wing-mounted antenna systems by means of a digital computer has been undertaken, the results of which are presented in this report. In particular, the design of an antenna system to give full hemispherical coverage in the aft region of an aircraft for quadrant detection at UHF has been of concern.

The principal objective of this study has been to determine the number and placement of elements and their excitation for arrays on the surfaces of the wings for a specified pattern. The constraints that are imposed are the frequency, element type, aircraft, stores and sector of coverage, all of which will be specified by the Naval Weapons Center (NWC).

This study has been undertaken in two phases. Phase I has concentrated on the optimization of the design of a wing-mounted array on the upper surface of the wings of a general aircraft. Classical array techniques were used to find the array spacing, scan angle and distribution of the antenna elements to best fit an ideal pattern. The Geometrical Theory of Diffraction (GTD) as developed at the ElectroScience Laboratory (ESL) has been used to include the effects of the aircraft structure. A bent plate model of the aircraft was initially used to determine the optimum array position. This bent plate aircraft model gave a worst case effect of the scattering from the fuselage. Measurements of a single slot element on an F-4 aircraft were taken at NWC to compare with the calculated results obtained by ESL. These comparisons pointed out the need to improve the model for the fuselage.

Phase II has been directed toward the improvement in the aircraft model using the GTD to represent the aircraft as a finite elliptic cylinder with flat plate wings. Techniques are also under development to be used in studying antennas mounted on the lower surface of wings with the stores and engine effects taken into account.

A method to present the volumetric pattern for an antenna mounted on an aircraft has been used to aid the system designer in viewing the performance of the antenna system in all space. The method is based on displaying different directive gain levels by different colors on a two-dimensional graph.

The following sections give the details of the techniques that have been developed.

## II. DESIGN PROCEDURE FOR THE ARRAYS

The objective of the design procedure for this antenna system is to determine the location, spacing, excitation and number of elements of the array necessary to give a best fit to a specified pattern. The NWC specified quadrant detection pattern is illustrated in Fig. 1. The pattern should be 6 dB down at the horizon and the slope of the pattern off the tail should be at least that of a cardiod pattern in that same direction. A two-way front-to-back ratio of 60 dB is desired, that is, a pattern with back lobes at least 30 dB down from the pattern maximum is needed. The ripple level in the quadrant of interest should not be severe. Of course, the ideal pattern illustrated in Fig. 1 is not realizable so the actual pattern must be a result of compromises imposed by the physical constraints of the problem.

As a result of this study, it has been ascertained that the various parameters of the problem are nearly independent for the various pattern aspects of interest. This section will discuss the effects element spacing, scan angle, positioning with respect to the wing edge, and excitation of the array elements have on the resulting patterns. The discussion of the relative positioning of the array with respect to the aircraft will be taken up in the next section.

A two-dimensional model is sufficient to find the array parameters mentioned above. The array of elements mounted on an infinite ground plane shows the basic shape of the radiation pattern, but a finite plate, illustrated in Fig. 2, is needed to study the energy being diffracted below the wing. The Geometrical Theory of Diffraction (GTD) is used to analyze the effects of the finite width of the plate.

The analysis is started with a two-element slot array. The normalized array factor is given as

$$(1) \qquad F(\theta) = \cos\left[k \frac{S}{2} (\cos\theta - \cos\theta_s)\right] \quad ,$$

where

$k = 2\pi/\lambda$
$S$ = element spacing
$\theta_s$ - scan angle.

It was initially thought that the front-to-back ratio could be at least 20 dB one-way. A value of 30 dB one-way was later determined to be better due to system considerations; however, a few results for the 20 dB level are shown to illustrate several points. First, if a scan angle $\theta_s = 0°$ is chosen, the element spacing to achieve

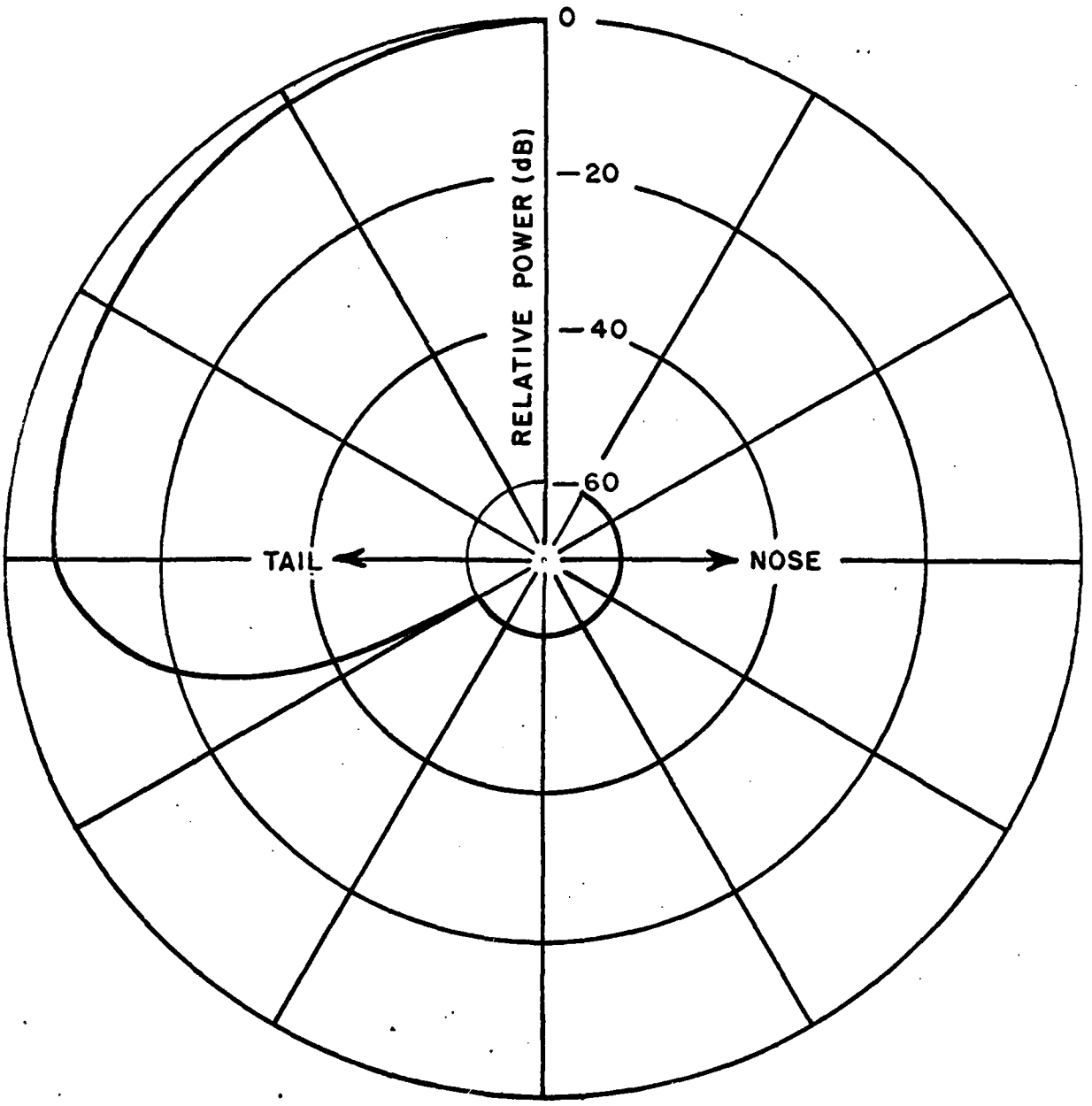


Fig. 1. Ideal elevation plane pattern.

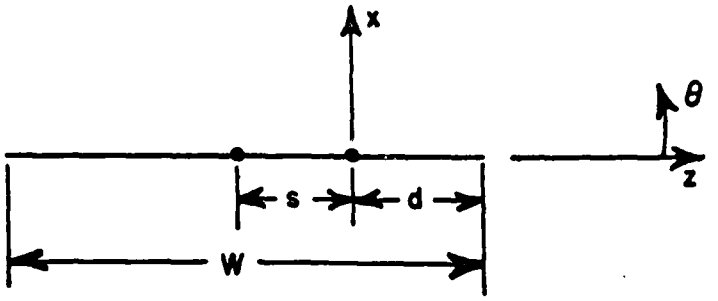


Fig. 2. Two-dimensional elevation plane model of wing.

a 20 dB front-to-back ratio can be determined from Eq. 1 to be $S = 0.267\ \lambda$. The resulting radiation pattern is shown in Fig. 3. If the value for S is chosen to be slightly off this value, the resulting front-to-back ratio changes drastically as shown in Fig. 4. Note the large increase in the backlobe level with relatively small change in S.

Second, since the antenna system is to be used for quadrant detection, it would be desirable to have the beam maximum in the center of the quadrant. To accomplish this, the array should be scanned at $\theta_s = 0°$, since the plate has a tendency to raise the beam peak off of the plate to an angle of $\theta \approx 45°$. If the scan angle had been made $\theta_s = 45°$ as in Fig. 5, the energy is spread much more into the forward quadrant. Consequently, a scan angle of $\theta_s = 0°$ concentrates most of the energy in the desired quadrant.

The above parameters mainly affect the basic shape of the patterns in the prime quadrant of interest as can be seen by comparing the finite plate and infinite ground plane results. The distance of the array from the tip of the wing, d, affects the ripple level in the main beam and the amount of energy diffracted into the lower quadrant. As the array position is moved to the trailing edge of the wing (array distance d from edge is decreased), the ripple in the main beam decreases but the energy diffracted below the wing increases. The distance $d = \lambda$ was used in the figures above. The value $d = 3\lambda$ is used in Fig. 6, for comparison to illustrate these effects. Note that the discontinuity at $\theta = 180°$ in the above patterns is due to the lack of including double diffraction in the GTD solution. This does not significantly affect the shape of the pattern in the region of concern, so double diffraction is not included in the analysis.

The above patterns illustrate that the radiation pattern will be approximately 6 dB down at the horizon ($\theta = 0°$) independent of the fact that the value d is varied. This is a consequence of the general

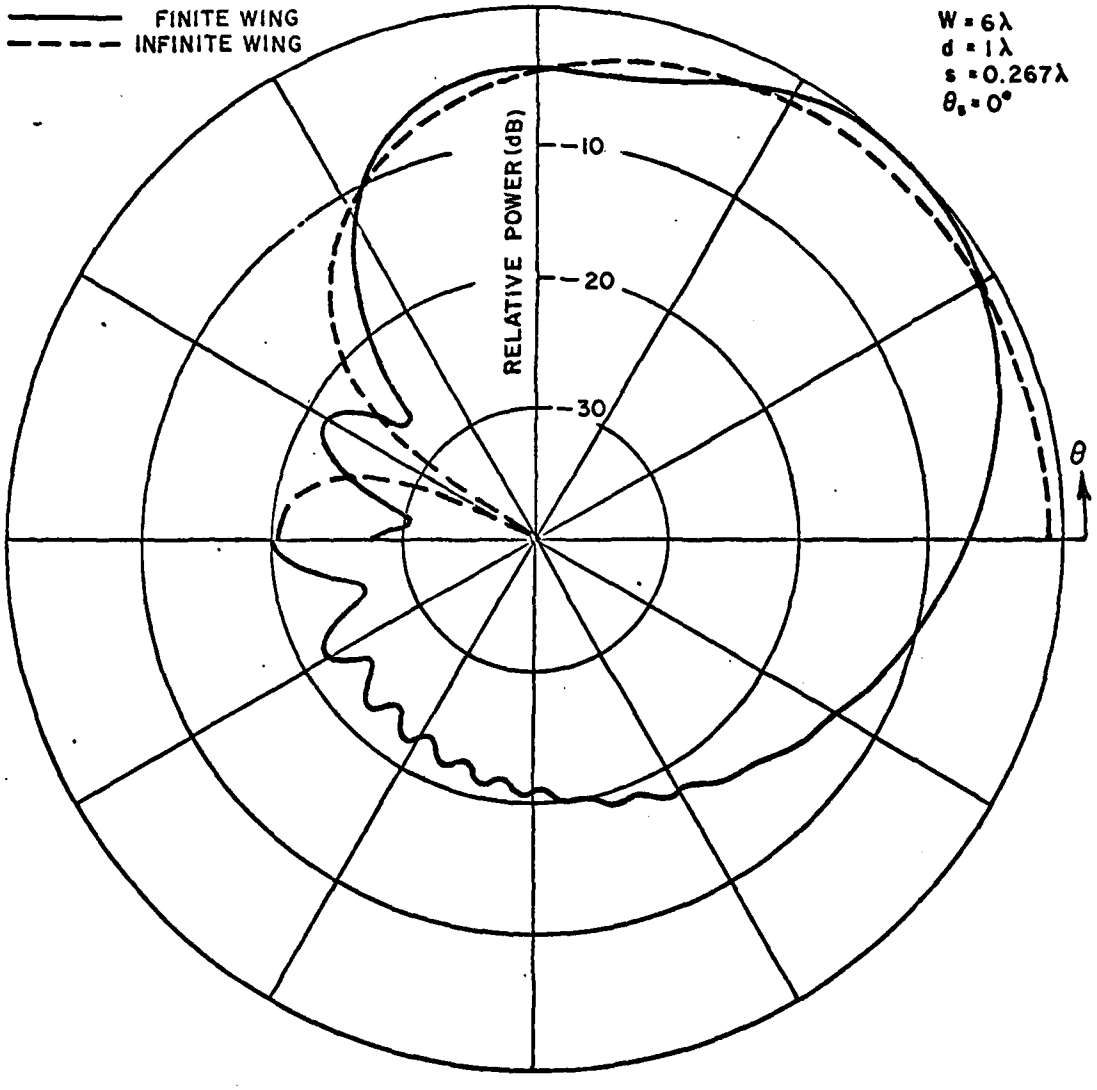


Fig. 3. Elevation Plane Pattern for two-dimensional wing model.

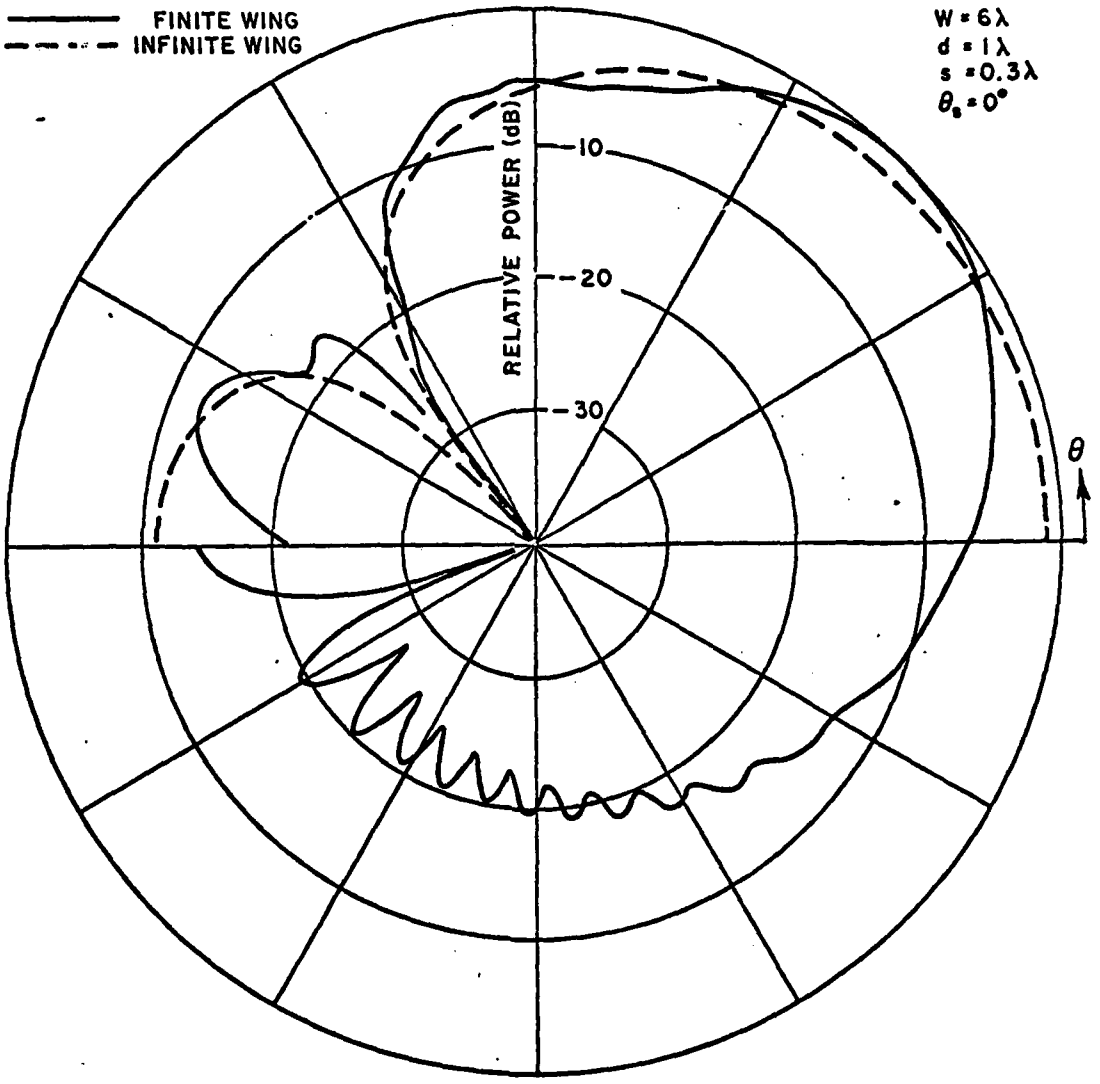


Fig. 4. Elevation Plane Pattern for two-dimensional wing model.

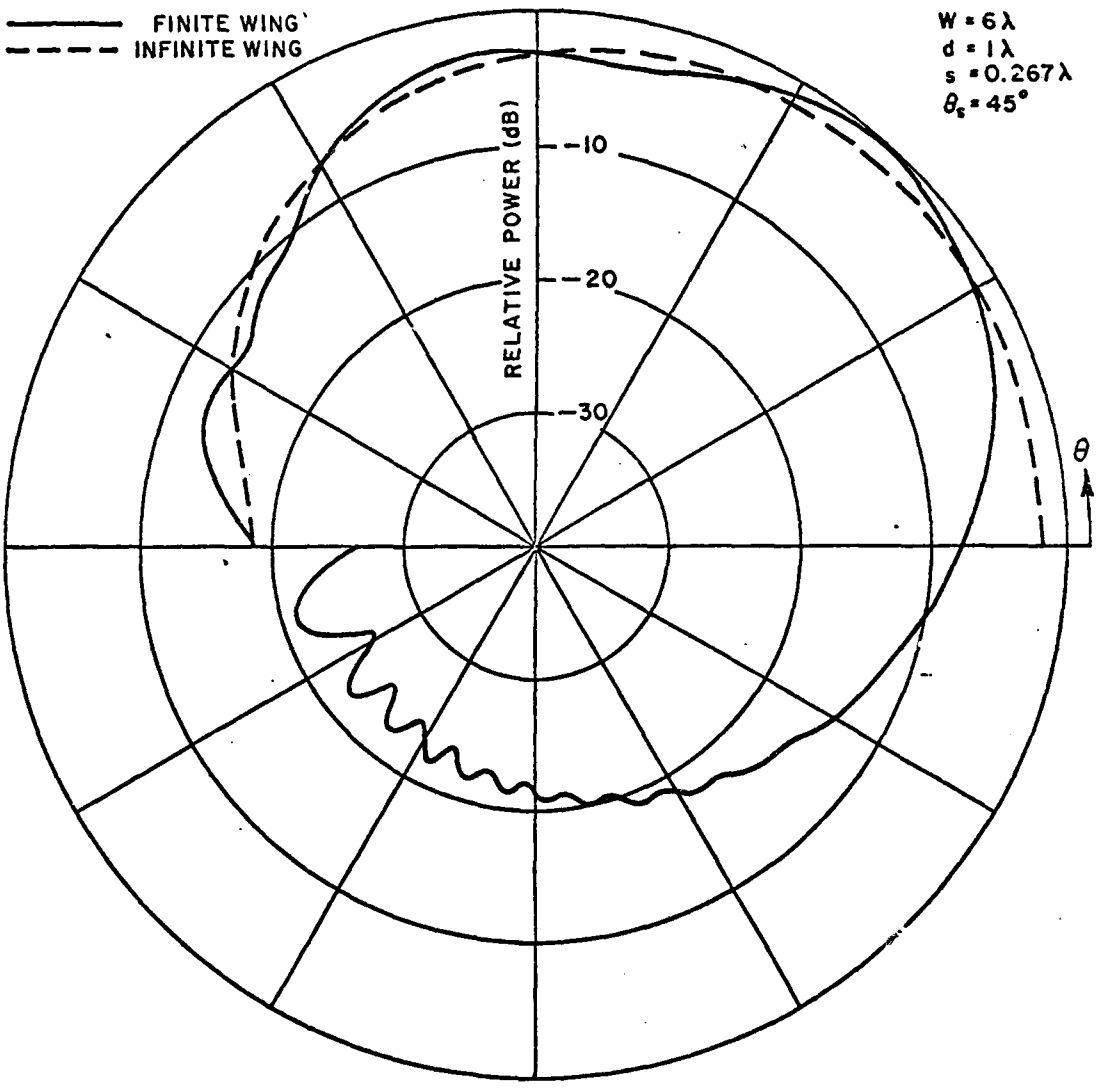


Fig. 5. Elevation Pattern for two-dimensional wing model.

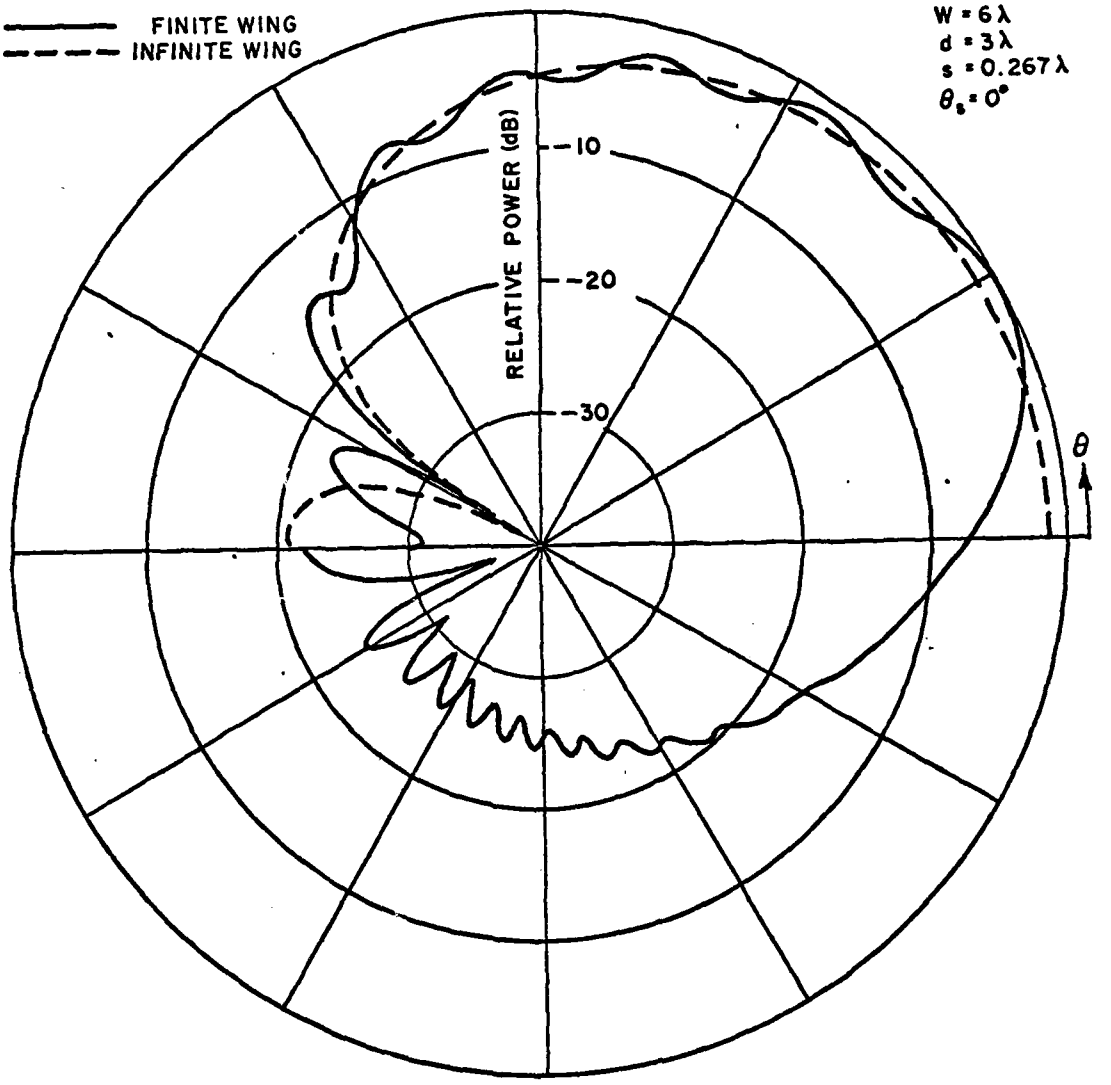


Fig. 6. Elevation Plane Pattern for two-dimensional wing model.

rule of GTD that states, that the total field at an incident shadow boundary will be approximately one-half of the incident field. Also, it can be shown from the theory of GTD that the slope of a cardiod pattern can be maintained for any distance from the wing edge greater than about $\lambda/10$. This does not present a problem since, in the above considerations, d is kept much larger than that value.

The pattern of a two-element array that was found to best approximate the ideal pattern is shown in Fig. 7. The desired front-to-back ratio of 30 dB one-way is obtained by solving for S in Eq. 1 such that the array factor has a null at $\theta = 180°$. This is achieved with an element spacing of $S = .25\,\lambda$. A wing width of $w = 4\lambda$ is chosen to simulate a typical width of an F-4 wing. The array is positioned ($d = 3\lambda$) as far as possible from the aft edge of the wing to minimize the energy diffracted in the region below the wing to prevent ground clutter interference. This has the disadvantage of increasing the ripple level in the quadrant of interest; however, the ripple does not appear to be severe.

In order to improve the pattern in Fig. 7 for quadrant detection, the next logical step is to consider a three-element array. The normalized array factor for a three-element array with uniform element weights, is given as

$$(2) \qquad F(\theta) = \frac{1}{3} + \frac{2}{3}\cos\left[k\,S\,(\cos\theta - \cos\theta_s)\right] \quad .$$

With the scan angle set to $\theta_s = 0°$, as in the case for the two-element array, the element spacing is determined to be $S = 0.1667\lambda$ in order to obtain a null at $\theta = 180°$. The resulting pattern is shown in Fig. 8. This does not present a significant improvement over the two-element case because the increased aperture length obtained by using three elements is not used to advantage with a scan angle of 0°. When the array is scanned to $\theta_s = 45°$ with a uniform amplitude distribution, the result shown in Fig. 9 is obtained. It can be seen that there is no significant change in the patterns. If a binomial amplitude distribution is used for the excitation of the elements, that is, if the amplitudes of the elements are (1/2, 1, 1/2), respectively, the energy in the top front quadrant is reduced. This result is shown in Fig. 10. Comparing this with the result for the two-element array in Fig. 7, there is found to be as much as 10 dB improvement in the pattern in the top front quadrant.

The two-dimensional results above are appropriate for any type of slot antenna element. The analysis was carried out without restricting the design to the physical constaints of a particular antenna element. The actual antenna elements proposed for the array are cavity backed slots capable of being excited with the first three waveguide modes. For the third mode to be excited, the

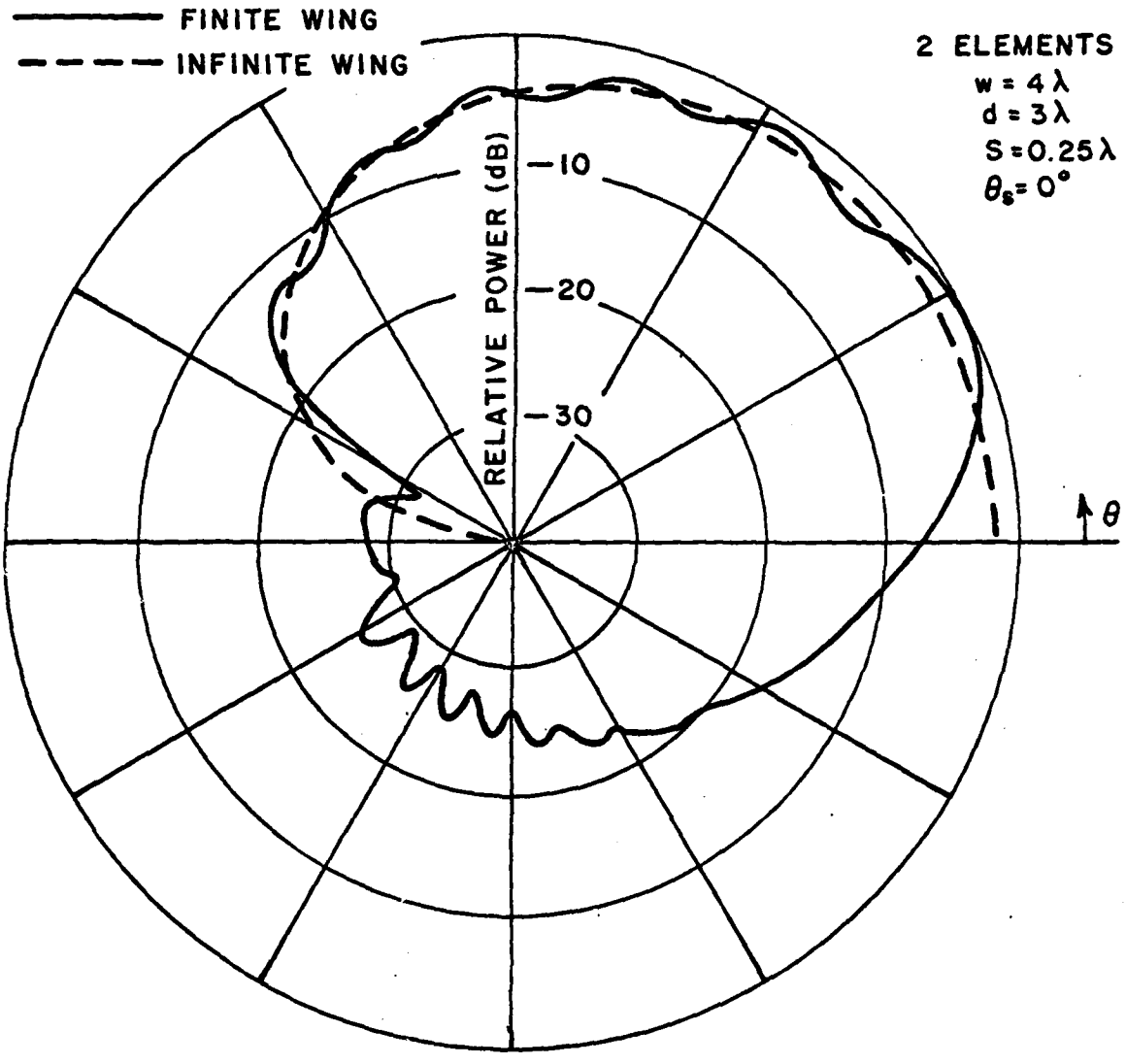


Fig. 7. Elevation Plane Pattern for two-dimensional wing model.

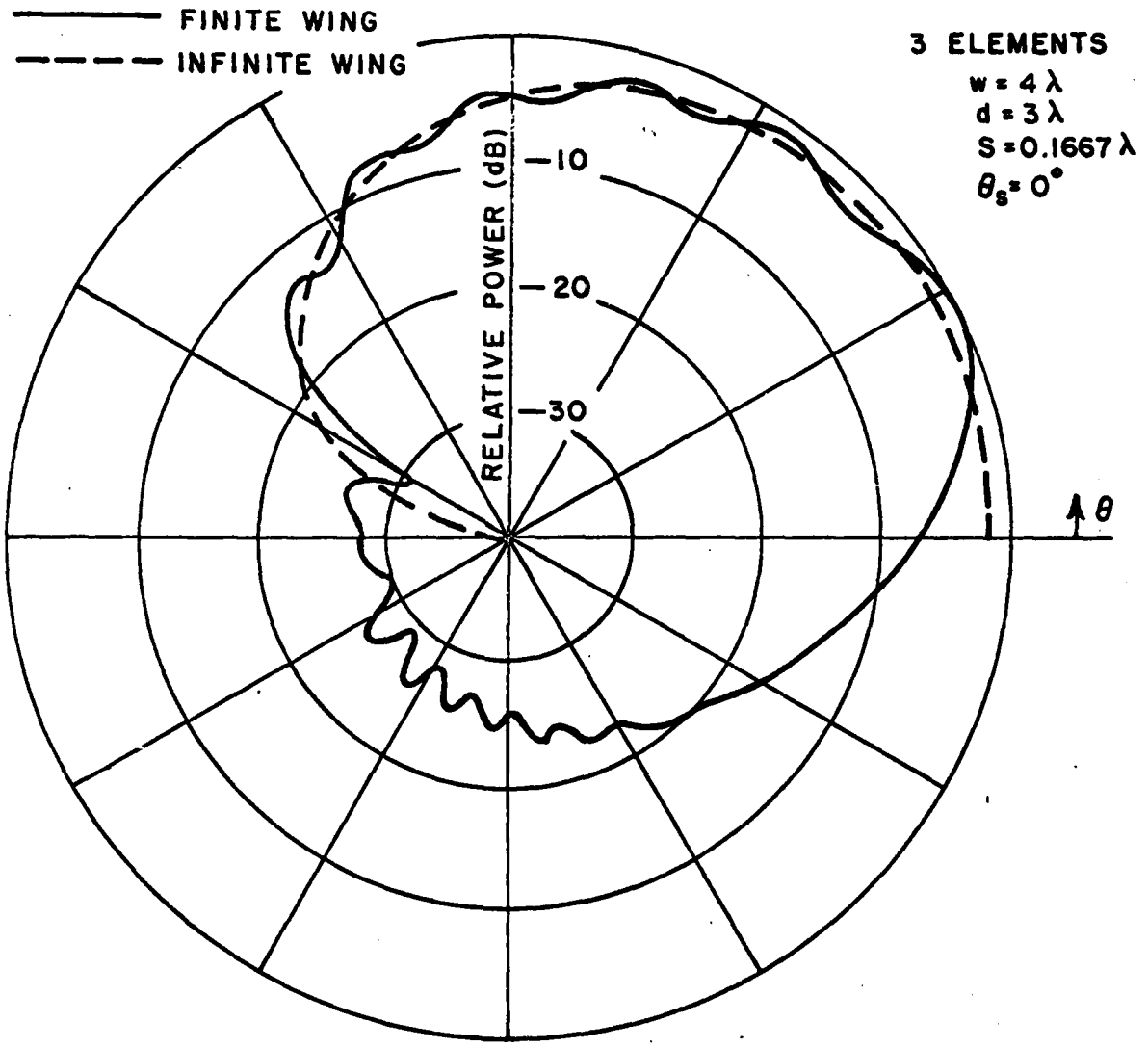


Fig. 8. Elevation Plane Pattern for two-dimensional wing model.

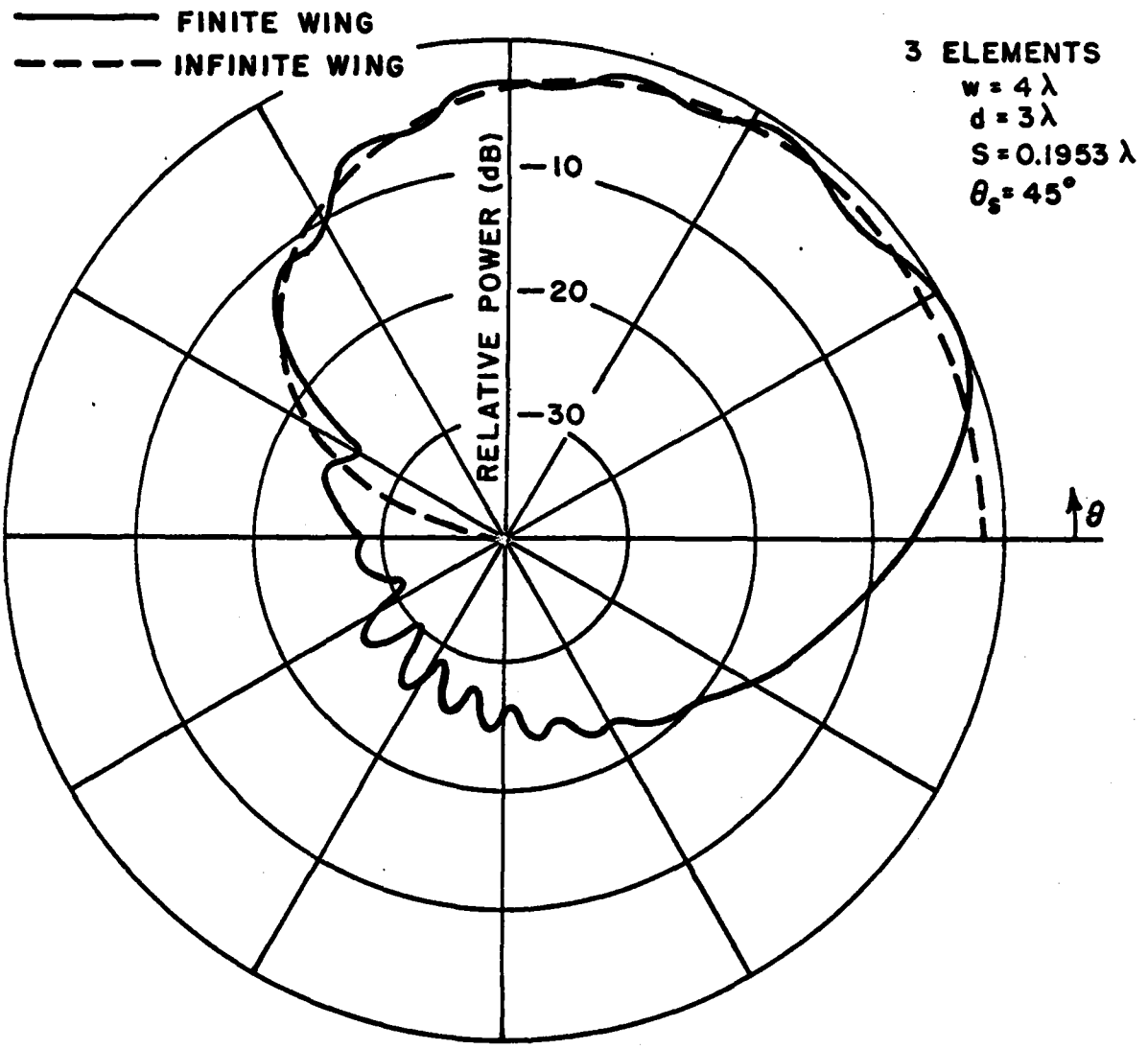


Fig. 9. Elevation Plane Pattern for two-dimensional wing model.

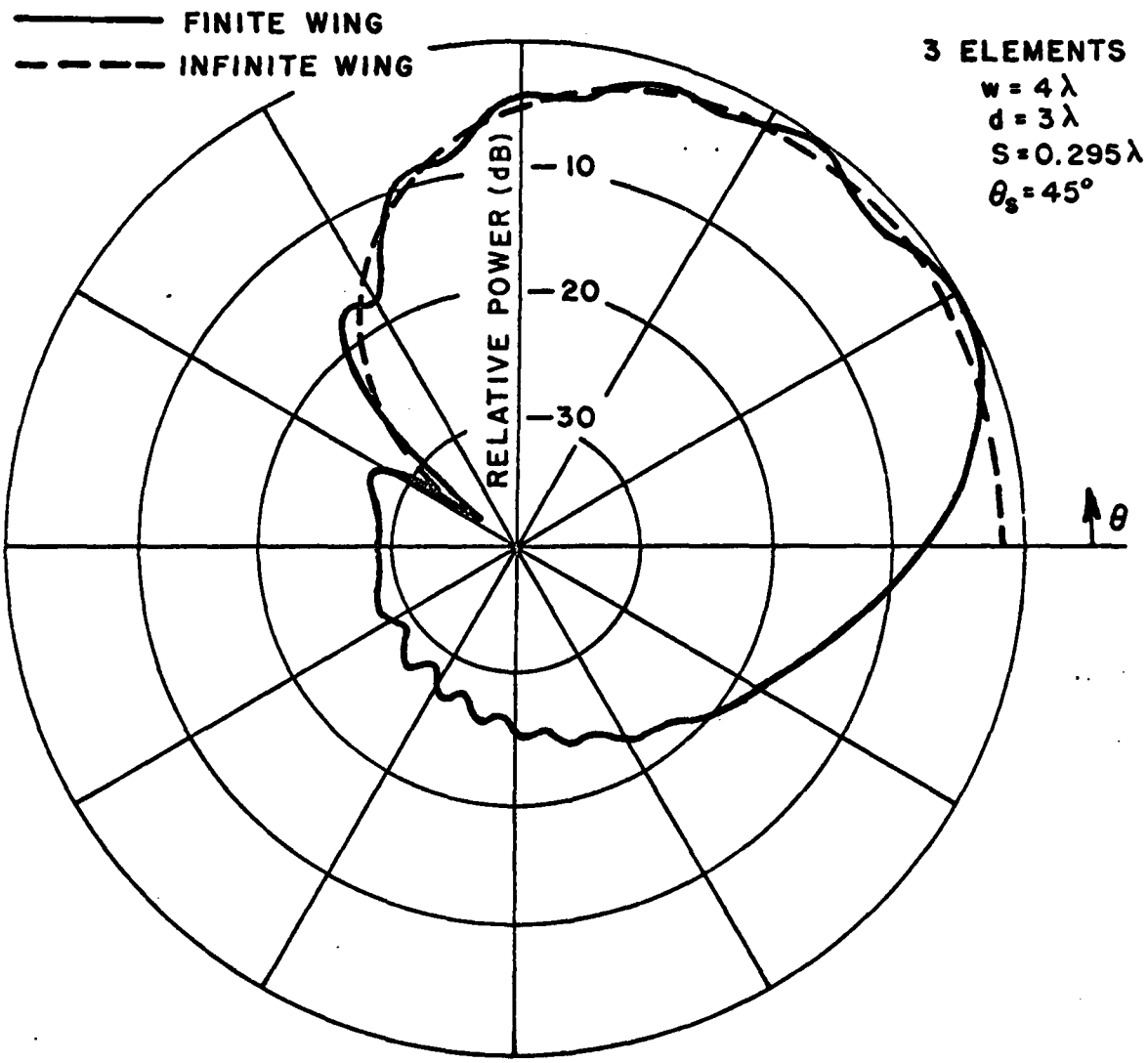


Fig. 10. Elevation Plane Pattern for two-dimensional wing model.

slot must be 1.5 $\lambda_e$ in the dielectric or approximately 0.984$\lambda$ in free space.

The normalized element patterns for various current excitation modes are given by

$$E_\phi^m = \frac{I_m (-1)^{\frac{m-1}{2}} \left(\frac{m\pi}{kh}\right) \sin\theta' \cos\left(\frac{kh}{2}\cos\theta'\right)}{\left(\left(\frac{m\pi}{kh}\right)^2 - \cos^2\theta'\right)}$$

odd m = 1, 3, 5, ...

$$E_\phi^m = \frac{-jI_m (-1)^{\frac{m}{2}} \left(\frac{m\pi}{kh}\right) \sin\theta' \sin\left(\frac{kh}{2}\cos\theta'\right)}{\left(\left(\frac{m\pi}{kh}\right)^2 - \cos^2\theta'\right)}$$

even m = 2, 4, 6, ...

where h is the length of the slot.

The azimuth patterns for the modes excited separately in the two- and three-element arrays on an infinite ground plane are shown in Figs. 11 and 12, respectively. The first mode, in both cases, produces essentially the desired pattern. The second mode will not benefit the desired pattern in that it has a null in the desired maximum direction. A little of the third mode, however, can be used to help shape the beam. A simple synthesis program was developed to help find a combination of the first and third modes that best approximates the ideal pattern. For the two-element array, the normalized mode current weights are $I_1 = 1.0 \angle 0°$, $I_2 = 0.$, and $I_3 = 0.246 \angle 180°$ with the resulting pattern shown in Fig. 13. For the three-element array, the normalized mode current weights are $I_1 = 1.0 \angle 0°$, $I_2 = 0.$, and $I_3 = 0.390 \angle 180°$ with the resulting pattern shown in Fig. 14. Note that in the azimuth plane there is a 10 dB reduction in the backlobes of the three-element array over the two-element array.

The use of the three-element array with a cavity-backed slot element presents a problem, however. This problem arises due to the fact that the element spacing needed for optimum results does not leave room for the cavity. To overcome this, limitation imposed by the cavity dimensions two alternatives can be tried. First, the

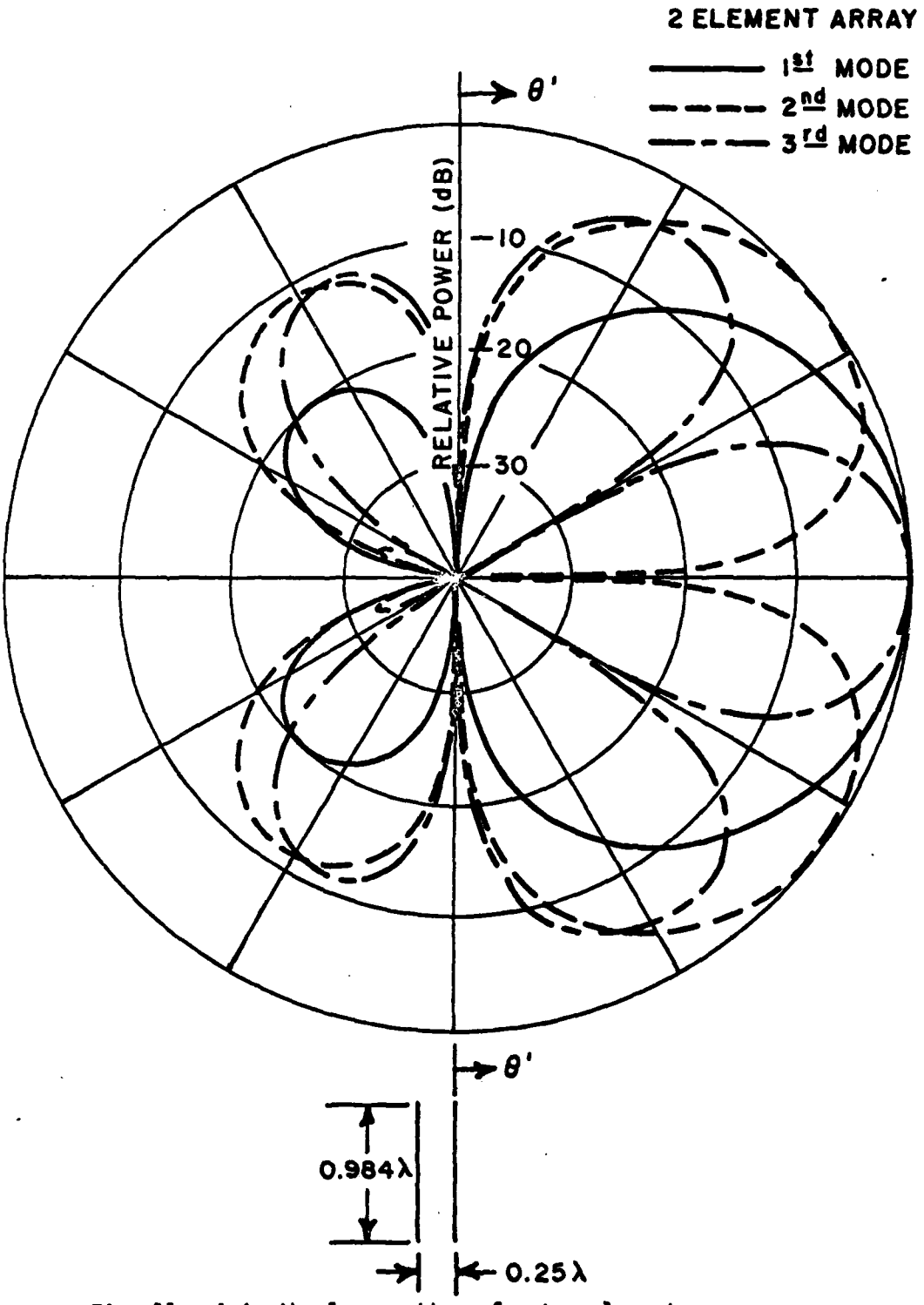


Fig. 11. Azimuth plane pattern for two-element array for individual modes.

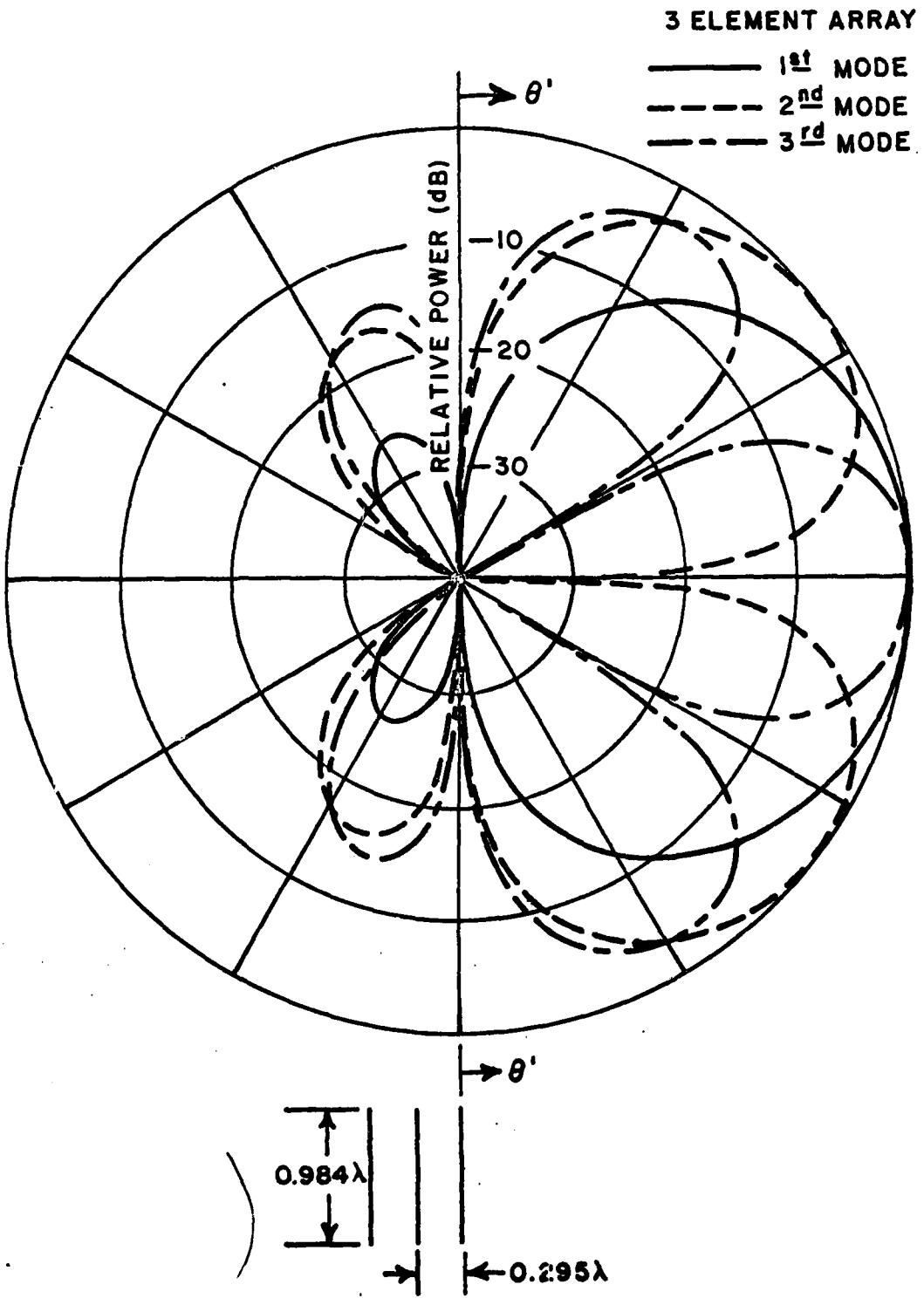


Fig. 12. Azimuth plane pattern for three-element array for individual modes.

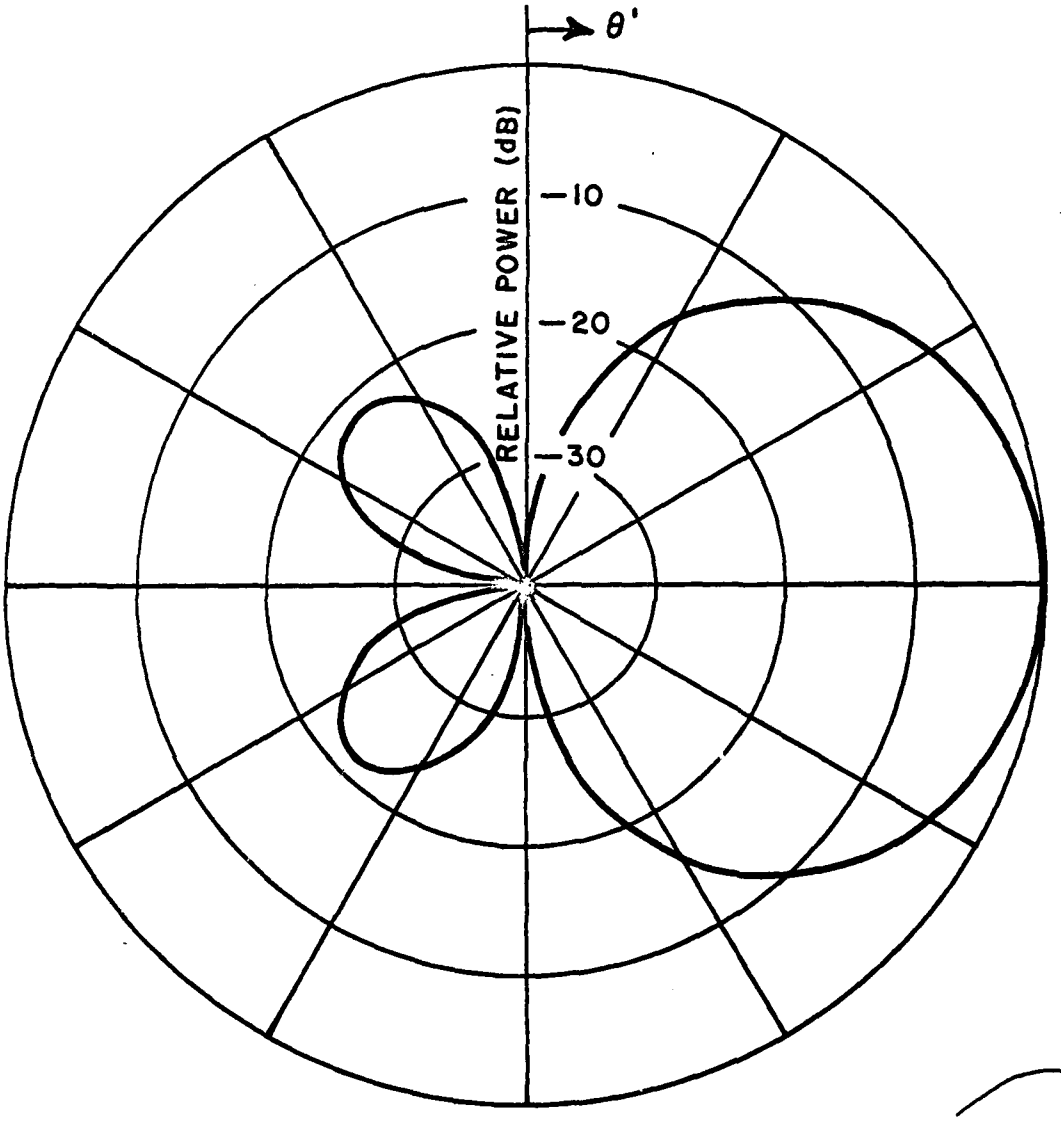


Fig. 13. Synthesized azimuth plane pattern for two-element array using first and third modes.

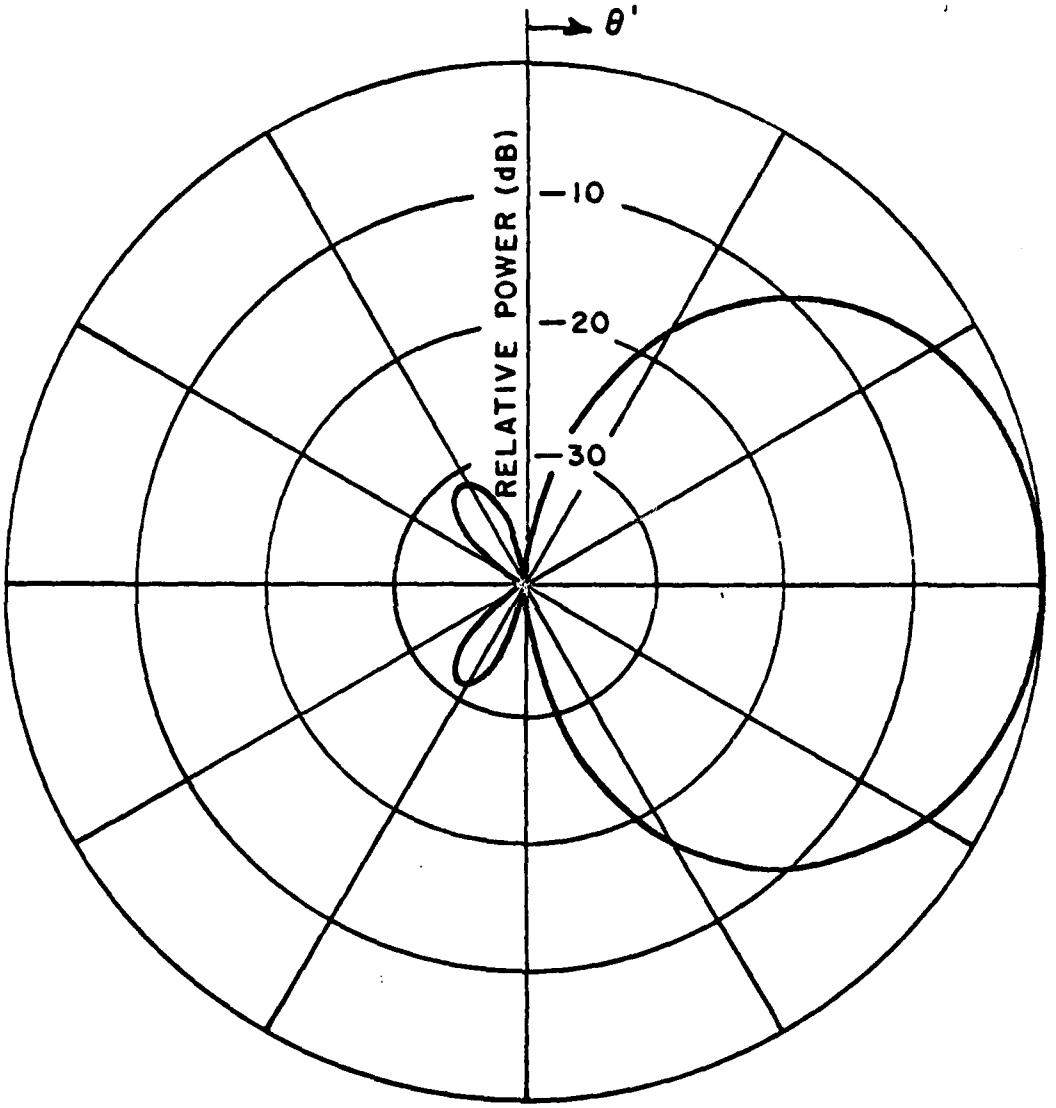


Fig. 14. Synthesized azimuth plane pattern for three-element array using first and third modes.

placement of two elements in a single cavity is considered. This, however, means that the elements in the same cavity must have essentially the same amplitude and phase. Figure 15 shows a result for the type of element used at NWC scanned at 45°, using only the first waveguide mode. The result for a four-element array with two elements per cavity is shown in Fig. 16. Note that there is no improvement in the antenna pattern over that of the two-element case. This is due to the fact that we cannot individually phase the elements. Thus, putting two elements per cavity is not advantageous in terms of the resulting patterns.

Another way to use a three-element array in a manner that will avoid the cavity problem would be to offset the elements. The result with no offset of the elements, that is, with all the elements in a line, is shown in Fig. 17. Note that only the first waveguide mode is used in the following discussion. The results for a slight offset of the elements is shown in Fig. 18. The results for an offset that would make possible the positioning of the elements so that the cavities do not overlap is shown in Fig. 19. As can be seen, the grating lobes due to the large spacing between elements for any of the offset array results are prohibitively large. Combining the various waveguide modes does not improve the patterns. Thus, offsetting the elements does not look advantageous. Given these constraints, the two-element array design given in Fig. 7 appears to be the most realistic design that is close to optimum.

## III. BENT PLATE MODEL

In order to thoroughly analyze an antenna system's performance when the antenna is mounted on the wing of an aircraft, the pattern distorting effects of the fuselage and the three-dimensional effects of the wings must be taken into consideration. These effects are initially included in this analysis by using a program developed at the ElectroScience Laboratory which allows the computation of the radiation pattern for an arbitrary source in the presence of a plate with bends and arbitrarily many sides [1]. This program allows the fuselage profile and wing outline to be modeled in a simple manner. The fuselage geometry for the bent plate model of an F-4 is shown in Fig. 20. The wing geometry is shown in Fig. 21. This solution represents the worst case for fuselage scattering since the flat plate will scatter energy in a much more severe manner than would a curved surface. This allows, however, a reasonable means of finding an optimum location for an antenna array that will minimize the adverse effects of the fuselage. The optimum locations found using this method are not intended to give exact locations on the actual aircraft, but only to give the antenna designer a good idea where to place the array with respect to the major features of the aircraft. The following results were obtained for the F-4, however, the program can be used for any aircraft.

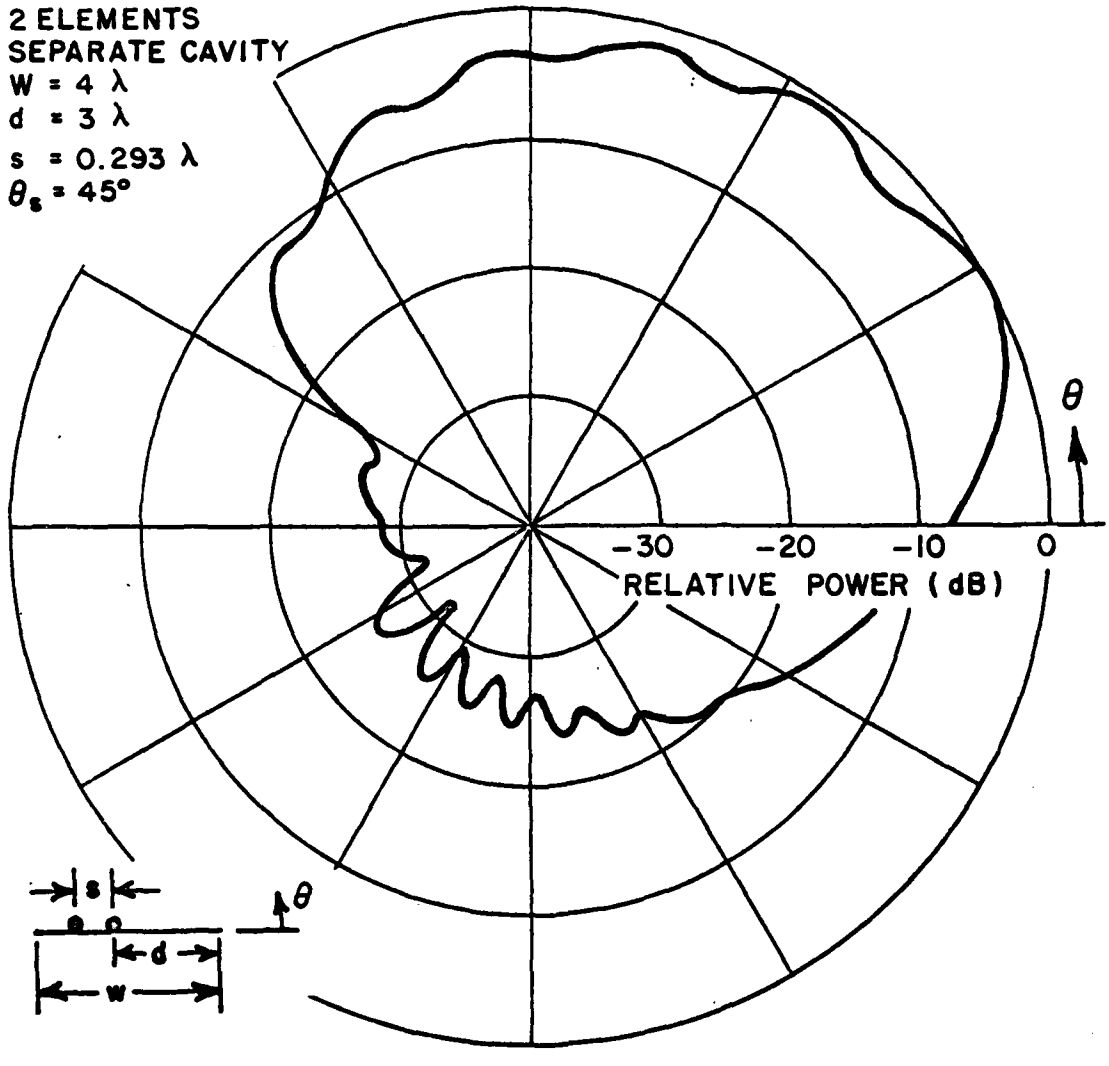


Fig. 15. Radiation pattern for two elements in different cavities on a finite ground plane.

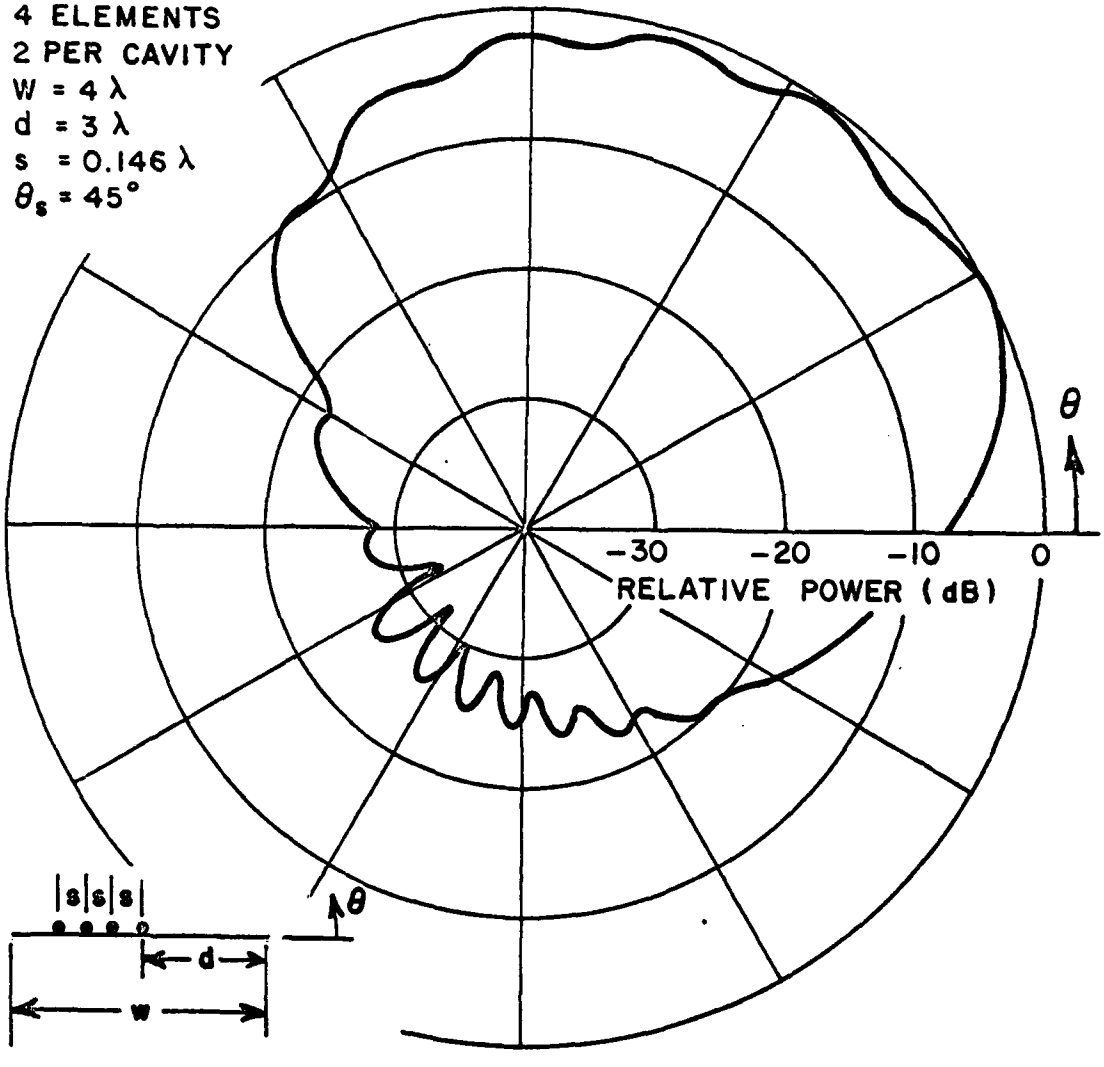


Fig. 16. Radiation pattern for four elements with two elements per cavity on a finite ground plane.

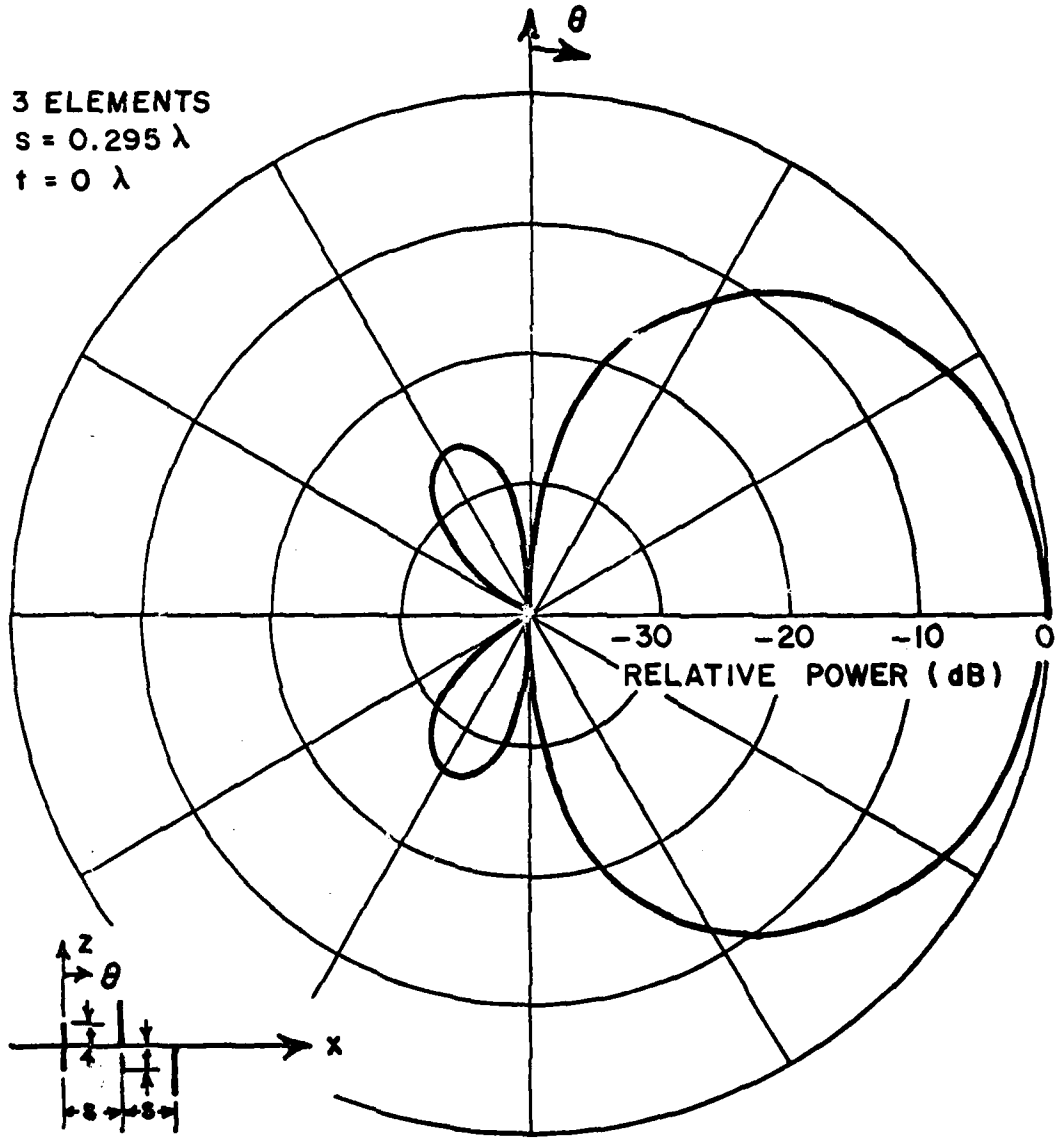


Fig. 17. Radiation pattern for a three-element array with no offset of the elements.

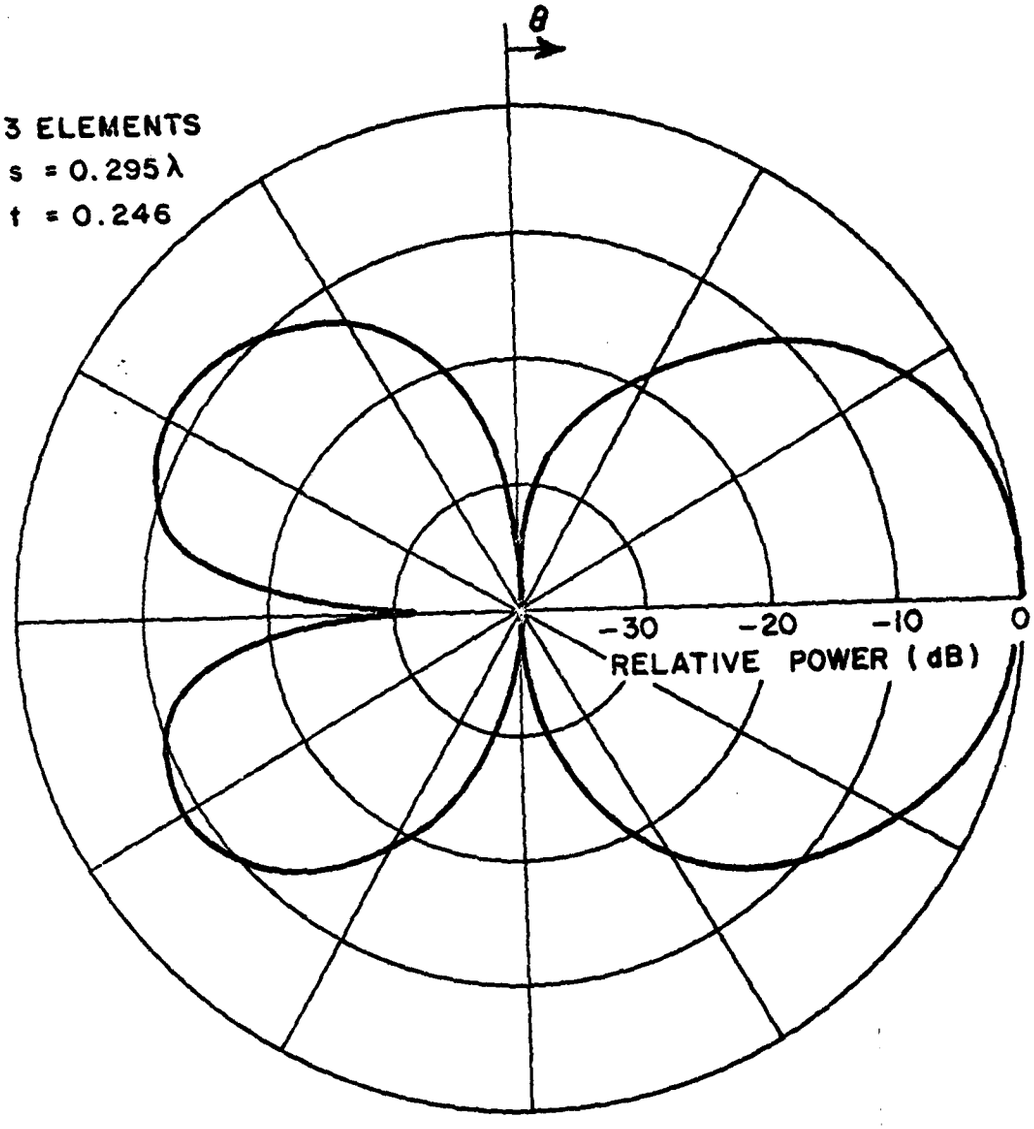


Fig. 18. Radiation pattern for a three-element array with a slight offset of the elements.

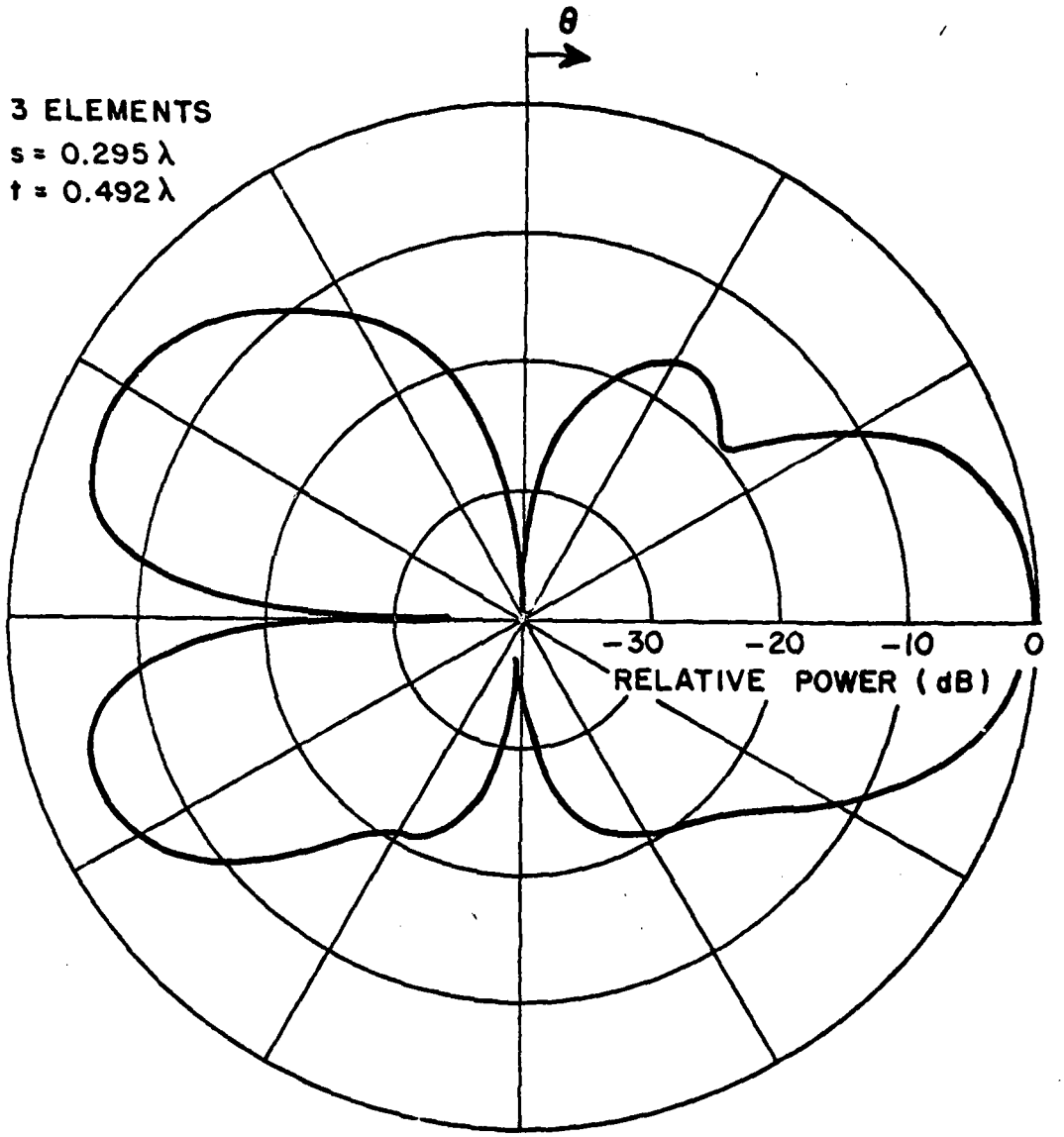


Fig. 19. Radiation pattern for a three-element array with the elements offset such that the cavities would not overlap.

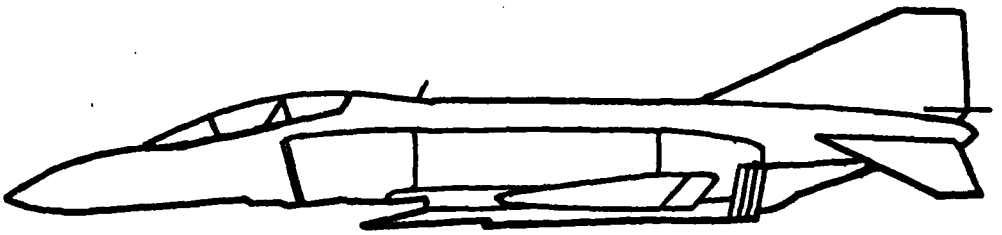

| POINT | y | x |
|---|---|---|
| 1 | 0.0 | 0.0 |
| 2 | 0.210 | 0.045 |
| 3 | 1.650 | 0.485 |
| 4 | 1.560 | 1.185 |
| 5 | 1.210 | 1.220 |
| 6 | 0.090 | 0.685 |
| 7 | -1.625 | 0.700 |
| 8 | -3.340 | 0.375 |
| 9 | -3.310 | 0.045 |
| 10 | -1.840 | 0.090 |

SCALE 1:126.5

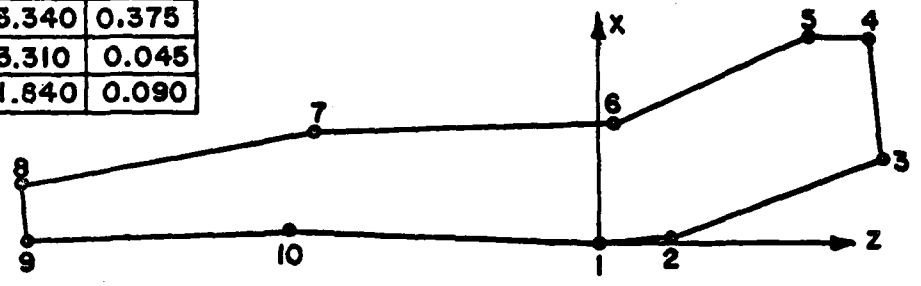


Fig. 20. Fuselage geometry for bent plate model of F-4 aircraft.

| POINT | z | y |
|---|---|---|
| 10 | -1.840 | 0.0 |
| 11 | -1.840 | 0.427 |
| 12 | -0.240 | 1.868 |
| 13 | 0,187 | 1.868 |
| 14 | -0.050 | 0.369 |
| 15 | 0.0 | 0.0 |
| 11' | -0.876 | 1.295 |
| 13' | 0.0966 | 1.295 |

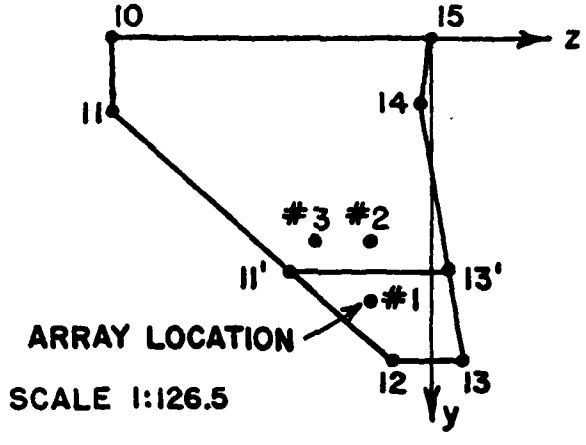


Fig. 21. Wing geometry showing array locations.

The flat plate program initially allowed only one bend in the plate. This bend is used at the fuselage-wing junction so that a bend in the wing (as F-4 wings) could not be included at first.

The array optimization proceeded concurrently with a modification of the program to allow another bend in the wing. First, to study the effects of a three-dimensional wing on the array design of Chapter II, a two-element array of $\lambda/2$ slots with a cosine aperture distribution was used with the parameters shown in Fig. 3. The elevation plane pattern for the bent wing aircraft shown in Fig. 22 compares favorably with the results in Fig. 3 for the two-dimensional model. The azimuth plane pattern for the bent plate model with the antennas positioned to give an endfire beam in the aft direction is shown in Fig. 23. This does not seem to be a desirable pattern since much of the energy is scattered into the wrong quadrant, and there are undesirable reflections off the fuselage. If the antennas are positioned to give and endfire beam at an angle of 45° with respect to the fuselage, the pattern is greatly improved. This result is shown in Fig. 24. Note in Fig. 24 that the beam maximum is in the center of the quadrant and the fuselage reflections have been reduced.

The optimum array designs for the two- and three-element cases, with the parameters presented in Chapter II, are next studied for the bent plate model. The results for the three-element array will be shown for comparison, even though the three-element array may not be practical for this particular element type.

The arrays are placed as far as possible from the aft wing edge to reduce diffractions below the wing. The array axis is at a 45° angle with respect to the z-axis. This is indicated as location #1 in Fig. 21, but without the bend at 11' and 13' included. The two-element array pattern in the plane containing the beam maximum (elevation plane), that is the plane coincident with the array endfire direction, is shown in Fig. 25. The three-element array pattern for this same plane is shown in Fig. 26. An improvement is observed in the level of the three-element array pattern in the top front quadrant. The two-element array azimuth plane pattern is shown in Fig. 27, and the three-element array azimuth pattern is shown in Fig. 28. The three-element pattern has about a 10 dB improvement in one of the backlobes as predicted earlier in the array studies of Chapter II.

With the bent plate program modified to allow two bends, a 15° bend was placed in the plate to represent an F-4 wing structure. Elevation plane patterns through the maximum of the main beam were computed for array location #1 with optimum array design. The pattern shown in Fig. 29 is for a two-element array and can be compared to Fig. 25 without the bend. The pattern in Fig. 30 is for a three-element array and corresponds to Fig. 26. In both cases, the major difference between the flat wing and bent wing results appears to be a side lobe in the pattern.

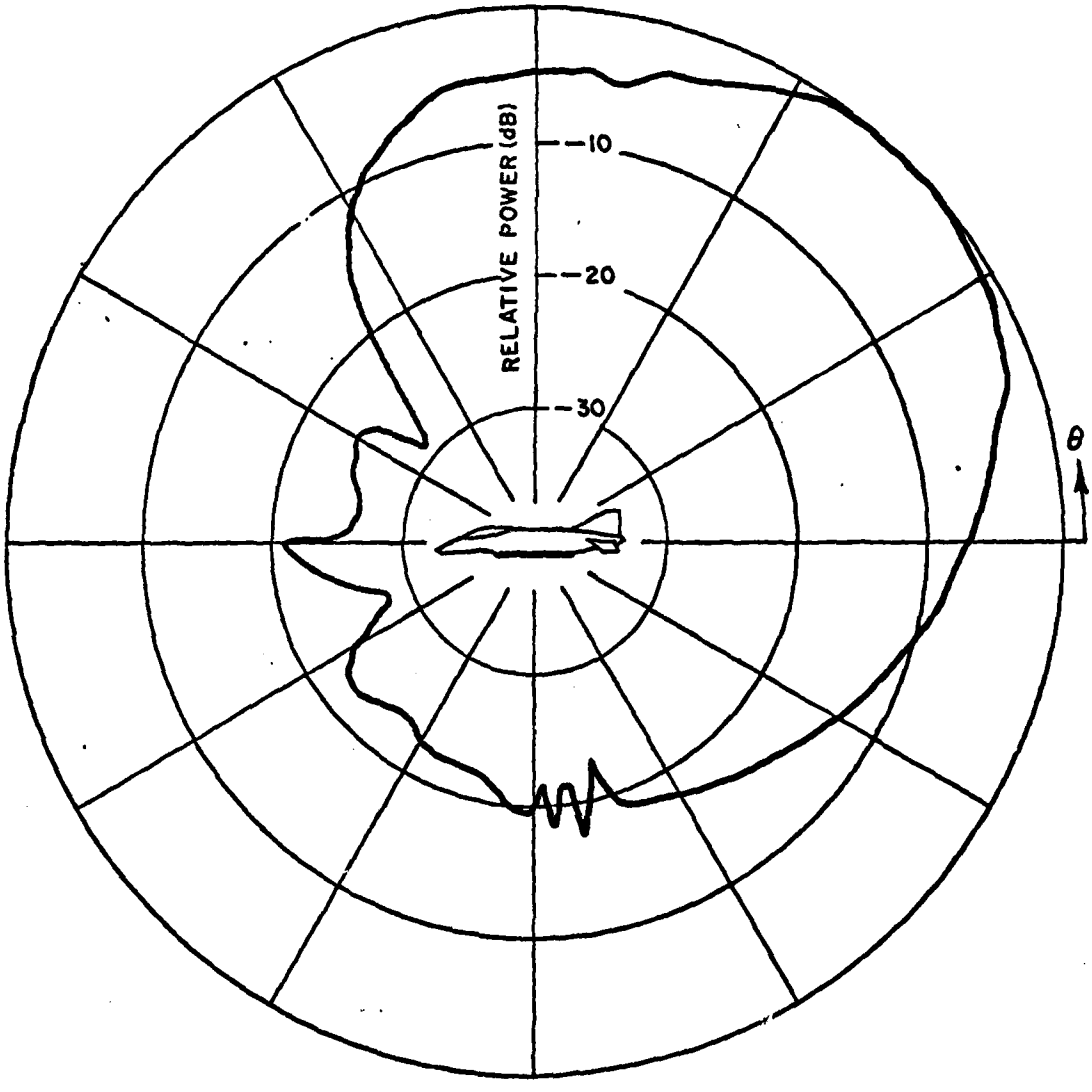


Fig. 22. Elevation Plane Pattern for bent plate model of aircraft.

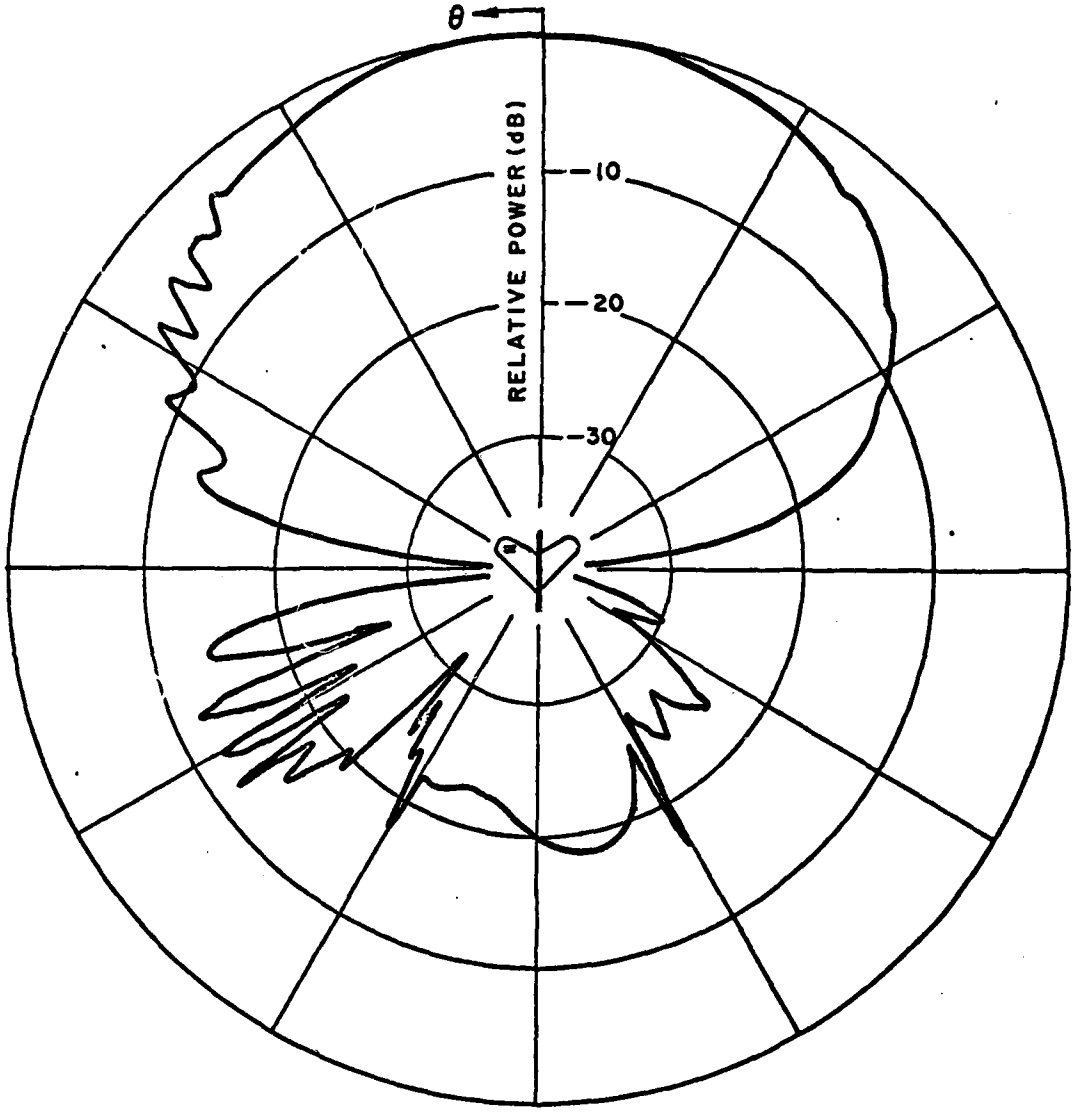


Fig. 23. Azimuth Plane Pattern for bent plate model of F-4 aircraft with antennas positioned to give an end-fire beam in aft direction.

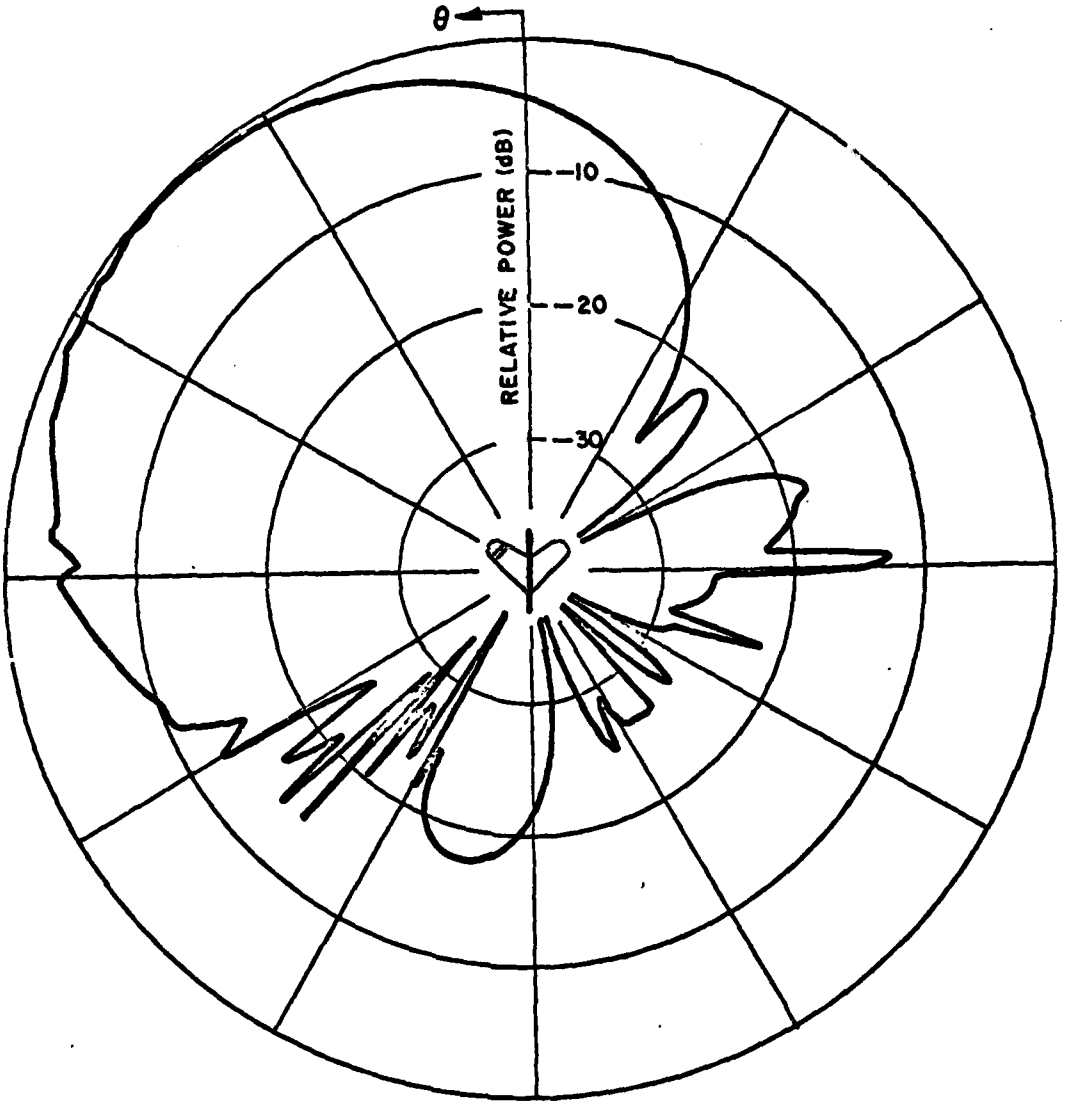


Fig. 24. Azimuth Plane Pattern for bent plate model of F-4 aircraft with antennas positioned to give an end-fire beam at an angle of 45° to the aft direction.

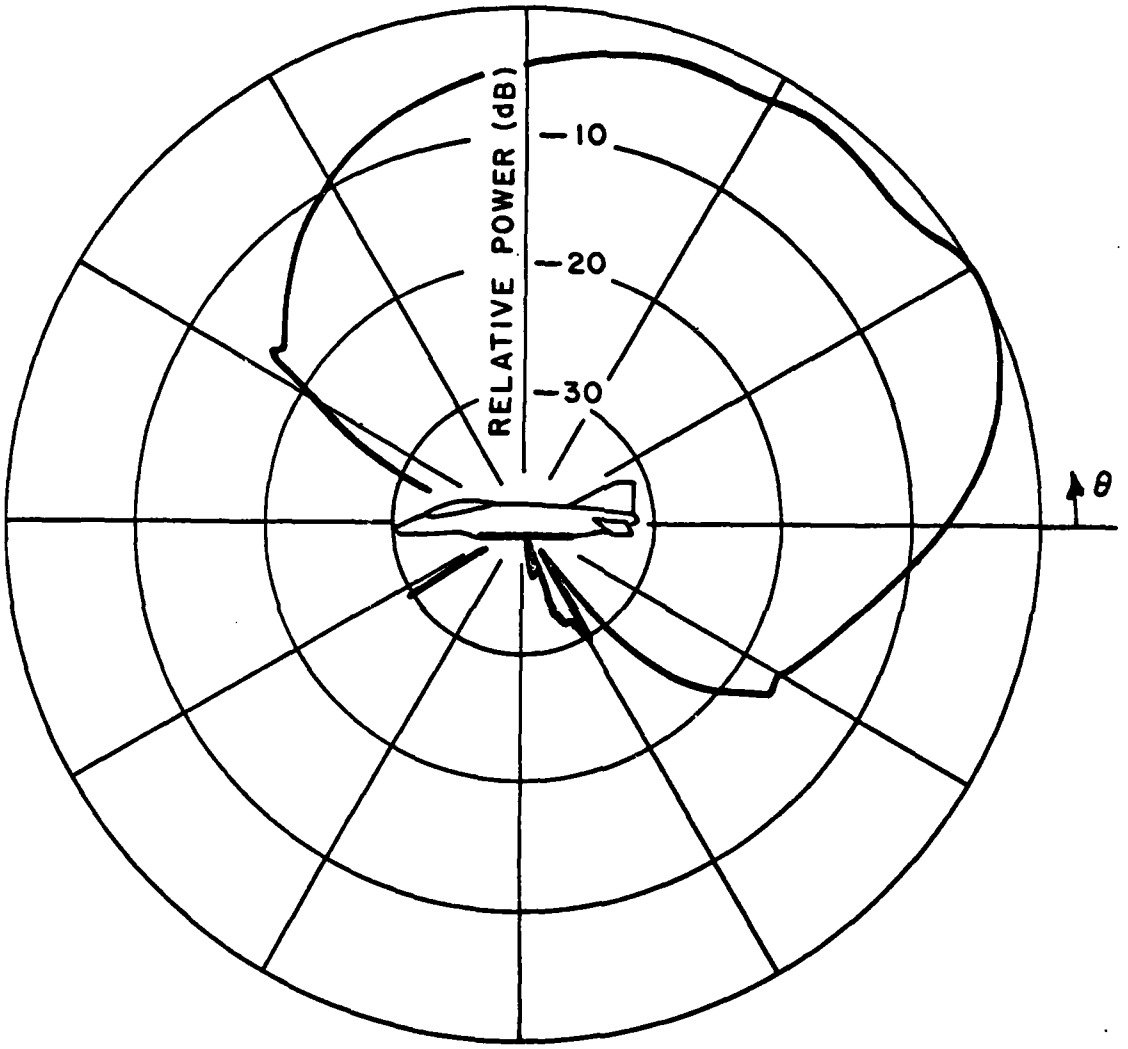


Fig. 25. Radiation pattern in plane containing the beam maximum for bent plate model of F-4 aircraft with two-element array design.

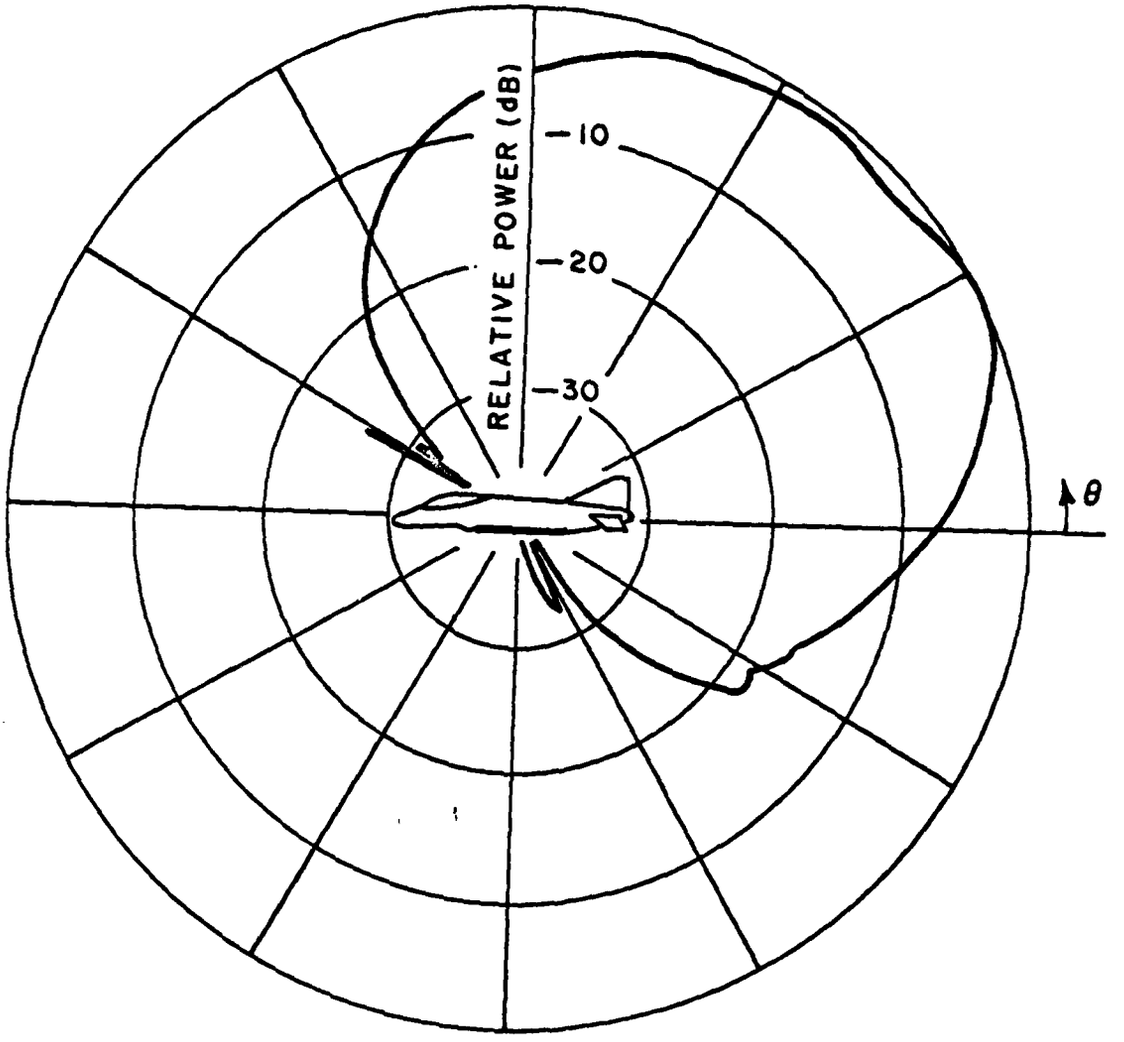


Fig. 26. Radiation pattern in plane containing the beam maximum for bent plate model of F-4 aircraft with three-element array design.

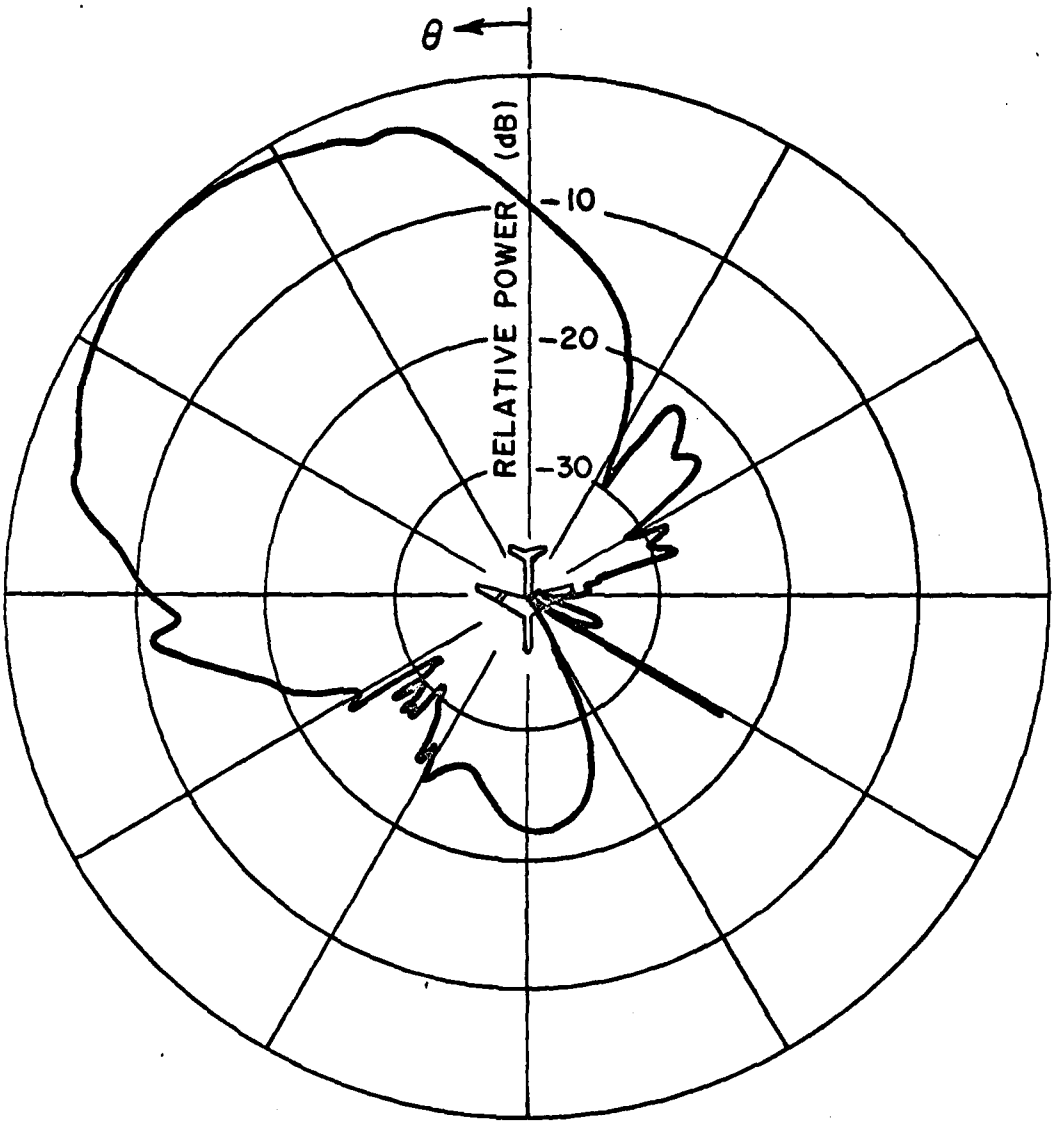


Fig. 27. Azimuth Plane Pattern for bent plate model of F-4 aircraft with two-element array design.

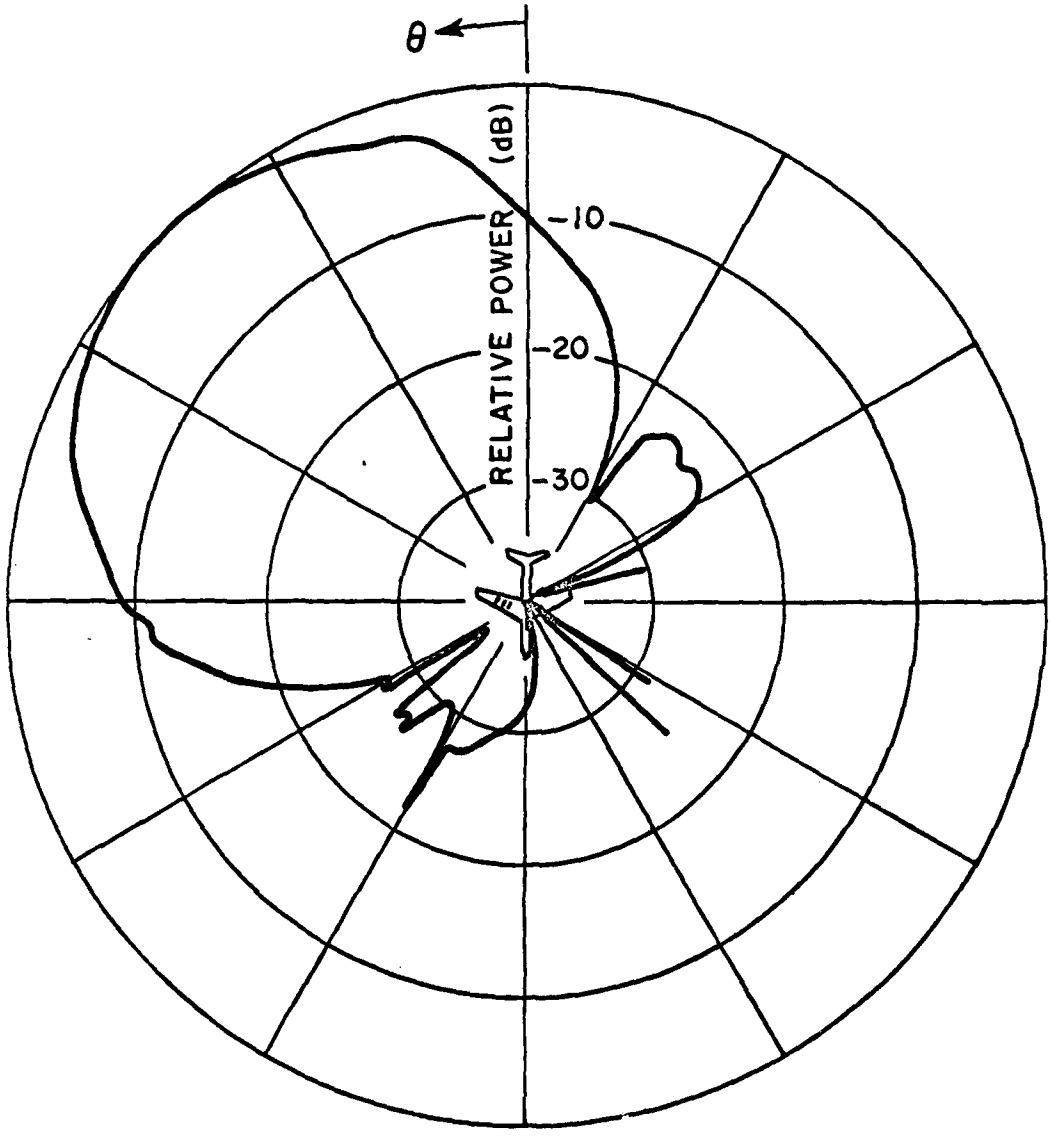


Fig. 28. Azimuth Plane Pattern for bent plate model of F-4 aircraft with three-element array design.

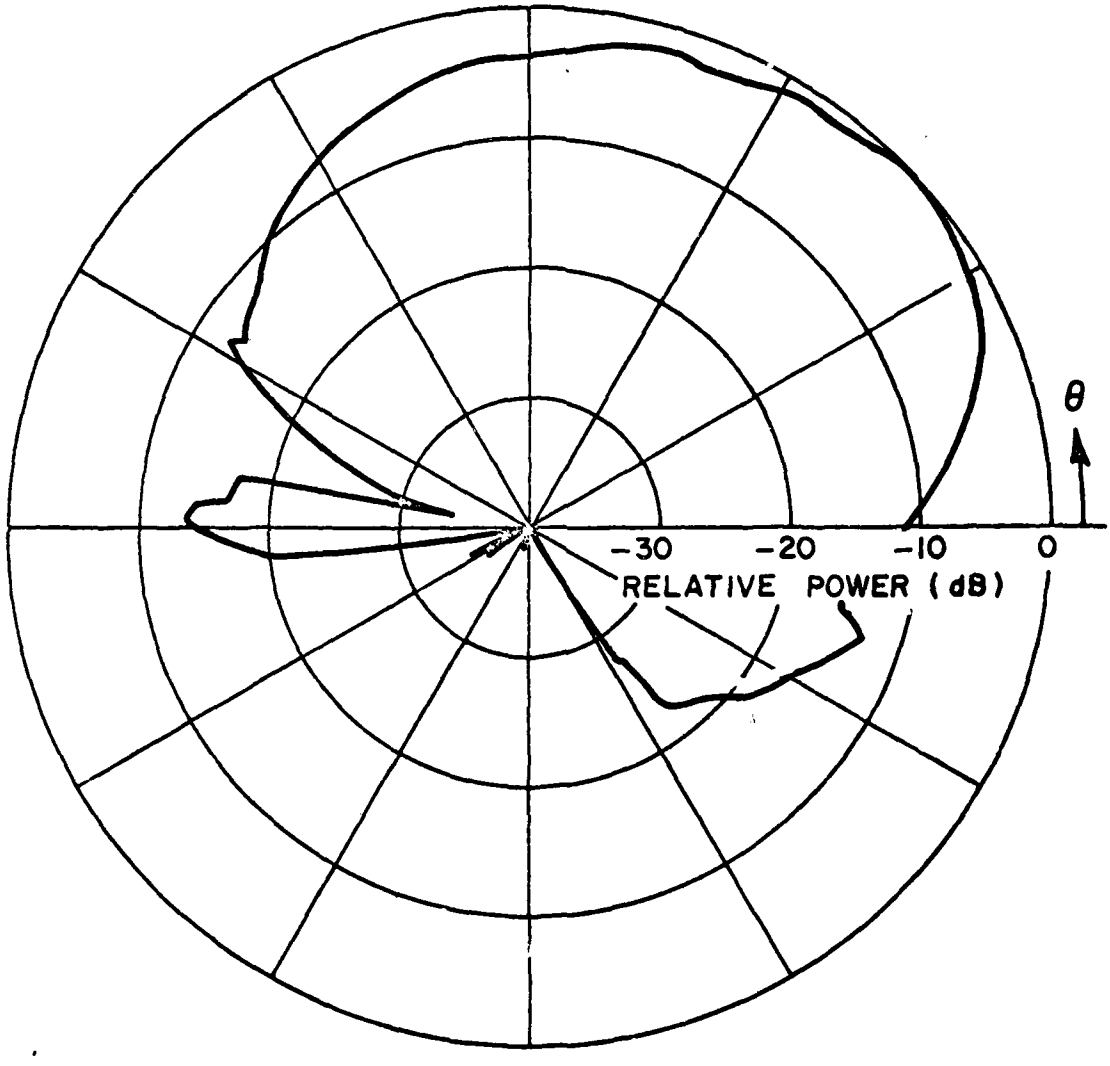


Fig. 29. Main beam elevation plane radiation pattern for two elements at location #1.

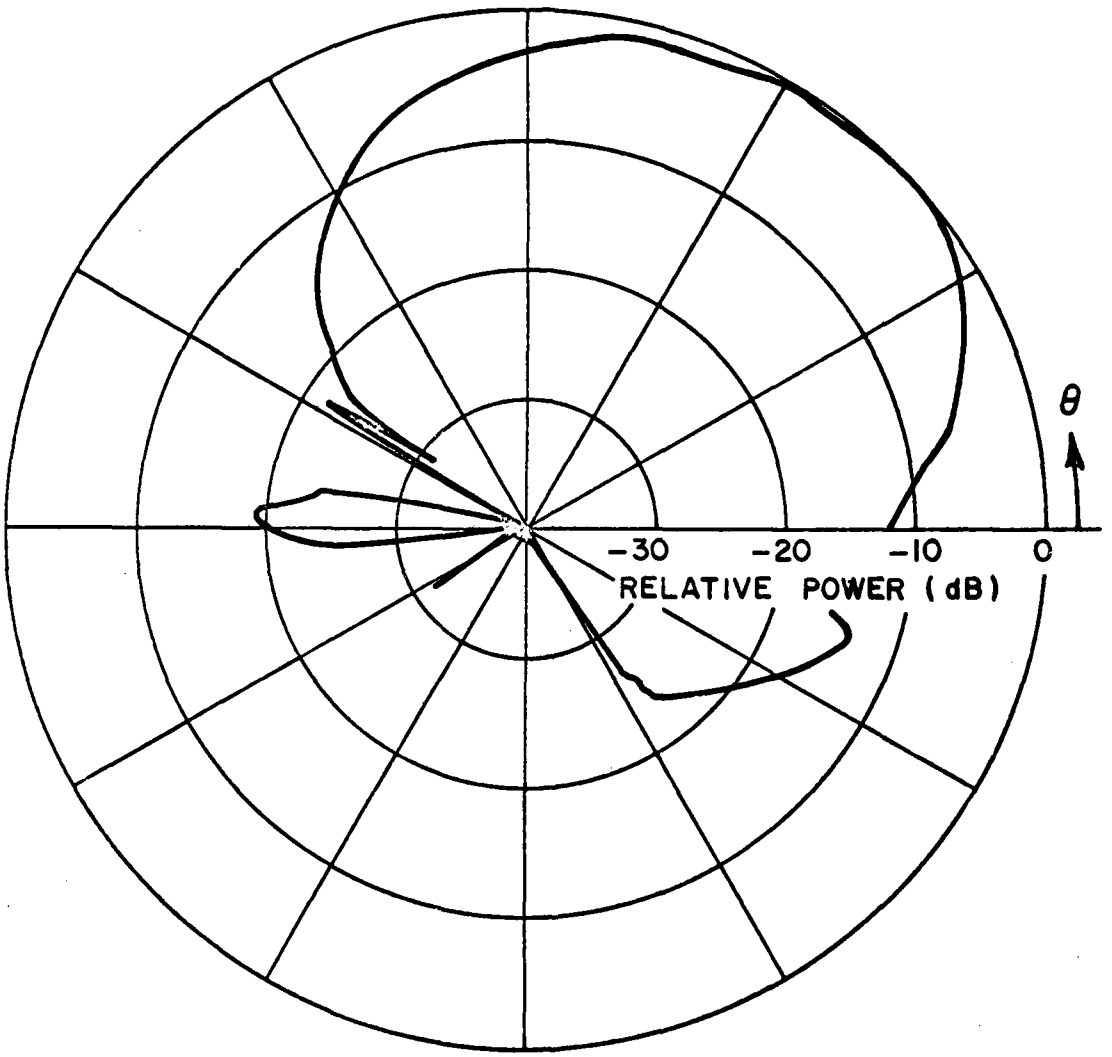


Fig. 30. Main beam elevation plane radiation pattern for three elements at location #1.

In order to avoid the sidelobes, the array is moved to location #2 in Fig. 21. The results for the two- and three-element arrays at location #2 are shown in Figs. 31 and 32, respectively. The patterns, however, have large amounts of ripple in the quadrant of interest. This may be reduced by moving the array as close as possible to the bend in the wing. Location #3 of Fig. 21 is such a position. This corresponds to coordinates on a full-scale model of (x = 0", y = 137.1", z = -100.1") for the first element and (x = 0", y = 141.3", z = -95.9") for the second element for the two-element array. The main beam elevation pattern for this case is shown in Fig. 33.

In order to check the validity of the approximations made in the bent plate computer program up to this point, experimental measurements were made at NWC using a scale model of an F-4 aircraft, shown in Fig. 34. Four different pattern cuts were made as illustrated in Figs. 35 a-d. Five different antenna locations on the wing were used as shown in Fig. 36. The antenna was a single cavity-backed slot of length $0.748\lambda$ in free space with only the first waveguide mode excited. The comparison of experimental and calculated main beam elevation plane pattern results (refer to Fig. 35 a) for the slot placed at a 45° angle with respect to the fuselage axis at locations #2 and #4 are shown in Figs. 37 and 38, respectively. The overall character of the measured and calculated patterns appears to agree; however, the finer details of the patterns do not compare very well. These results point out the fact that higher order diffraction terms are needed in the bent plate program than are included in these results. These higher order terms include slope diffraction, corner diffraction, and double diffraction fields. The means of including these will be discussed below.

An important benefit of the GTD method can be observed here. That is, even though our numerical solution may produce some errors, the solution does not hide the errors by being erroneously continuous, but, rather, the solution shows discrete jumps in the pattern which illustrate problem areas. If these discontinuities are large, it indicates further work must be done. If these discontinuities are small, however, the pattern computations can be deemed essentially correct for design purposes.

The above comparisons also indicate that the flat plate representation does not adequately represent the smooth curved surface of the aircraft fuselage. The single element mounted at 45° with respect to the fuselage, however, transmits much more energy toward the fuselage than would the optimum array design used in the quadrant detection application. To minimize the fuselage effects, a measurement was made on the F-4 model with the antenna main beam pointed straight behind the aircraft. This result is shown in Fig. 39. Some of the detail compares slightly better; however, the shifting of some of the ripple and the broadness of the pattern at $\theta = 180°$ indicates a problem with the measurements that turns up in all the comparisons.

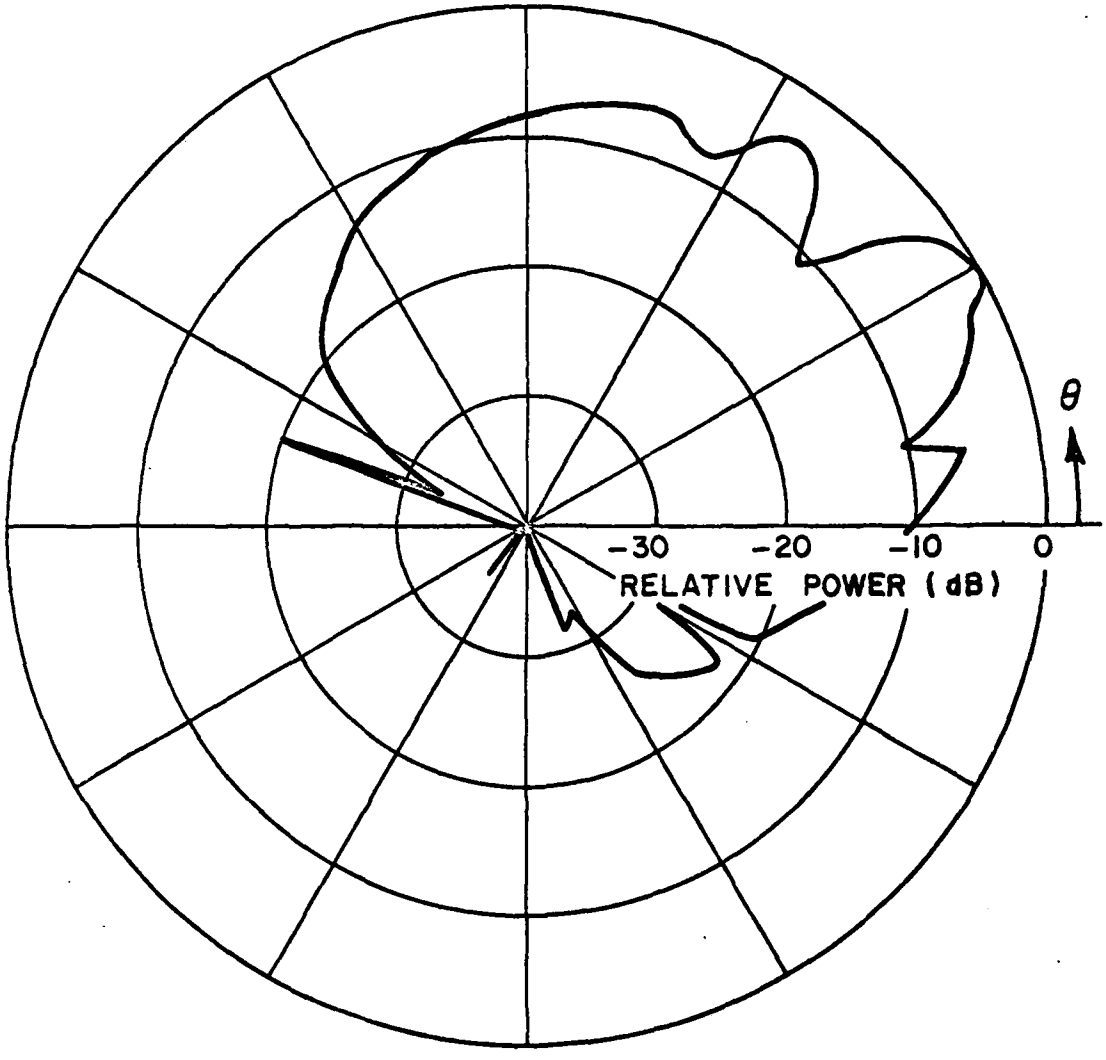


Fig. 31. Main beam elevation plane radiation pattern fo
two elements at location #2.

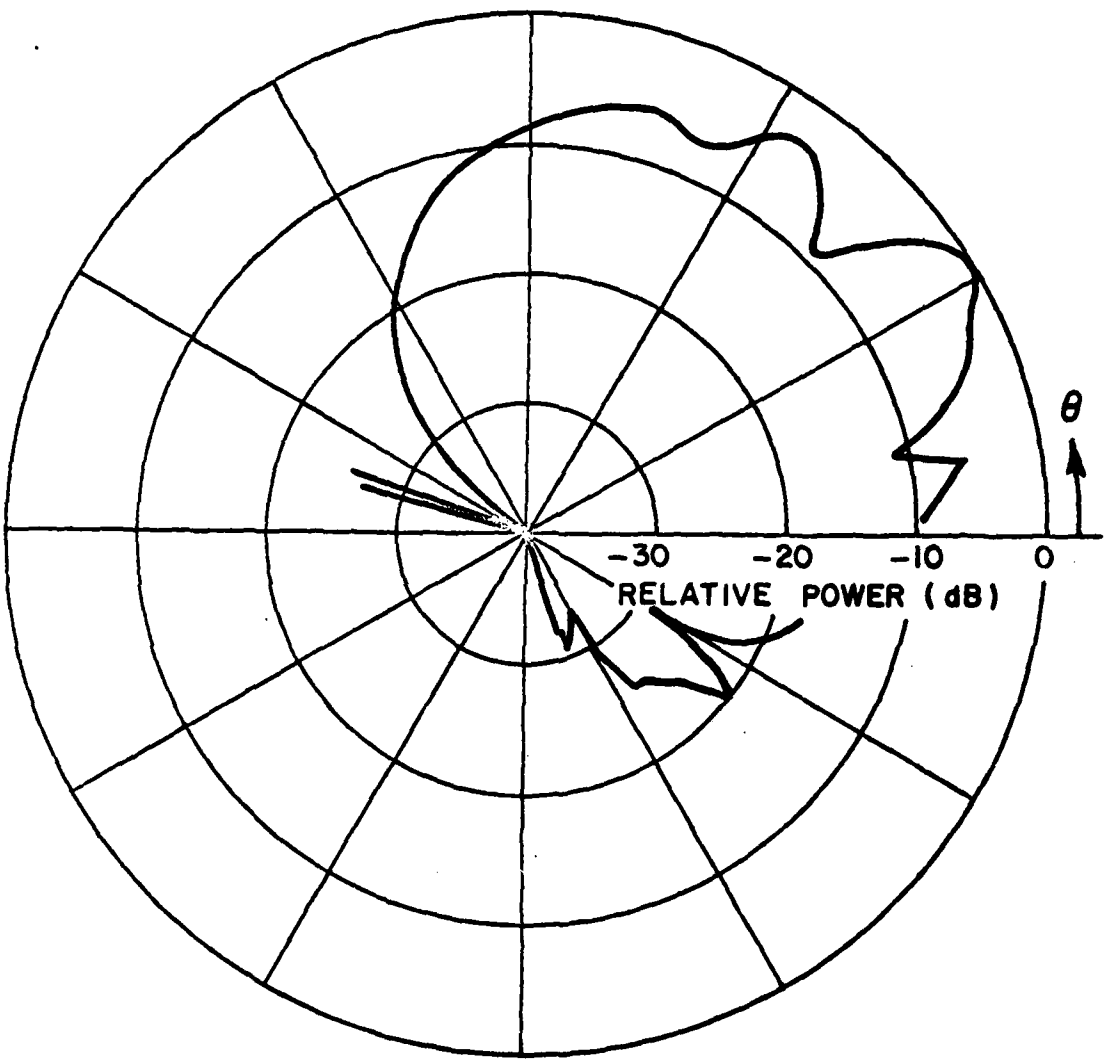


Fig. 32. Main beam elevation plane radiation pattern for three elements at location #2.

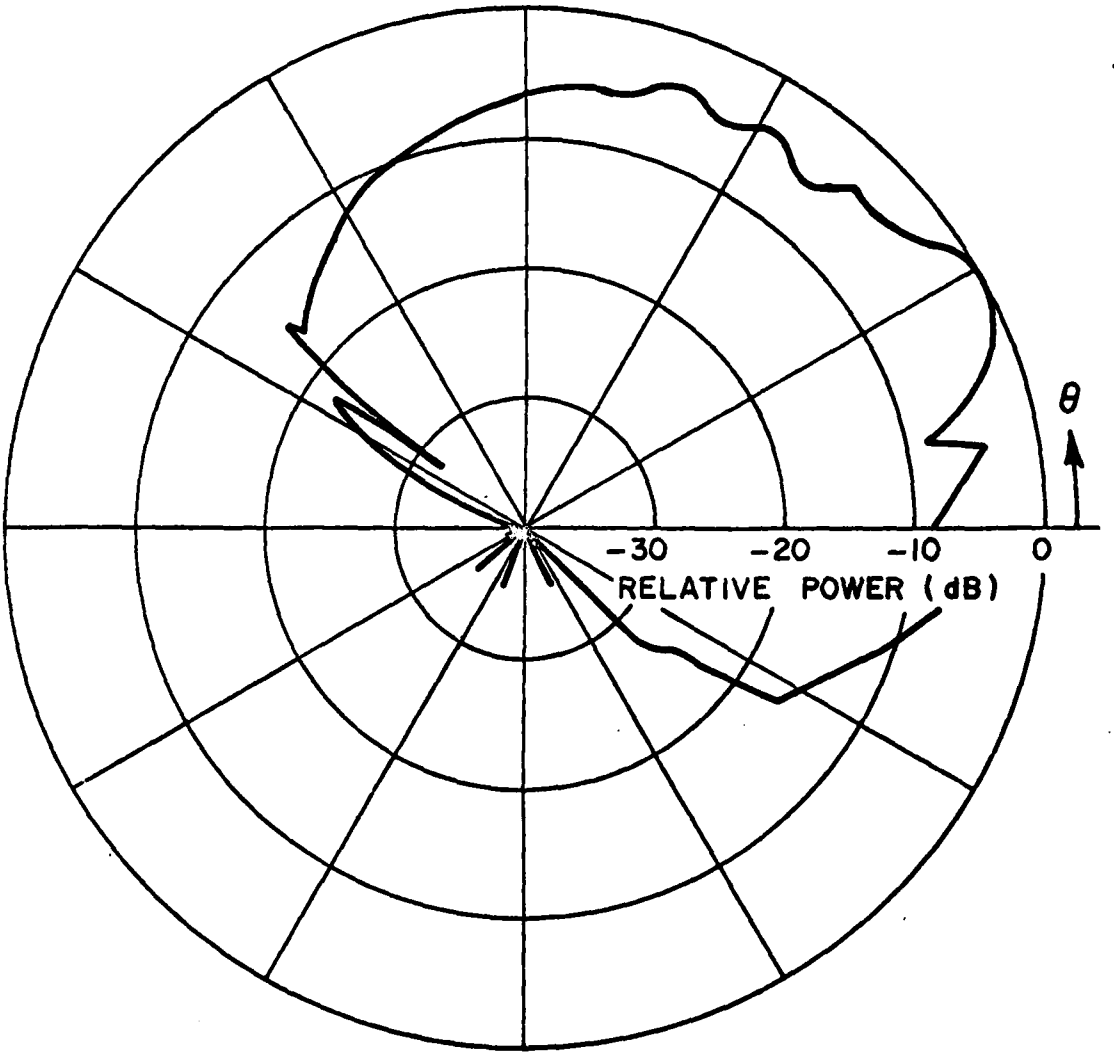


Fig. 33. Main beam elevation plane radiation pattern for two elements at optimum location.

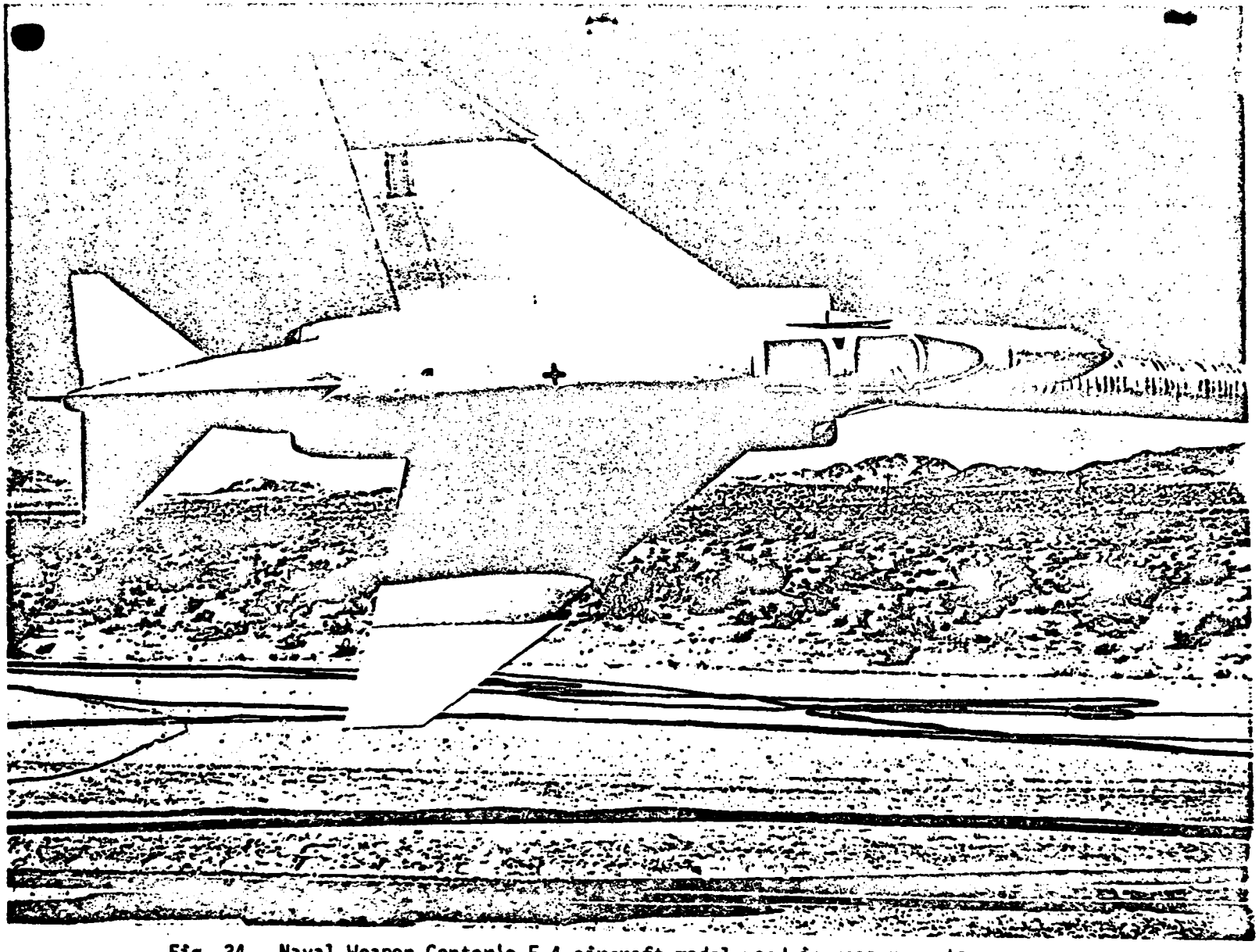

Ffg. 34. Naval Weapon Center's F-4 aircraft model used in measurements.

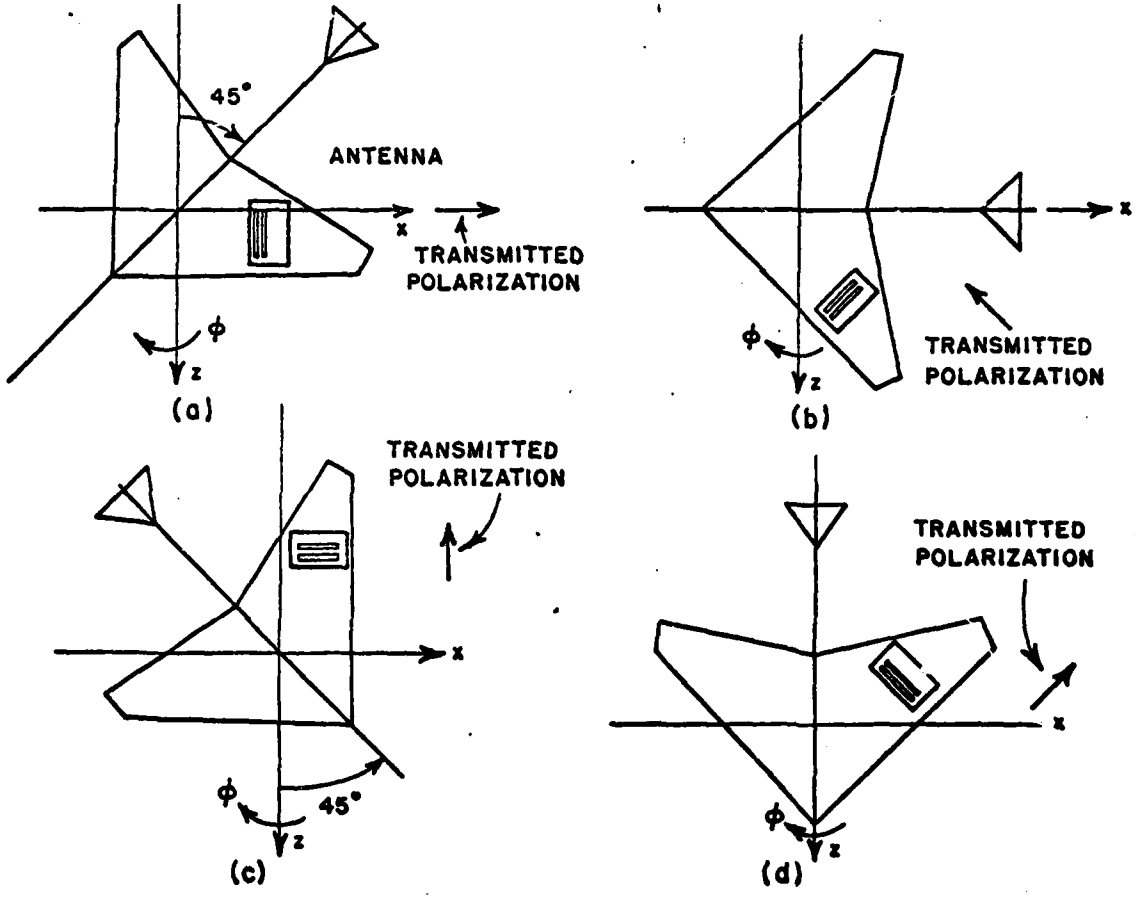


Fig. 35. Illustration of pattern cuts and transmitted polarization for measured results: (a) main beam elevation plane; (b) elevation plan; (c) main beam roll plane; (d) roll plane.

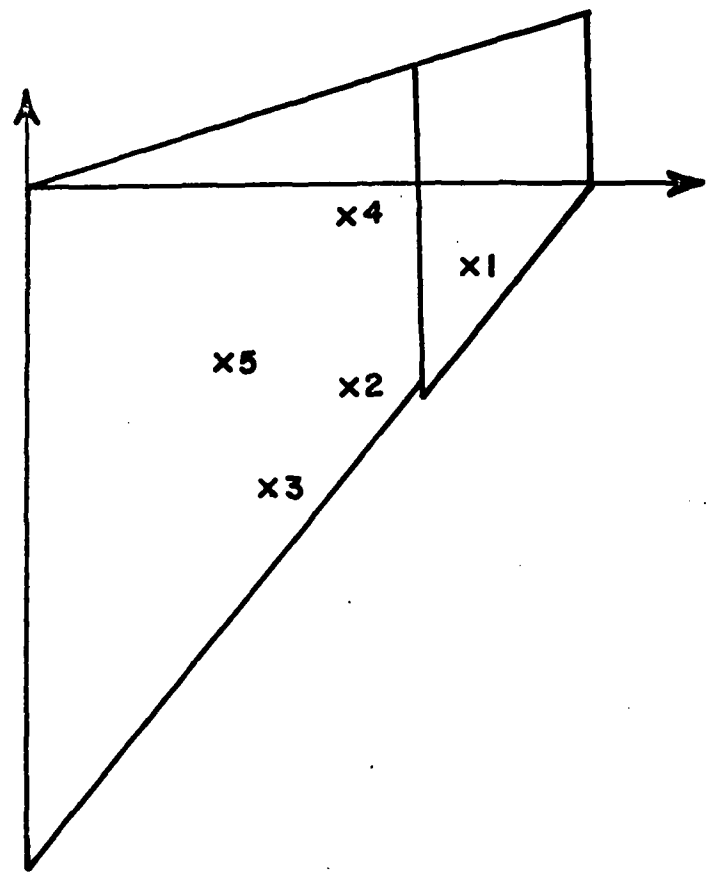


Fig. 36. Antenna locations on F-4 wing used in measured results.

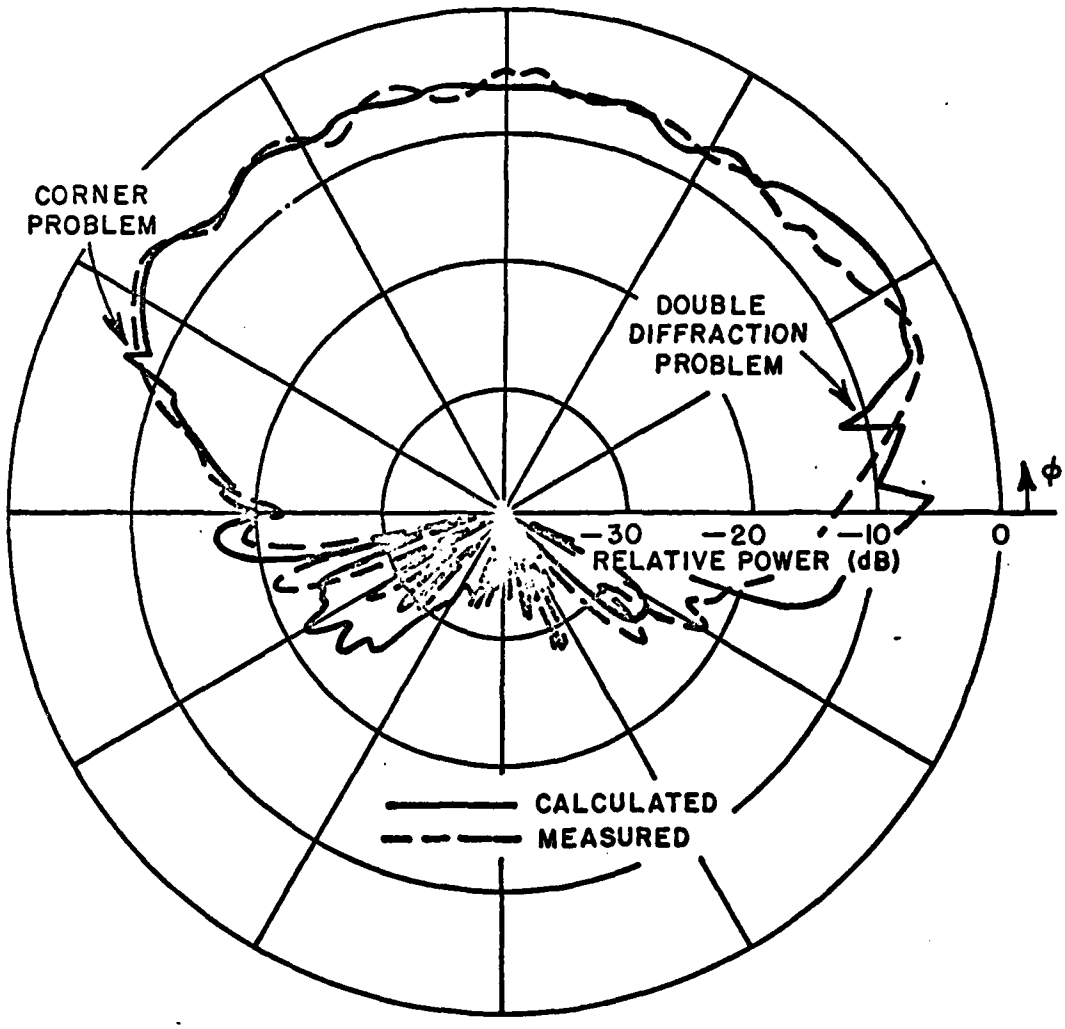


Fig. 37. Main beam elevation pattern for single slot mounted on F-4 at location #2.

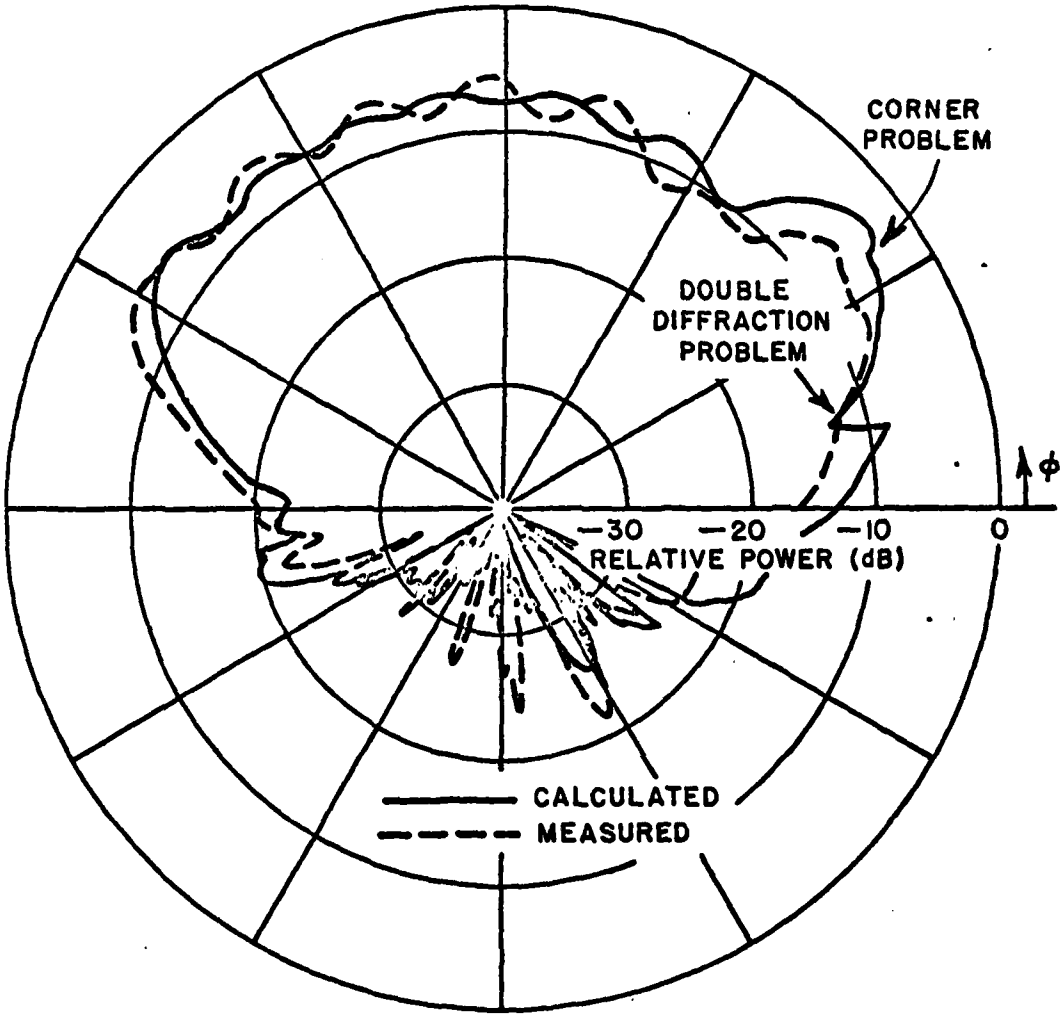


Fig. 38. Main beam elevation plane pattern of single slot mounted on F-4 at location #4.

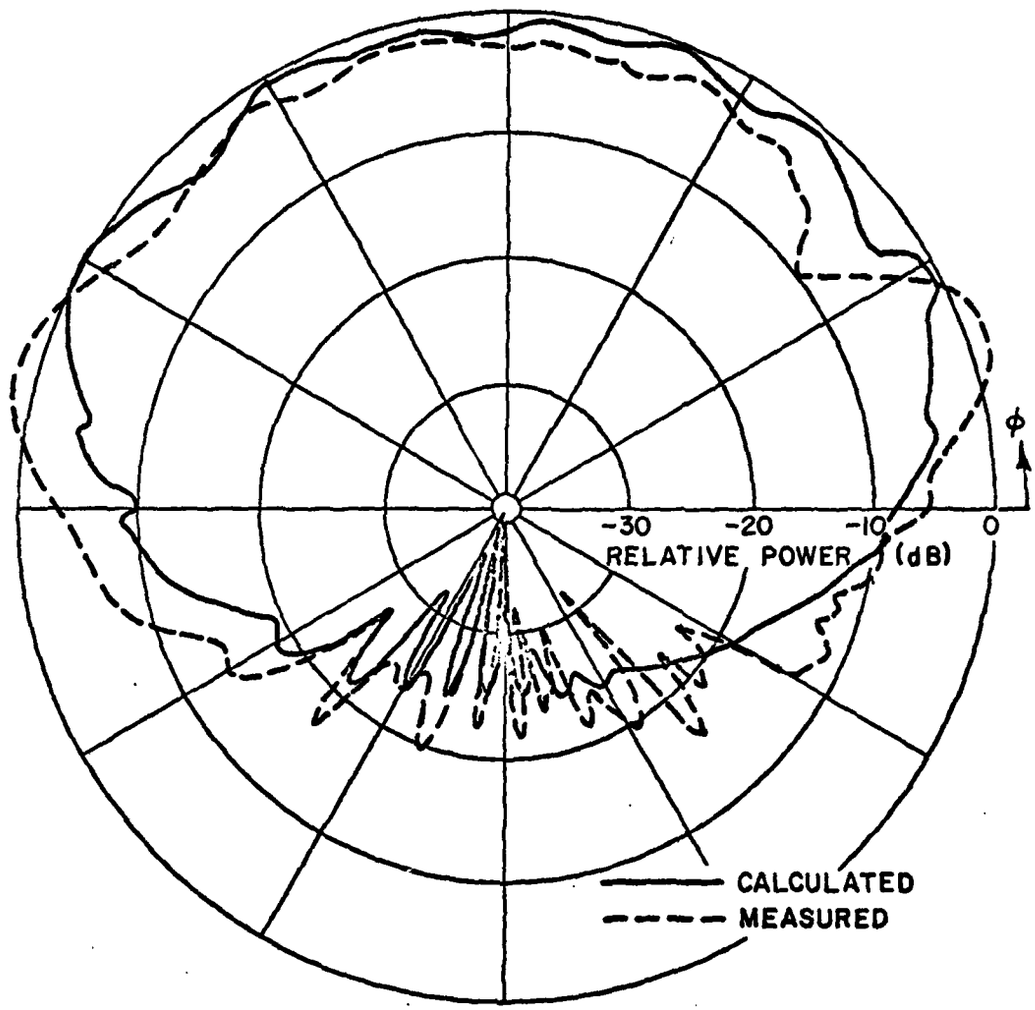


Fig. 39. Elevation plane pattern of single slot mounted on F-4 wing.

The problem is that the measurements were taken in the near field of the aircraft. As a result, one cannot directly compare the measured near-field and calculated far-field patterns. Of course, there is also the possibility of slight inaccuracies in the measured results due to variations in the placement of the antenna, ground reflections, etc. The comparisons are good enough, however, to show that the flat plate model although moderately successful needs improvement.

The modelling of the fuselage by a smooth curved surface to improve the computer aircraft model will be taken up in the next chapter. Other improvements due to higher order terms needed in both models are discussed briefly here. The question as to whether a flat plate adequately models a rounded wing tip is studied by comparing the results of a two dimensional thick wing model with the knife edge used in the flat plate model. The rounded wing tip is modeled by a circular cylinder mounted on a thick wall as shown in the insert of Fig. 40. The radiation patterns are compared in Fig. 40 for a tip of 1/16 radius and the knife edge model. Note there is very little difference in the two results. This implies that the knife edge is a good approximation for a wing tip at the frequencies of interest.

Recently slope diffraction coefficients have been derived at the ElectroScience Laboratory. They are of particular importance to slot antennas mounted on wings. A two-dimensional model has been analyzed to show this effect. A comparison of the calculated radiation pattern of a strip slot antenna mounted on a flat plate with and without slope diffraction is shown in Fig. 41. Note that there is no field predicted below the plate when slope diffraction is not used. This shows that the three-dimensional extension of these results is needed in the flat plate program. With this done, nulls that were previously predicted at the horizon for some cases with a slot mounted on an F-4 wing will be filled in as was shown to be the case in the NWC experimental results.

The discontinuity due to the lack of including the corner diffraction term in the flat plate program can be seen in Figs. 37 and 38. Usually corner diffraction has only a small effect on the patterns except for small angular sectors; however, when one antenna is close to a corner or the pattern is computed in a plane that includes the corner this term can be significant. A method was developed at first whereby equivalent currents on a rounded corner could be used to include these effects. This method allows one to place a current along each of the edges of the plate to represent the diffracted field. The geometry used is indicated in Fig. 42. The pattern for a short monopole on a square plate $8\lambda$ on a side was caluclated at $\phi=45°$, that is, directly over the corner using GTD without corner effects and is shown in Fig. 43. The large discontinuity at $\theta=90°$ is due to the lack of an appropriate corner diffraction coefficient. The pattern for a short monopole on a square plate with rounded corners ($B=1\lambda$), as shown in Fig. 42b, was calculated at $\phi=45°$ using the equivalent current concept and is shown in Fig. 44. The pattern for a corner of radius $B=2\lambda$ is shown in Fig. 45. These patterns show a much improved result at $\theta=90°$.

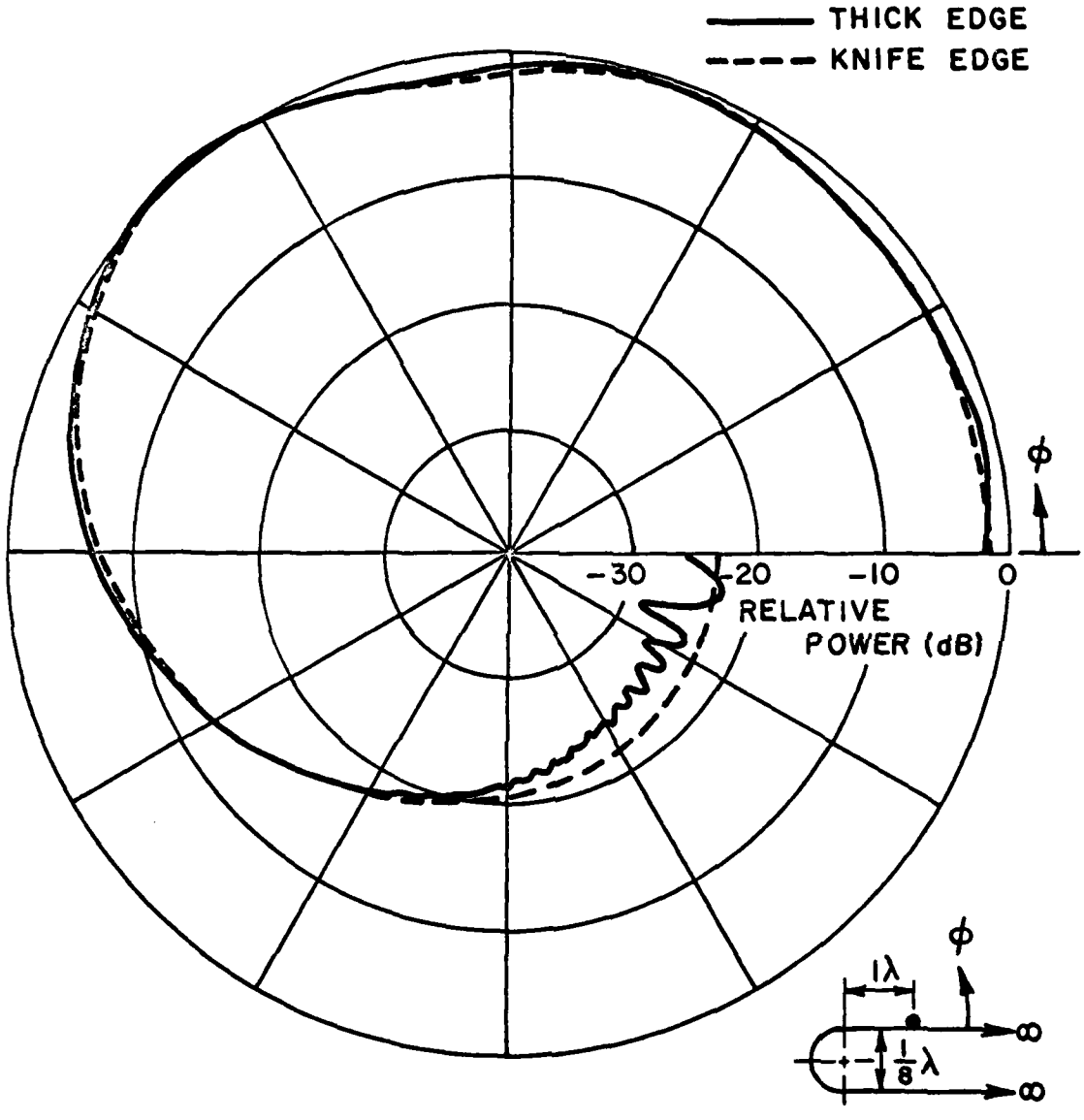


Fig. 40. Comparison of the radiation patterns of a slot on a thick edge plate to that of a slot on a knife edge plate.

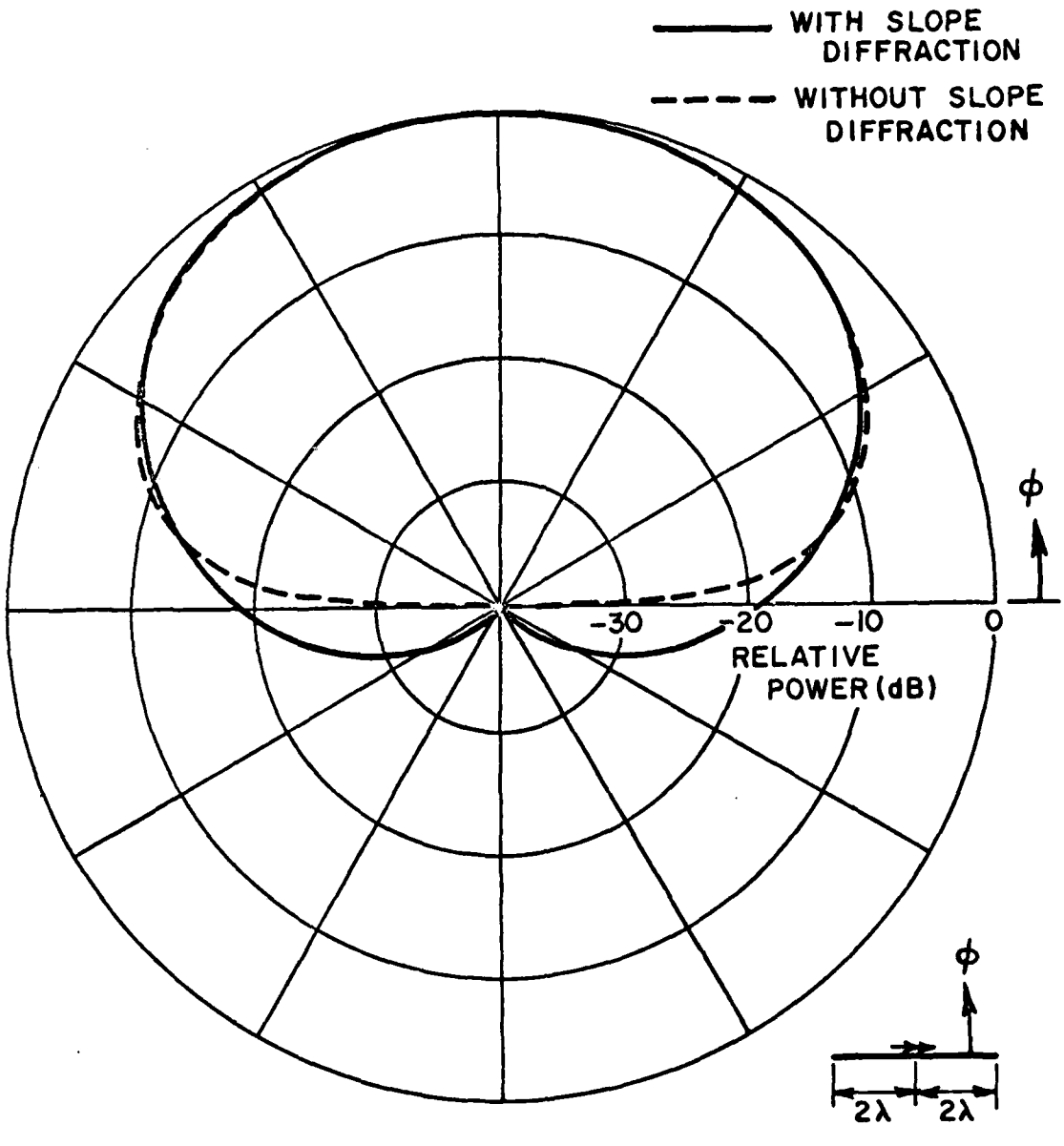


Fig. 41. Comparison of the radiation pattern of a strip slot on a plate with and without slope diffraction.

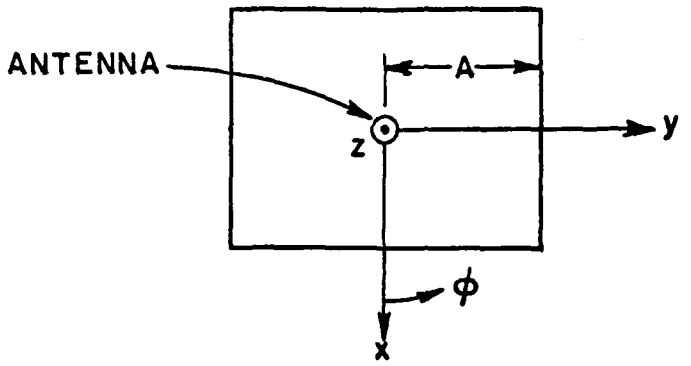


(a)

Geometry of a square plate.

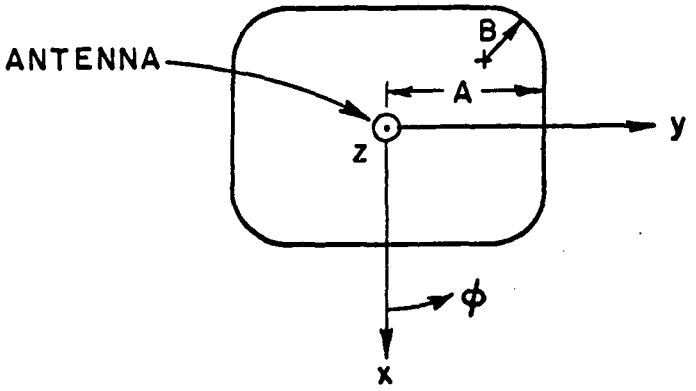


(b)

Geometry of square plate with rounded corners.

Fig. 42.

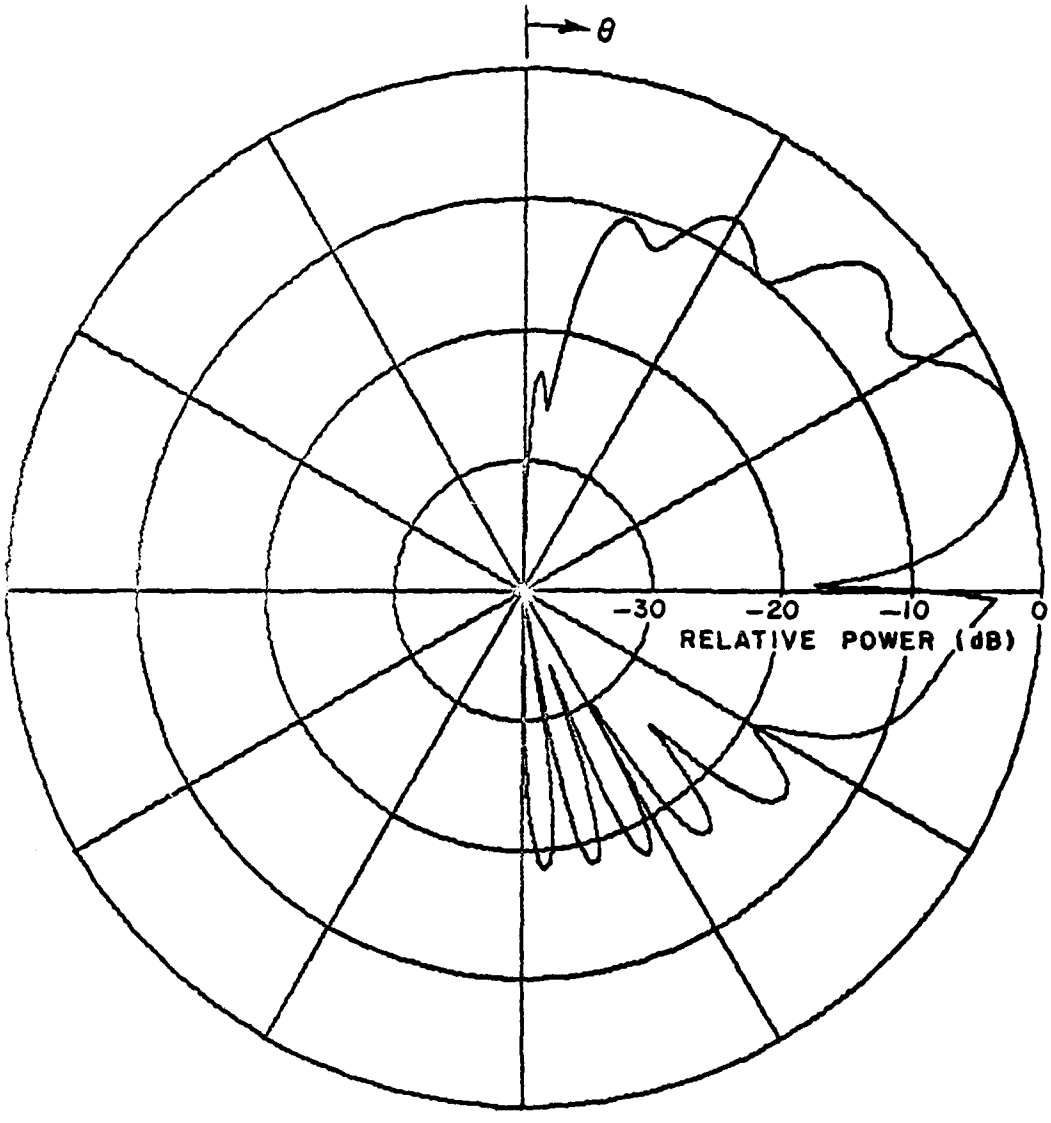


Fig. 43. Radiation pattern of a short monopole on a square plate A=4λ without corner diffraction taken in the plane φ=45°.

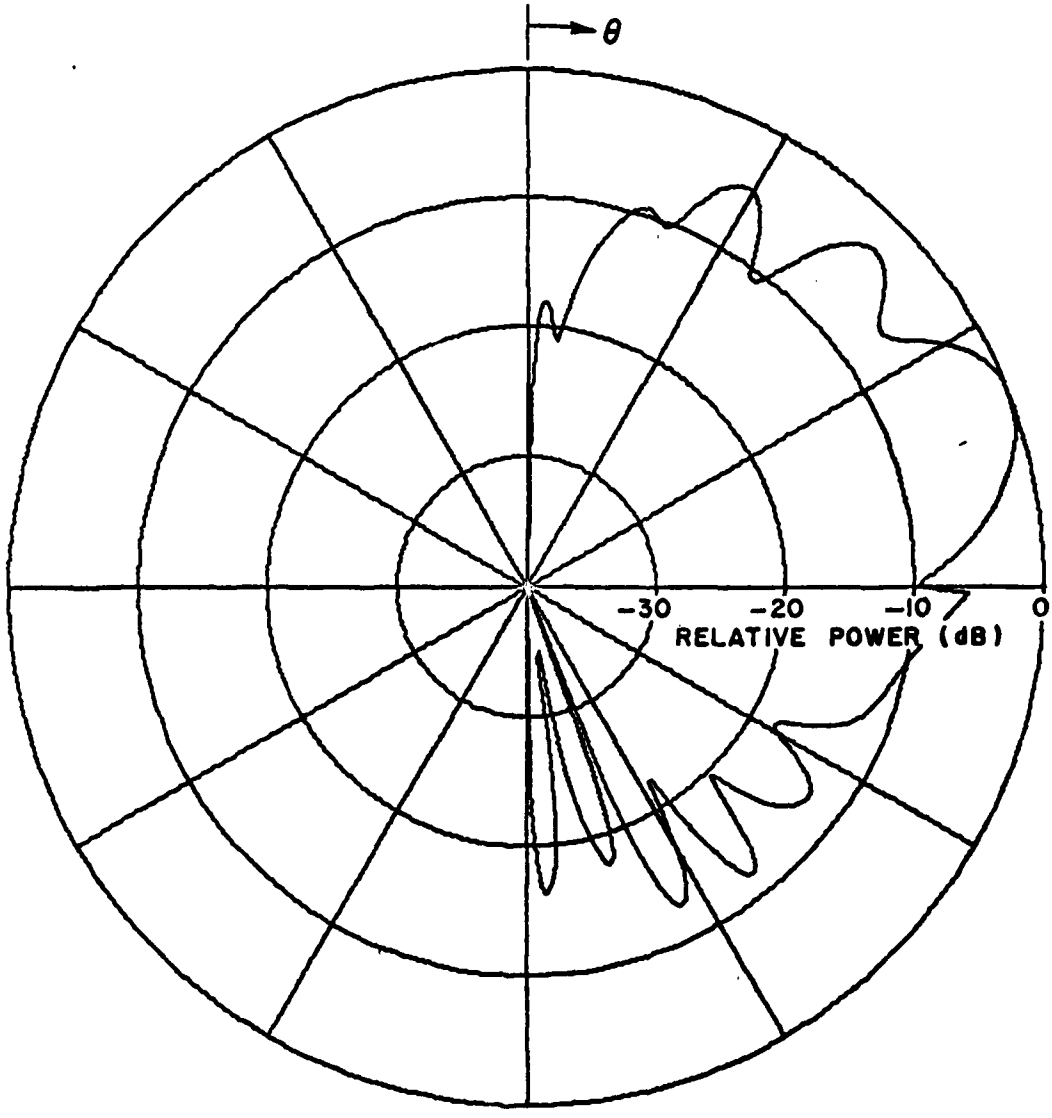


Fig. 44. Radiation pattern of a short monopole on a square plate A=4λ with rounded corners B=1λ taken in the plane $\phi$=45°.

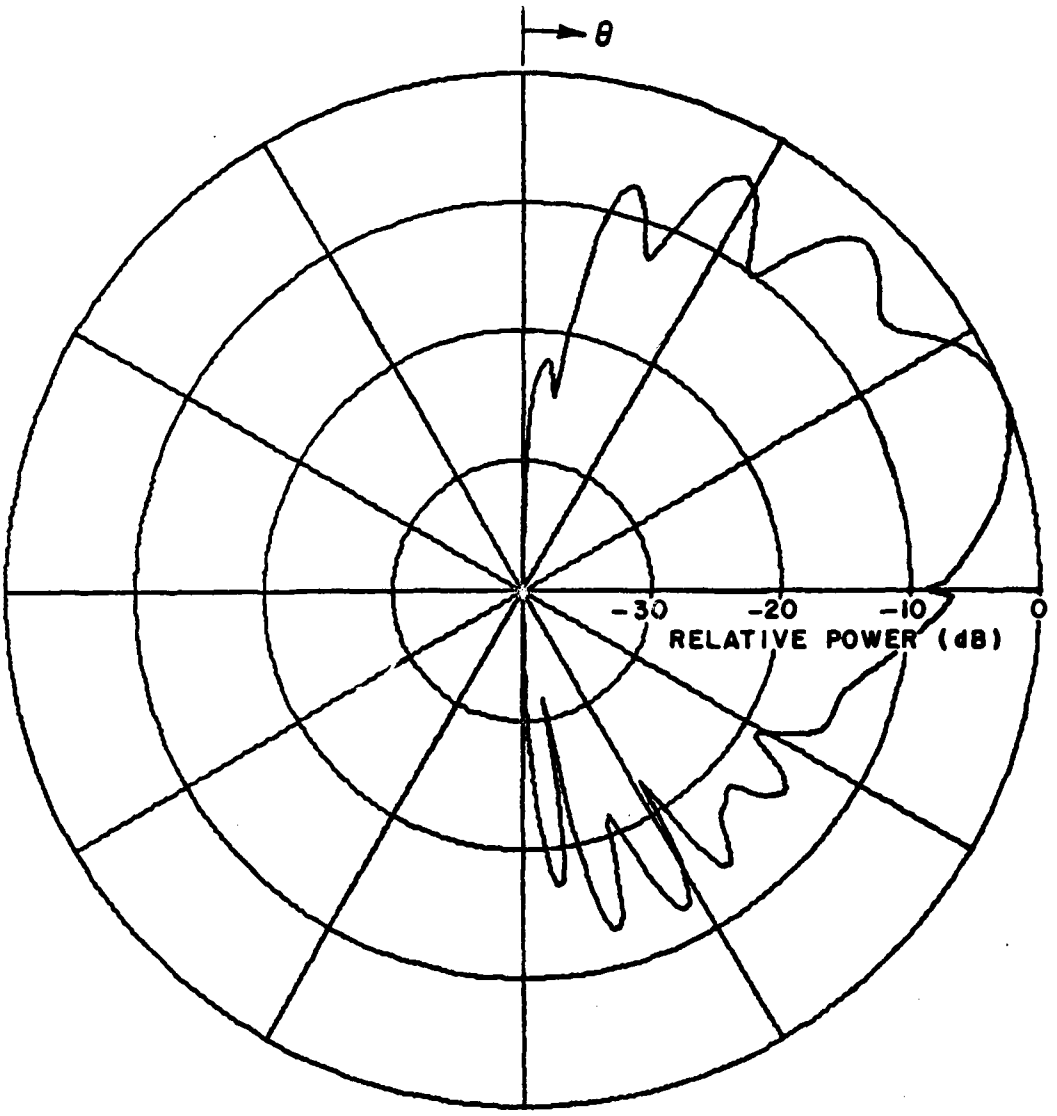


Fig. 45. Radiation pattern of a short monopole on a square plate A=4λ with rounded corners B=2λ taken in the plane $\phi$=45°.

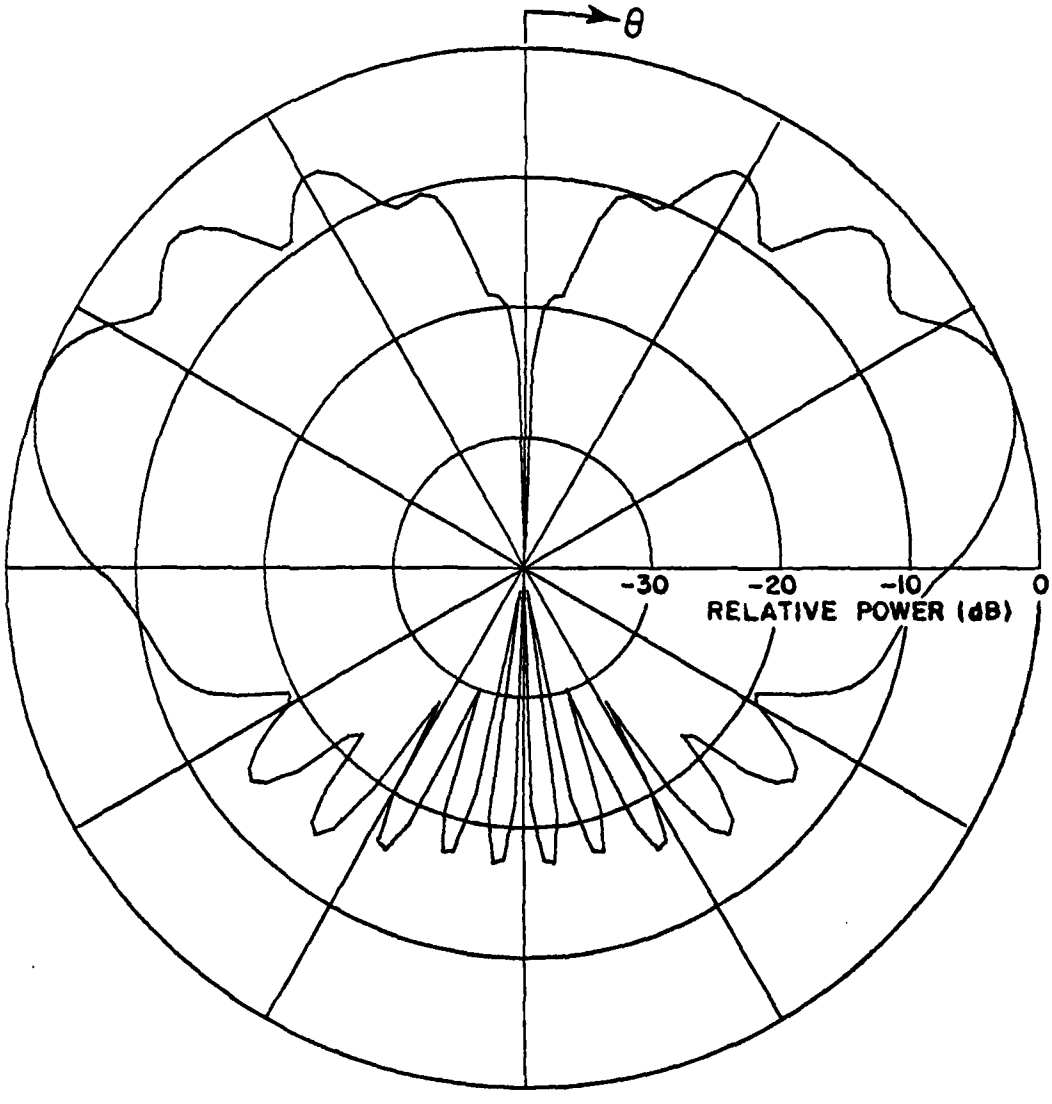


Fig. 46. Radiation pattern of a short monopole on a square plate A=4λ with corner diffraction coefficient taken in the plane φ=45°.

The slight discontinuity present is probably due to the lack of double diffraction in the solution. This method, however, does not give a direct comparison of results since the solutions represent slightly different problems due to the rounded corners. Furthermore, this method is more time consuming because of the need to integrate the equivalent currents for each observation angle as opposed to the numerically efficient GTD diffraction coefficient method. Such a diffraction coefficient was sought and has been recently developed at the ElectroScience Laboratory. It is based on the equivalent current concept above, but now the current is integrated asymptotically in terms of a stationary phase point near an end point. The stationary phase point is simply the point of diffraction along an infinite edge; whereas, the end point is simply the corner. This gives an additional Fresnel Integral which modifies the original diffracted field to make it continuous. The pattern for a short monopole on a square plate $8\lambda$ on a side, as shown in Fig. 42a, was calculated at $\phi=45°$ using this new GTD corner diffraction coefficient and is shown in Fig. 46. This diffraction coefficient should prove to be very effective in modelling wing-mounted antennas as well as any other problem invovling finite plate geometries.

From the Phase I study of a systematic design of a wing-mounted antenna system it may be concluded that the bent plate model is helpful in determining an optimum location for the array design; however, it is evident from the above results that improvements are needed in the aircraft modelling techniques for wing-mounted antennas. Phase II was directed toward solving the problems encountered in Phase I.

## IV. FINITE ELLIPTIC CYLINDER MODEL

Phase II of this study has been directed toward the improvement of our numerical aircraft modelling techniques for analyzing wing mounted antenna systems. Phase I had shown that higher order diffraction terms are needed when modelling wing mounted antennas than had previously been used. It also pointed out the need to model the fuselage of an aircraft with a more complex shape than a flat plate model for antennas that might strongly illuminate the fuselage. The high frequency solution for the scattered fields from a finite elliptic cylinder has been developed for this purpose. This shape can also be used to model external stores and engines for antennas mounted below the wings. This means that the numerical model of an aircraft pursued in this analysis will consist of a large finite elliptic cylinder representing the fuselage with flat or bent plate wings, horizontal and vertical stabilizers, and smaller flat plates or finite elliptical cylinders that represent engines and/or external stores as illustrated in Fig. 47.

The finite elliptic cylinder solution requires the use of a newly developed transition region solution for determination of the fields at the shadow boundary of the incident and reflected rays of an antenna near the surface [2]. The determination of the geometrical optics reflected fields also becomes more complex because the curved surface is present. In fact, the determination of the simple reflection point on the surface of the elliptic

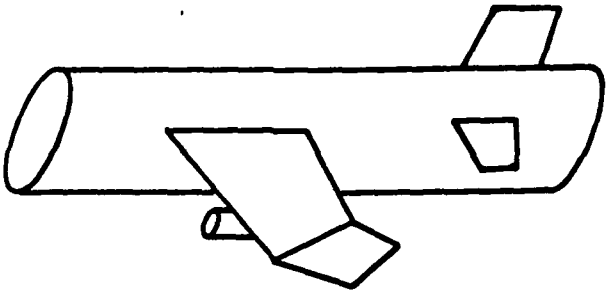

Fig. 47. Illustration of aircraft model for antennas mounted on the wings.

cylinder requires the solution of a sixth-order polynomial. This polynomial may be solved by using standard numerical techniques; however, this is very time consumming since this must be done for every visible observation direction.

To increase the computation efficiency, an approximate method for finding reflection points off of the elliptic cylinder from a fixed source has been derived. This incremental method has been developed based on the idea that if the observation direction changes only slightly, the reflection point will change only slightly. A linearlization of the reflection point equations is achieved using a first-order Taylor series expansion. This solution has been shown to be at least an order of magnitude faster than the polynomial solution and within desired numerical accuracy. There is one drawback in that the incremental method needs a known starting point.

In addition, in order to handle the curved edges at the ends of the finite cylinder, the curved edge diffraction coefficients are needed. In some cases a caustic term from the end caps can appear. The use of the equivalent current concept in these regions is under investigation.

The roll plane radiation pattern for a small electric dipole mounted parallel to the axis of a cylinder is shown in Fig. 48. This pattern was calculated using the newly developed solutions.

The attachment of flat plates to represent the wings of the aircraft was started in a systematic manner. The presence of the various plates and cylinders in close proximity requires the inclusion of many higher-order interactions in the solution. Obviously, it is not practical to include all of the multiple interactions between the various scattering structures. Therefore, a systematic development of the solution is followed in order to include only those terms that are of engineering importance. As mentioned before the GTD method is well suited to this method since errors appear as discontinuities in the resulting patterns. The diffraction mechanisms associated with these discontinuities may be added or neglected as deemed necessary for the problem. For this problem second-order interaction terms appear to be significant.

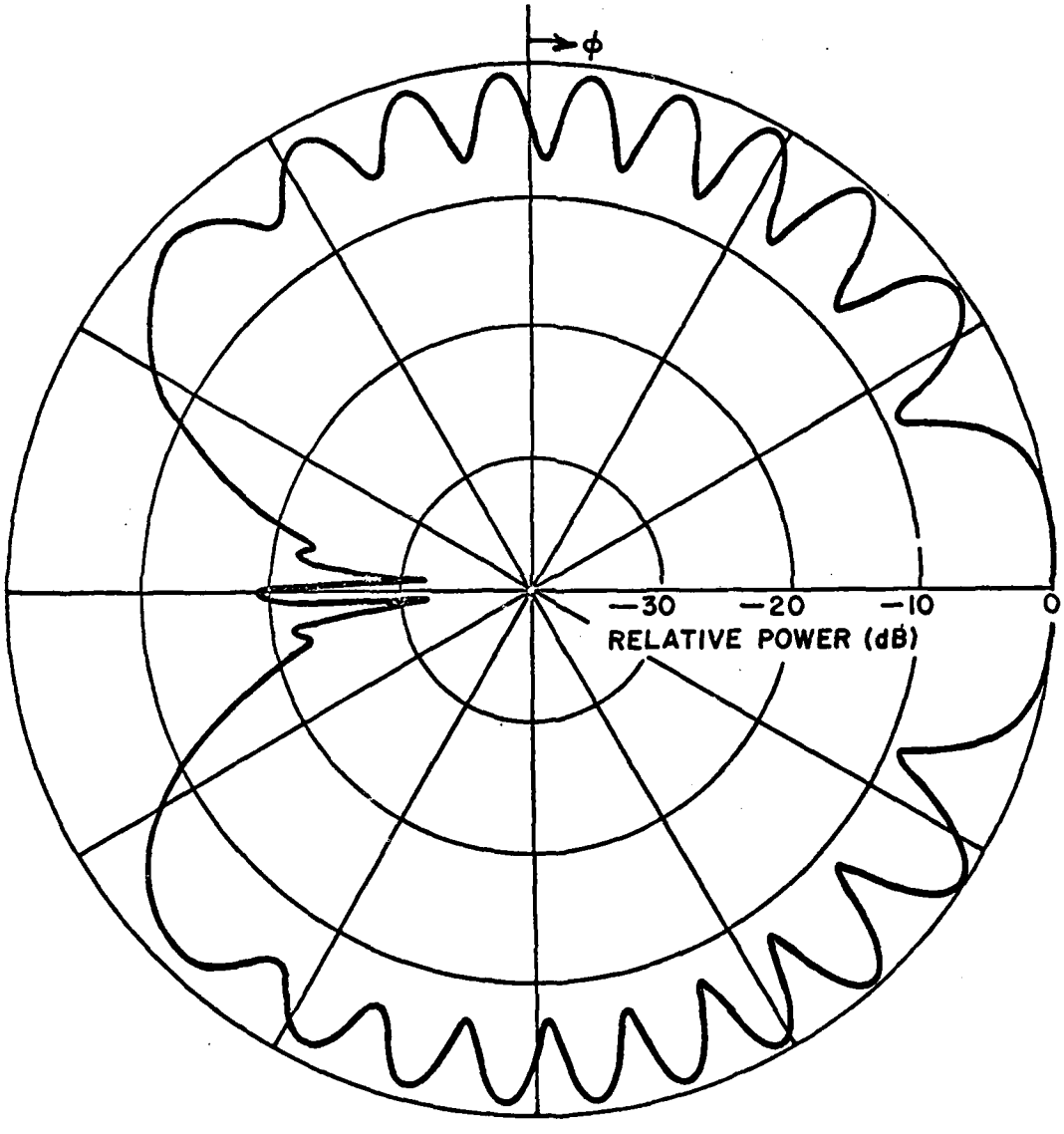


Fig. 48. Roll plane radiation pattern of small electric dipole mounted parallel to z-axis.

The preliminary model consisted of one flat plate attached to the finite elliptic cylinder in x-y plane as shown in Fig. 49. This is studied to test the shadowing routines and the first-order diffraction mechanisms. The elevation plane radiation pattern for an infinitesimal slot mounted parallel to the y-axis is shown in Fig. 50. Note that the cylinder has little affect in this plane. The roll plane radiation pattern for the same source is shown in Fig. 51. The need for a corner diffracted term is shown by the discontinuity in the right side of the backlobe of the pattern. The result using the recently developed corner diffraction term is shown as the dotted line in the same figure. The discontinuity in the left side of the backlobe is due to shadowing by the cylinder. The roll plane radiation pattern for an infinitesimal slot located parallel to the z-axis is shown in Fig. 52. Note the lack of a reflected-diffracted term in the $\phi$=90° direction is shown by the large discontinuity. Even for this simple structure, the interactions between the different parts are large and immediately apparent if neglected.

The reflected-diffracted term, which is a reflection off the elliptic cylinder then a diffraction off of a plate edge, was shown above to be important. Also, it can be shown that a diffracted-reflected terms can be important in certain cases. The determination of either of the ray paths associated with these mechanisms turns out to be very complicated if not impossible to solve exactly. This is due to the nonlinear nature of the equations governing their trajectories. However, the incremental method discussed above has proved to be a very effective method of solving these equations in an approximate way. The determination of a starting location for the reflection-diffraction point problem has been accomplished by the derivation of a sixth-order polynomial solution for the reflection off an elliptic cylinder with both a near field source and observation point. The benefit of including this term can be seen by the dotted line in Fig. 52.

The multiple interactions between the plates themselves are pretty well understood from the previous flat plate model. However, as was found at that time, the double diffraction terms between edges can be important. A method for determining the important double diffracted terms (that is, the terms from edges that lie in the same plane) has been developed and has shown promise in some cases.

To test the validity of the approximation involved in the finite elliptic cylinder aircraft model, an experimental model that resembled the computer model was built and tested. The model consisted of a finite cylinder with two plates as shown in the insert of Fig. 53. The comparison of calculated and measured results for the roll plane radiation pattern is shown in Fig. 53. The overall agreement between the two results is very good, even down to some of the small backlobes. The disagreement at $\phi$=-90° is due to the lack of a diffracted-reflected-diffracted term. This third-order term is hard to calculate and seems to be important only in this particular pattern cut. Therefore, it does not seem necessary to include this term at this time. The discontinuity at $\phi$=120° is due to some higher order terms involving the second wing which were not included. Again, these do not appear to be of engineering significance so they will be left out of the solution.

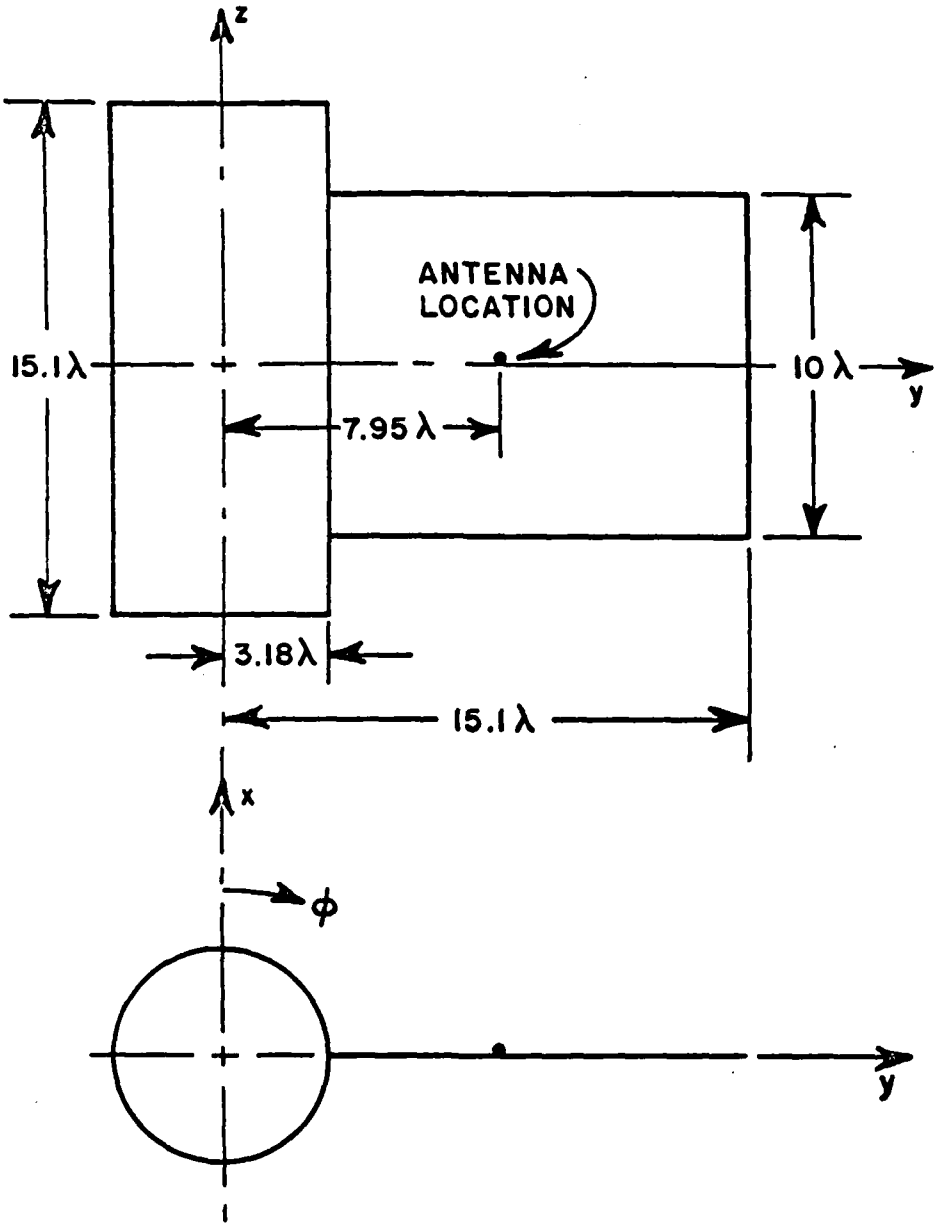


Fig. 49. Geometry of a preliminary model.

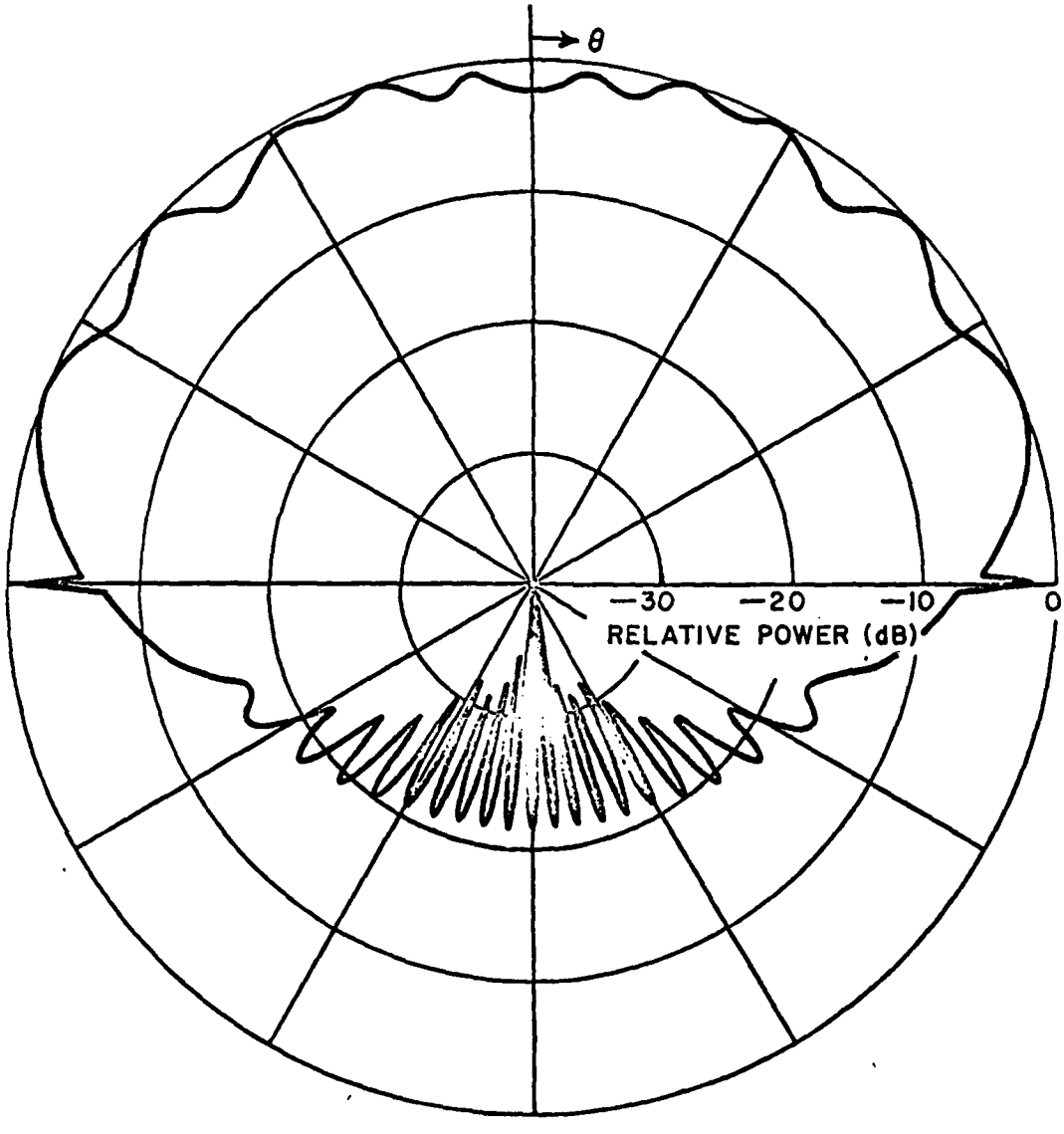


Fig. 50. Elevation plane radiation pattern of small slot mounted parallel to y-axis on plate.

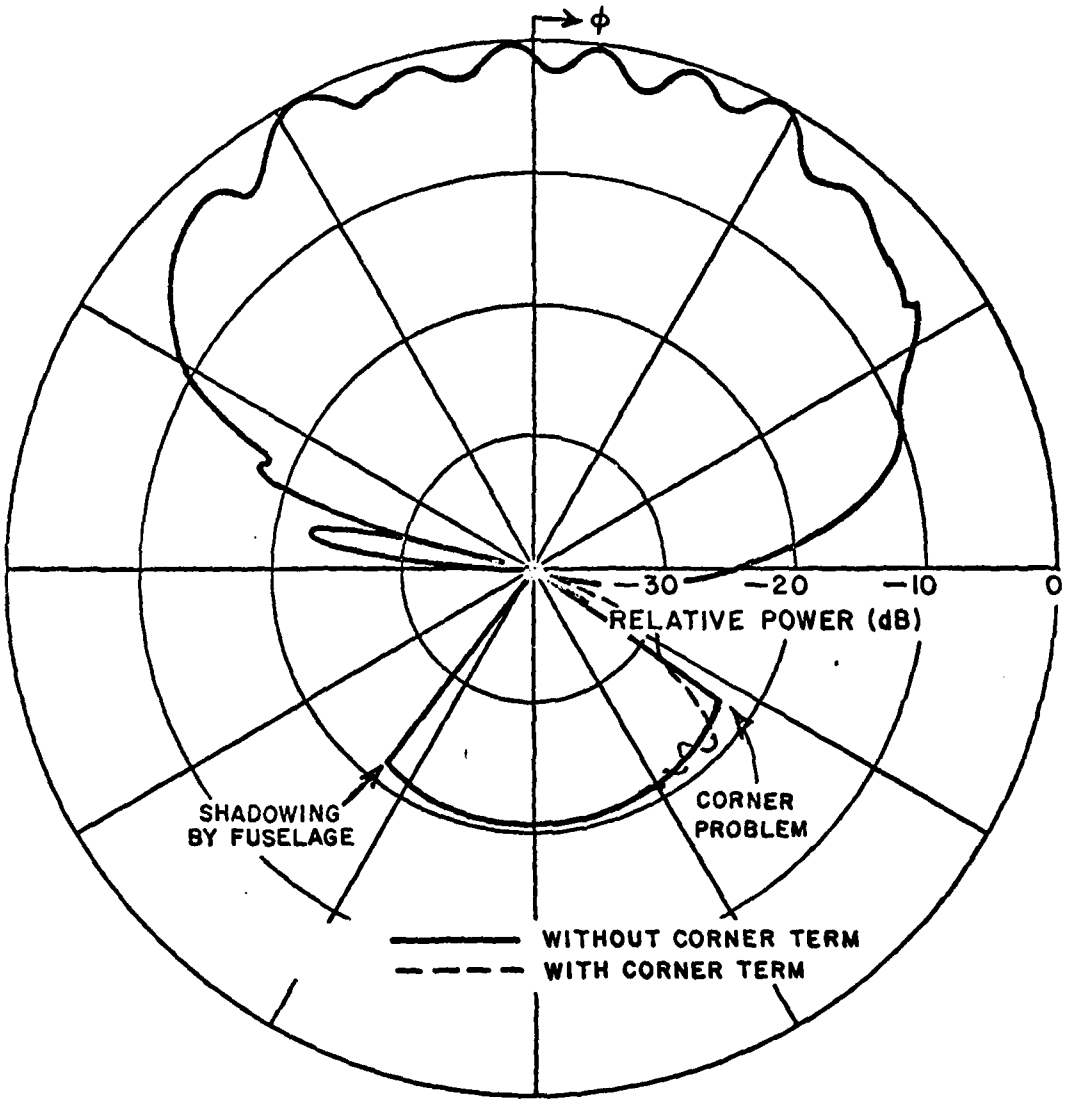


Fig. 51. Roll plane radiation pattern of small slot mounted parallel to y-axis on plate, showing effect of corner diffraction term.

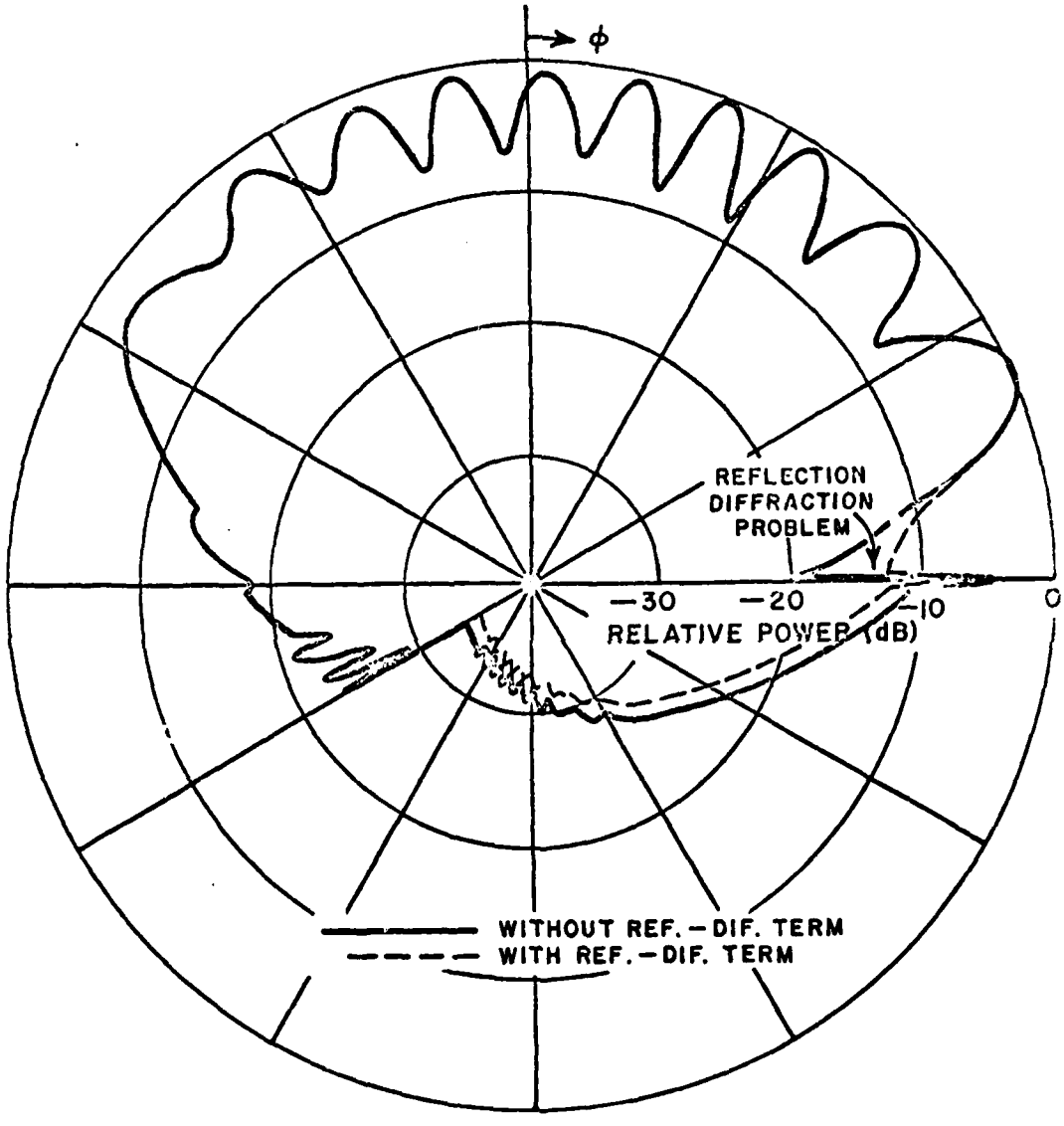


Fig. 52. Roll plane radiation pattern of small slot mounted parallel to z-axis on plate, showing effect of reflected-diffracted term.

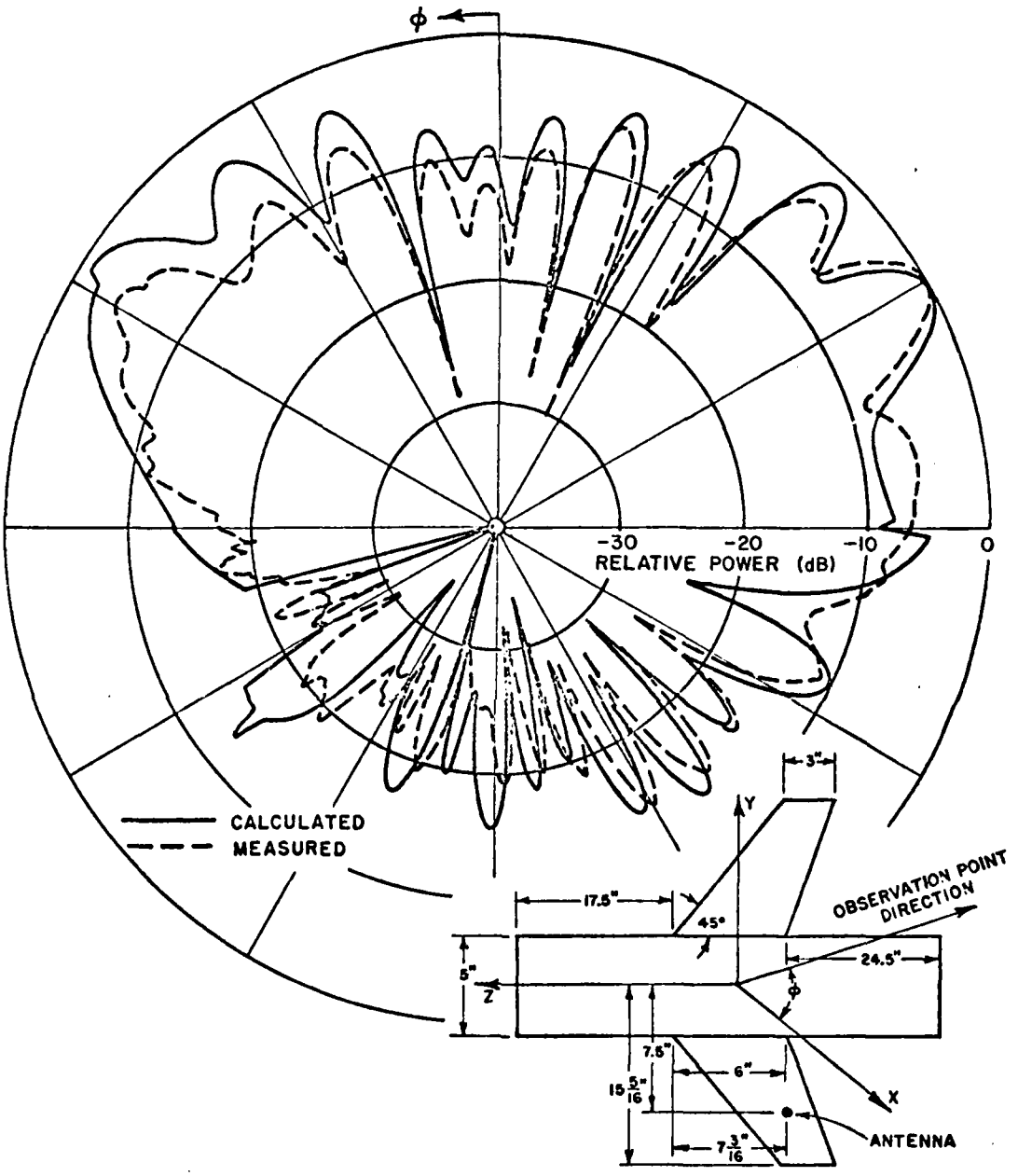


Fig. 53. Comparison of measured and calculated results for the roll plane radiation pattern of a single aircraft model with a short monopole mounted on its wing.

The finite elliptic cylinder aircraft model has been used to compute some of the patterns that were measured at NWC using a single slot on the wing of the F-4 scale model discussed in Section III. The geometry for this computer model is shown in Fig. 54. The dimensions for the model are listed in Table I. A comparison of the measured and calculated radiation patterns for the main beam elevation plane for the slot at location #2 (refer to Fig. 36) is shown in Fig. 55. These results can be compared with the bent plate results in Fig. 37. Note that the ripple level due to the reflections off the fuselage has been improved. The same problem of comparing near field measured results and far field computed results still exist in all of these patterns. However, a few of the results for the various cases will be shown here for illustrative purposes. In each case, Figs. 35a-d shows the aircraft pattern orientation. The polarization of the patterns was computed in the same way the measurements were taken, that is, with the probe aligned with the antenna to give the dominant polarization.

The comparison of the main beam elevation plane of an antenna at location #4 is shown in Fig. 56. This result can be compared with Fig. 37. The elevation plane results for an antenna oriented facing straight to the aft of the aircraft at location #5 is shown in Fig. 57. This result can be compared with Fig. 39. The main roll plane (Fig. 35c) pattern for an antenna at location #2 is shown in Fig. 58. The elevation plane (Fig. 35b) pattern for location #2 is shown in Fig. 59 and it's roll plane (Fig. 35d) pattern is shown in Fig. 60.

In all of the above results, the major characteristics of the patterns do show some agreement. In this model the horizontal stabilizers were shown to have little effect so they are neglected for this problem. Some higher interaction terms do show the lack of their presence in some of the various cuts; however, it was not deemed feasible to include them at this time. Further study is needed on some of these terms in the future. Even with the comparison difficulties, the results are felt to have great promise in aiding an antenna designer in the design of a specific antenna system. It is expected that more compatible results can be obtained in the future.

In the design of aircraft systems, the system designers need to be concerned with the pattern characteristics of an antenna in all space surrounding the aircraft. This is best accomplished by displaying the volumetric pattern for the given antenna design. The volumetric patterns for the 2-element optimum array designed in Sections II and III and placed at location #2 has been computed using the finite elliptic cylinder aircraft model. The geometry is shown in Fig. 61. The directive gain has been computed using the following equation,

$$G_d(\theta,\phi) = \frac{4\pi r^2(|E_\theta|^2 + |E_\phi|^2)}{P_r\sqrt{\mu_o/\epsilon_o}}$$

TABLE I

DIMENSIONS FOR FINITE ELLIPTIC CYLINDER MODEL OF F-4

All Dimensions in Inches

## Fuselage

$A_{Top} = 87.$
$A_{Bottom} = 19.$
$B = 54.$
$Z_{End\ Cap\ Nose} = -420.,\ \theta_{Nose} = 90°$
$Z_{End\ Cap\ Tail} = 26.6,\ \theta_{Tail} = 20°$

## Wings

### Plate 1

| Corner | X | Y | Z |
|---|---|---|---|
| 1 | 0. | 54. | -228. |
| 2 | 0. | 166.2 | - 86.2 |
| 3 | 0. | 166.2 | 32.8 |
| 4 | 0. | 54. | 0. |

### Plate 2

| Corner | X | Y | Z |
|---|---|---|---|
| 1 | 0. | 166.2 | -86.2 |
| 2 | 0. | 166.2 | -96.2 |
| 3 | 19.7 | 228.7 | 0. |
| 4 | 19.7 | 228.7 | 53.4 |
| 5 | 0. | 166.2 | 32.8 |

TABLE I cont.

Plate 3

| Corner | X | Y | Z |
|---|---|---|---|
| 1 | 0. | -54. | 0. |
| 2 | 0. | -166.2 | 32.8 |
| 3 | 0. | -166.2 | -86.2 |
| 4 | 0. | -54. | -228. |

Plate 4

| Corner | X | Y | Z |
|---|---|---|---|
| 1 | 0. | -166.2 | 32.8 |
| 2 | 19.7 | -228.7 | 53.4 |
| 3 | 19.7 | -228.7 | 0. |
| 4 | 0. | -166.2 | -96.2 |
| 5 | 0. | -166.2 | -86.2 |

Plate 5

| Corner | X | Y | Z |
|---|---|---|---|
| 1 | 87. | 0. | 205.1 |
| 2 | 149.9 | 0. | 197.3 |
| 3 | 154.3 | 0. | 153.1 |
| 4 | 87. | 0. | 11.4 |

Source Coordinates

| Source | X | Y | Z |
|---|---|---|---|
| 1 | 5.14 | 182.5 | -36.91 |
| 2 | 0.00001 | 149.1 | -73.6 |
| 3 | 0.00001 | 126.3 | -102.5 |
| 4 | 0.00001 | 150.3 | -4.6 |
| 5 | 0.00001 | 111. | -74.1 |

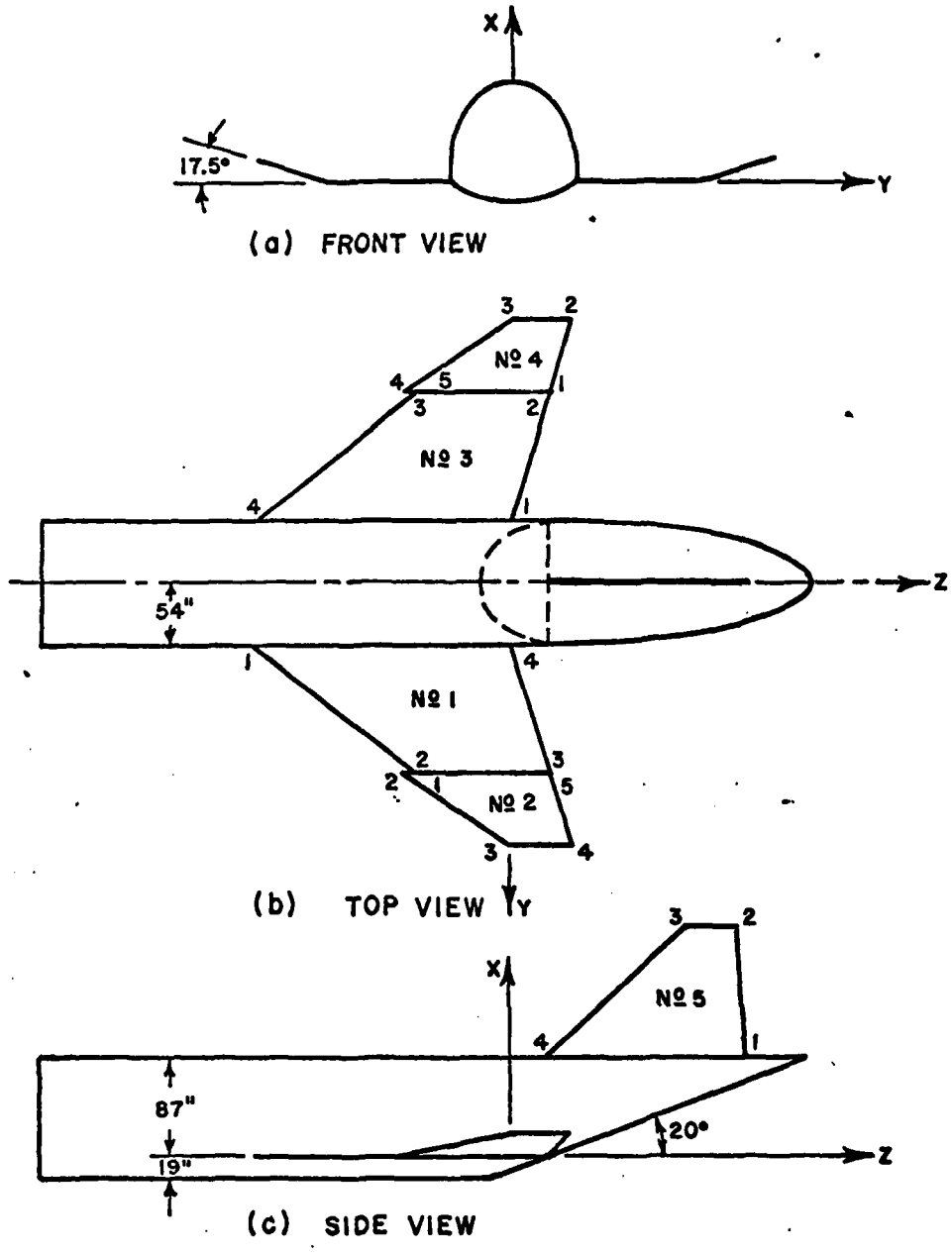


Fig. 54. Illustration of geometry of F-4 aircraft model used in finite elliptic cylinder model.

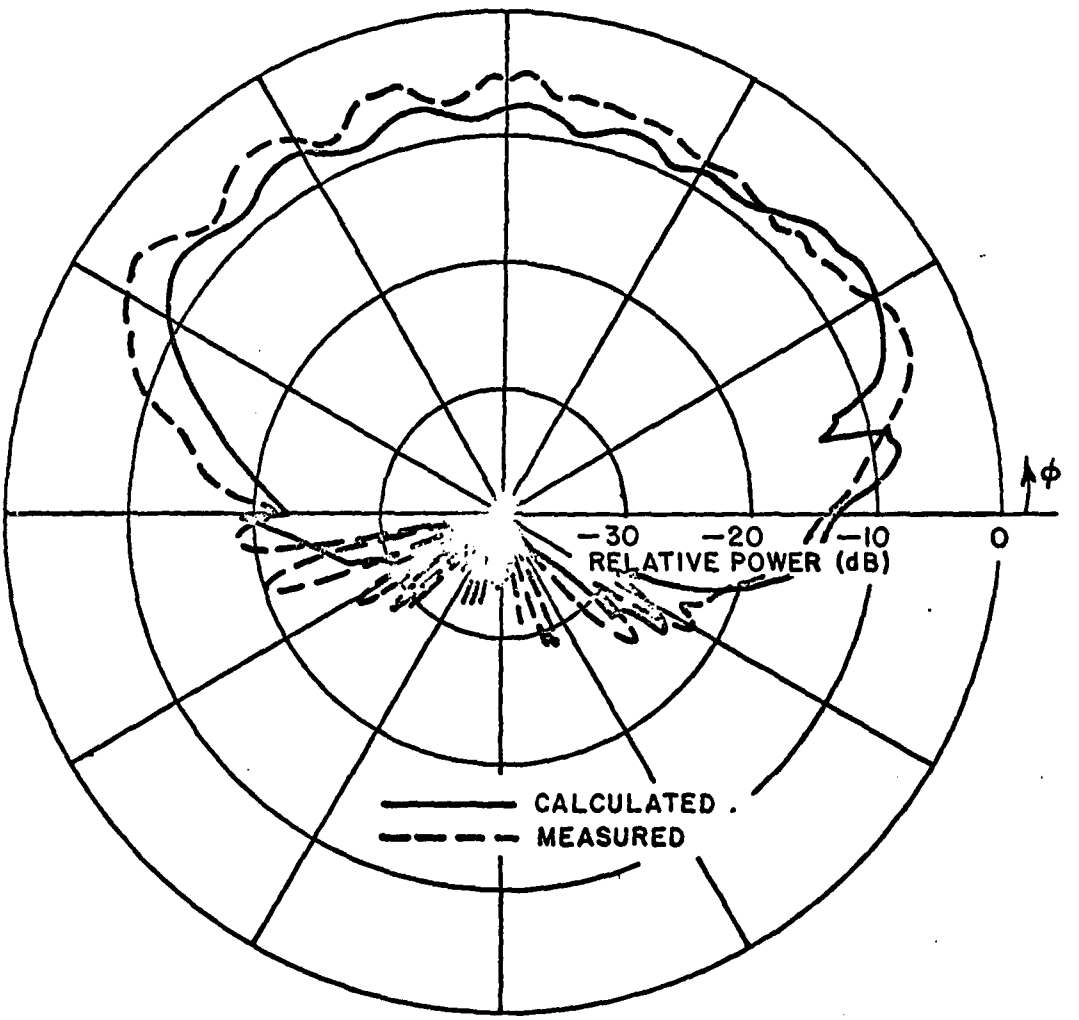


Fig. 55. Comparison of NWC measured results on an F-4 model with the finite elliptic cylinder model results of main beam elevation plane radiation pattern for an antenna location #2.

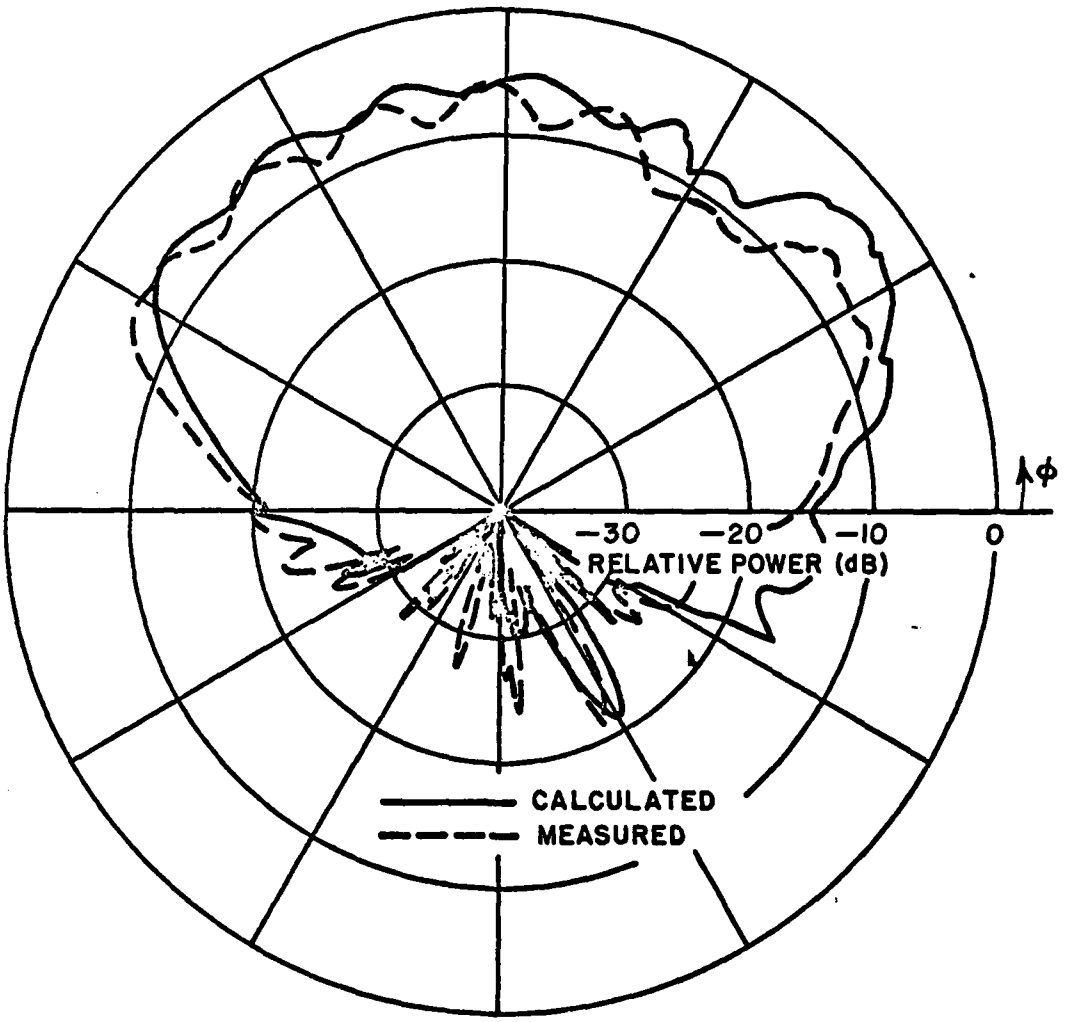


Fig. 56. Comparison of measured and calculated results of main beam elevation plane pattern for antenna location #4.

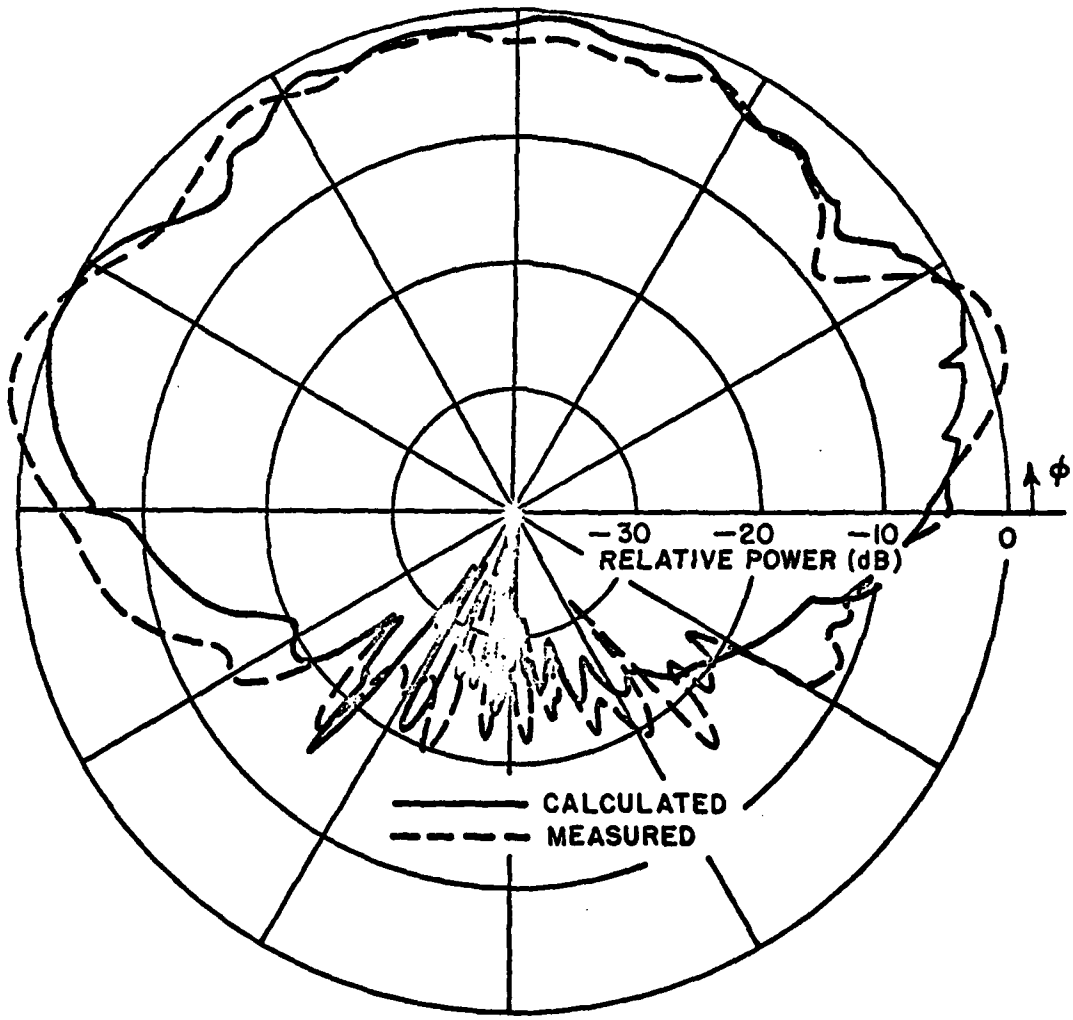


Fig. 57. Comparison of measured and calculated results of elevation plane pattern for antenna location #5 with array pointed straight aft of aircraft.

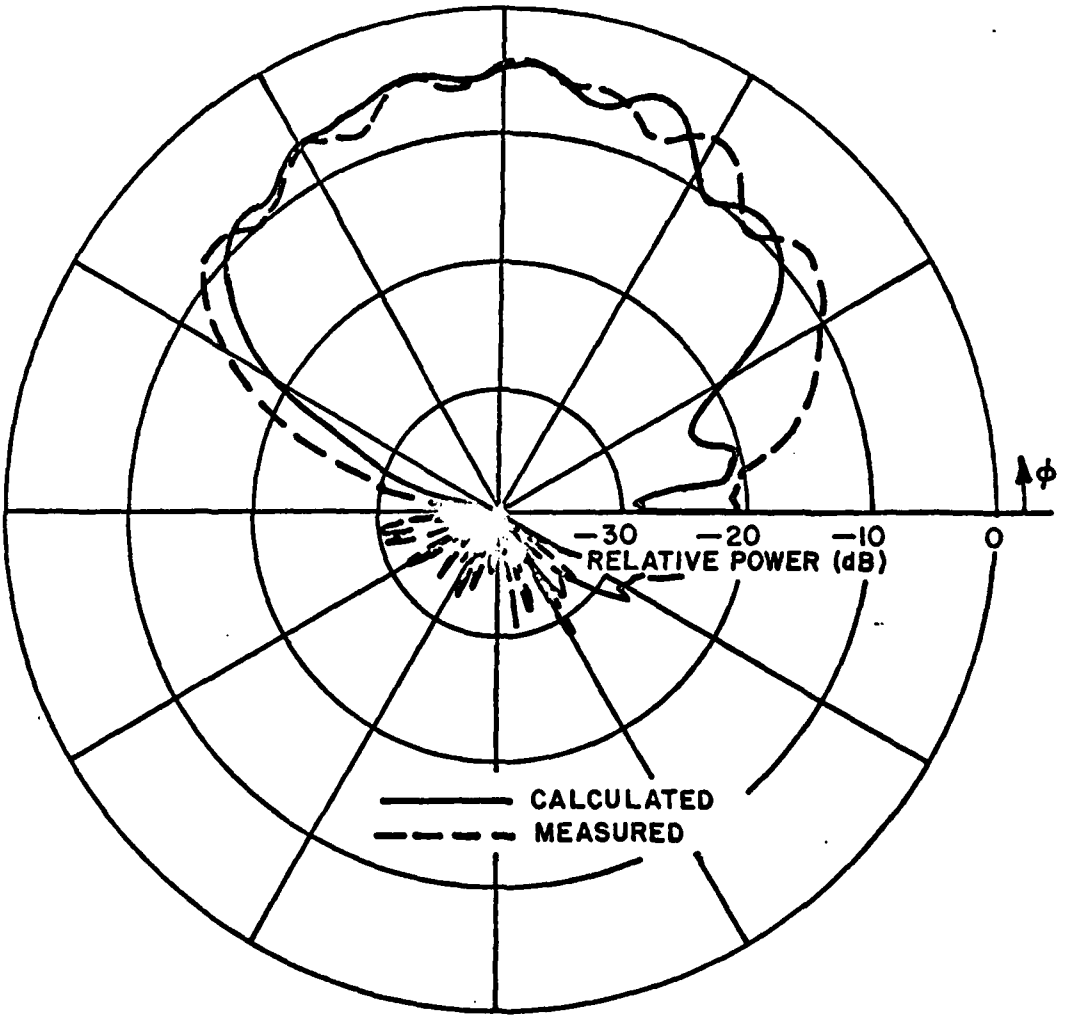


Fig. 58. Comparison of measured and calculated results of main roll plane pattern for antenna location #2.

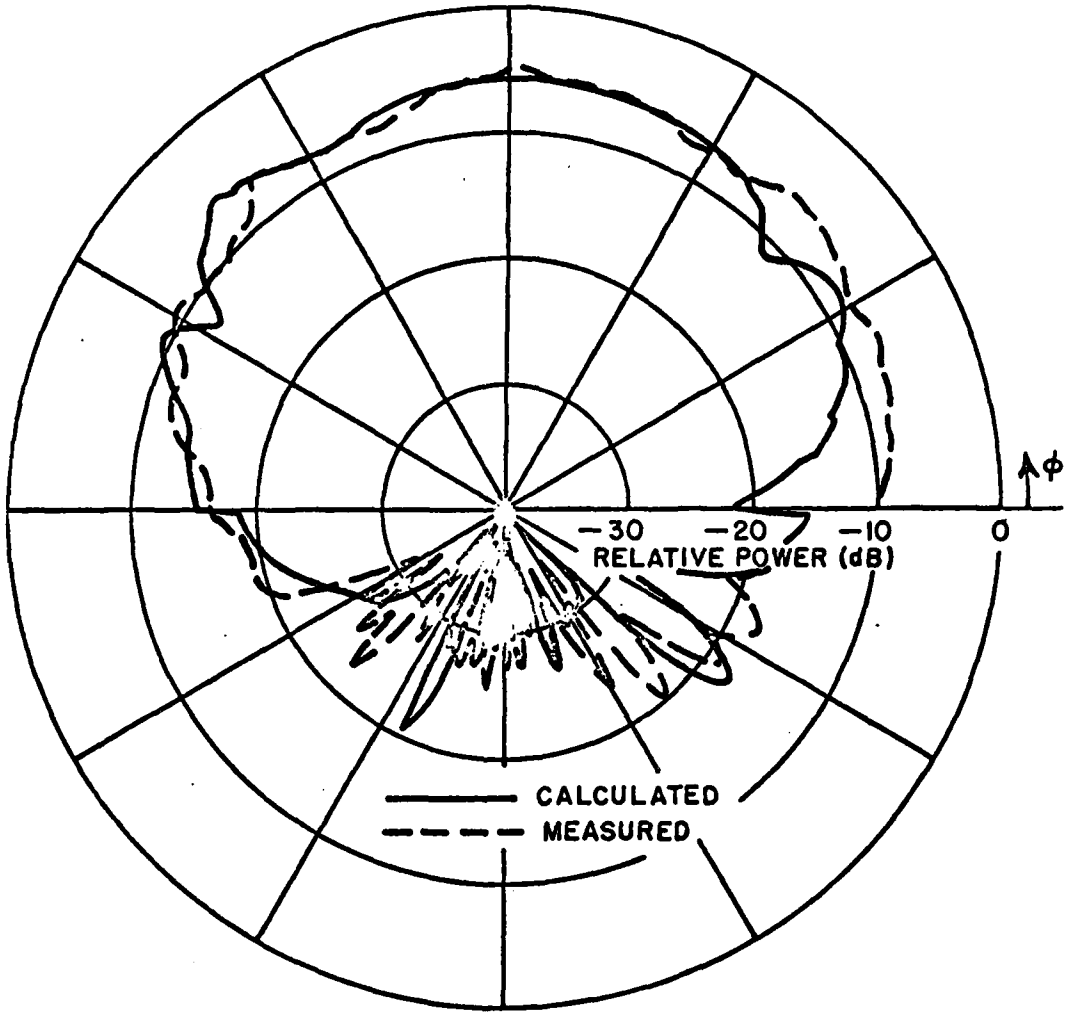


Fig. 59. Comparison of measured and calculated results of elevation plane pattern for antenna location #2.

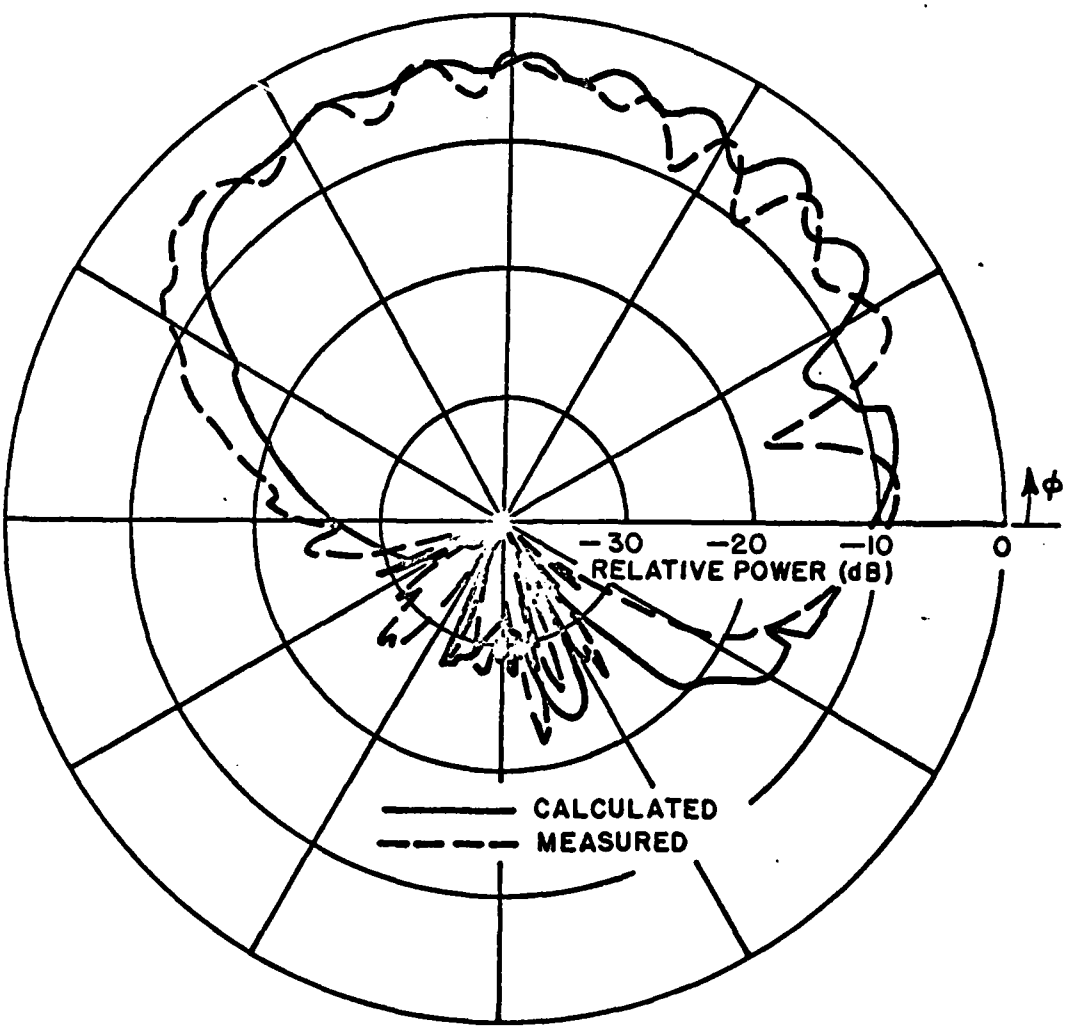


Fig. 60. Comparison of measured and calculated results of roll plane pattern for antenna location #2.

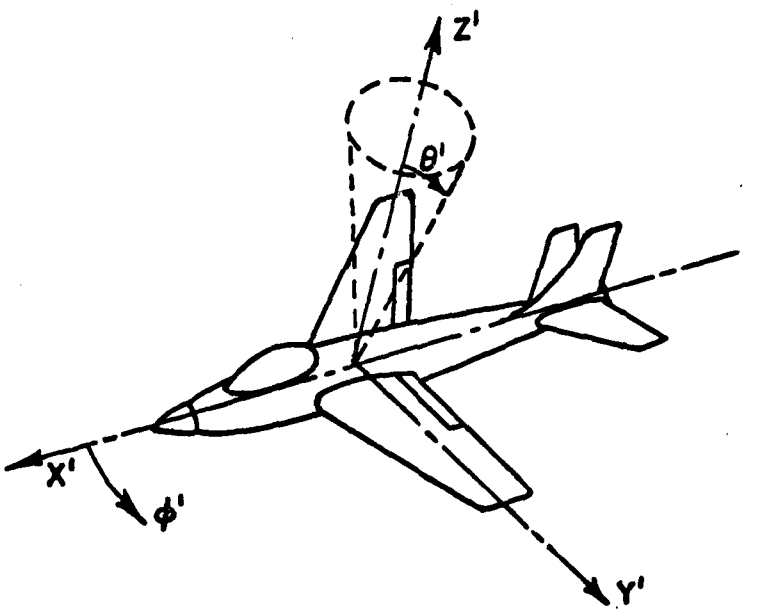


Fig. 61. Coordinate system used for volumetric patterns.

where for this case $P_r$ is the time average power radiated by an antenna in free space, and in the far field

$$P_r = \frac{1}{\sqrt{\mu_o/\epsilon_o}} \iint_S r^2(|E_\theta|^2 + |E_\phi|^2)\sin\theta \; d\theta \; d\phi \; . \qquad [3]$$

The directivity, which is the maximum directive gain, for the antenna system in place on the aircraft was determined to be 12.34 dB. The directive gain is plotted in Fig. 62 using different colors to represent the different gain levels. For example, all sections of space that have a gain of between 12.34 dB and 5 dB are pink in color. Each color change after that represents a 5 dB window showing regions of further reduction in the gain.

Note that the volumetric pattern shows that the 2-element array design does a realistic job of approximating the desired objectives. Consequently, our two-element array design should provide the quadrant coverage necessary for application on the wing of an F-4 aircraft. To further illustrate the antenna system performance the directive gain elevation patterns normalized to 0 dB have been plotted in thirty degree steps from 0° to 150° and are shown in Figs. 63a-f. The main beam elevation plane pattern at angle 135° is shown in Fig. 64.

## V. CONCLUSIONS AND RECOMMENDATIONS FOR FUTURE STUDIES

### A. Conclusions

Under the present contract a systematic design of a wing-mounted antenna system by means of a numerical solution has been undertaken. Our principal objective has been to determine the number and placement of elements and their excitation when mounted on the wing surfaces with constraints on the frequency, element type, aircraft, stores and sector of coverage as specified by NWC. Mainly, the program has been concerned with the design of an antenna system to give full hemispheric coverage in the aft region of an aircraft for quadrant detection at UHF. The project was carried out in two phases.

The first phase was concerned with the design of the antenna array and with the placement of the array on an F-4 wing. Classical array analysis was used to find the element spacing, scan angle, and distribution in order to obtain the desired pattern shape above the wing. In this case for a two-element array, the best pattern is obtained with the elements spaced a quarter-wavelength apart and phased to scan end-fire.

The element type chosen for this application is a cavity backed slot capable of being excited by the first three waveguide modes. Because of limitations imposed on spacing due to the cavity, a two element array

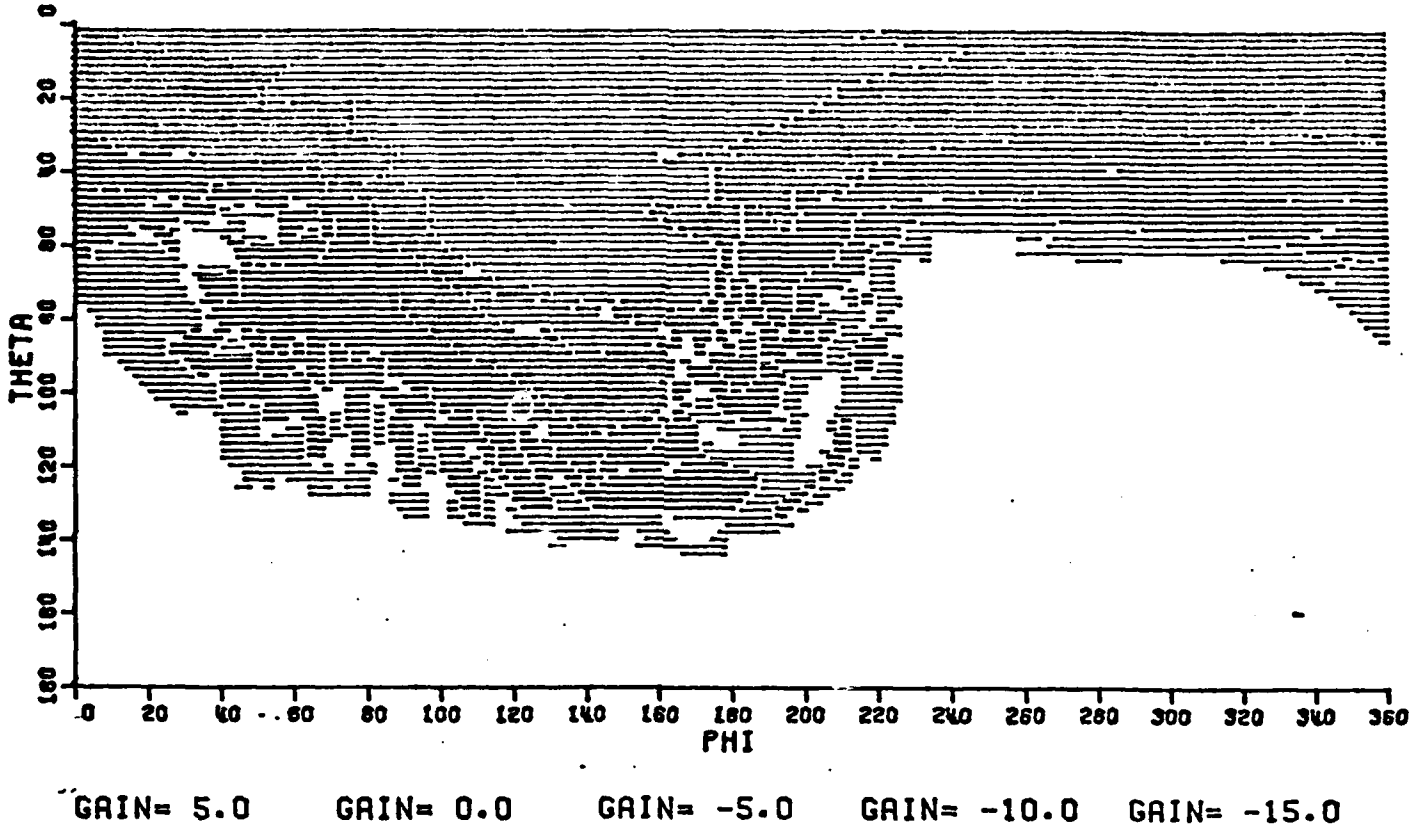


Fig. 62. Volumetric directive gain results with various gain levels represented in different colors for optimum two element array design mounted on the wing of an F-4 model.

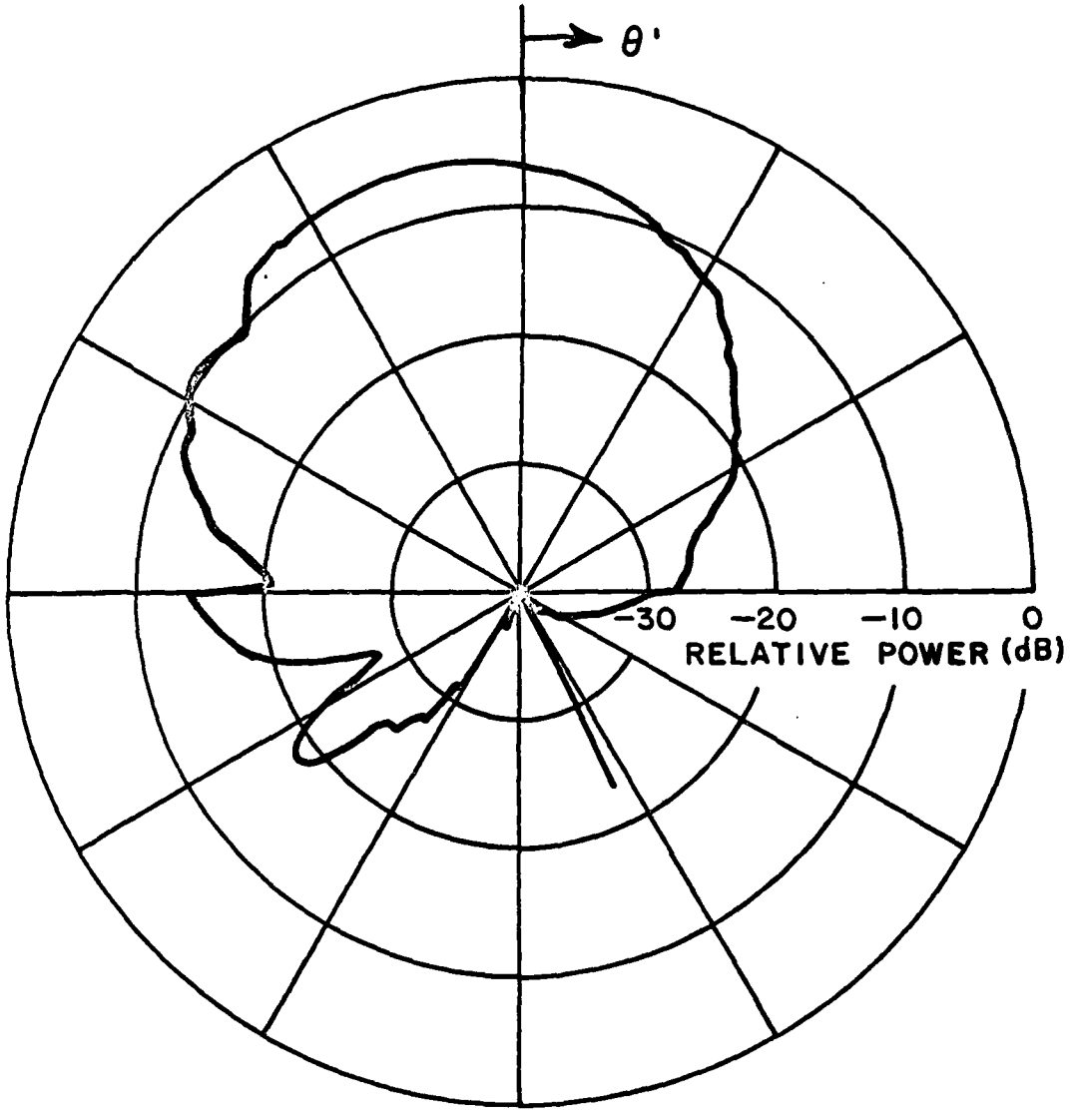


Fig. 63a. Directive gain pattern for optimum two-element array design mounted on the wing of an F-4 model in the $\phi' = 0°$ plane.

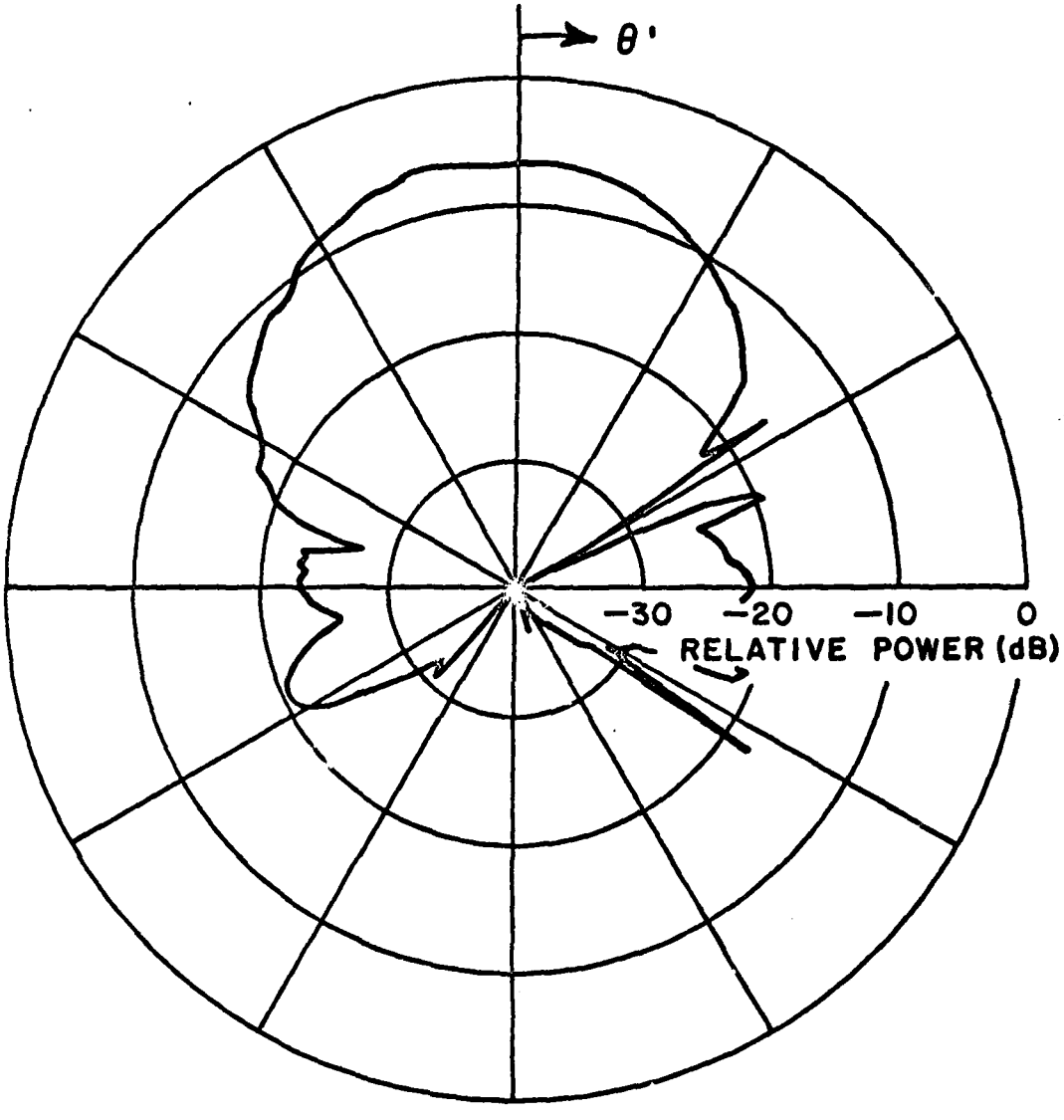


Fig. 63b. Directive gain pattern for optimum two-element array design mounted on the wing of an F-4 model in the $\phi' = 30°$ plane.

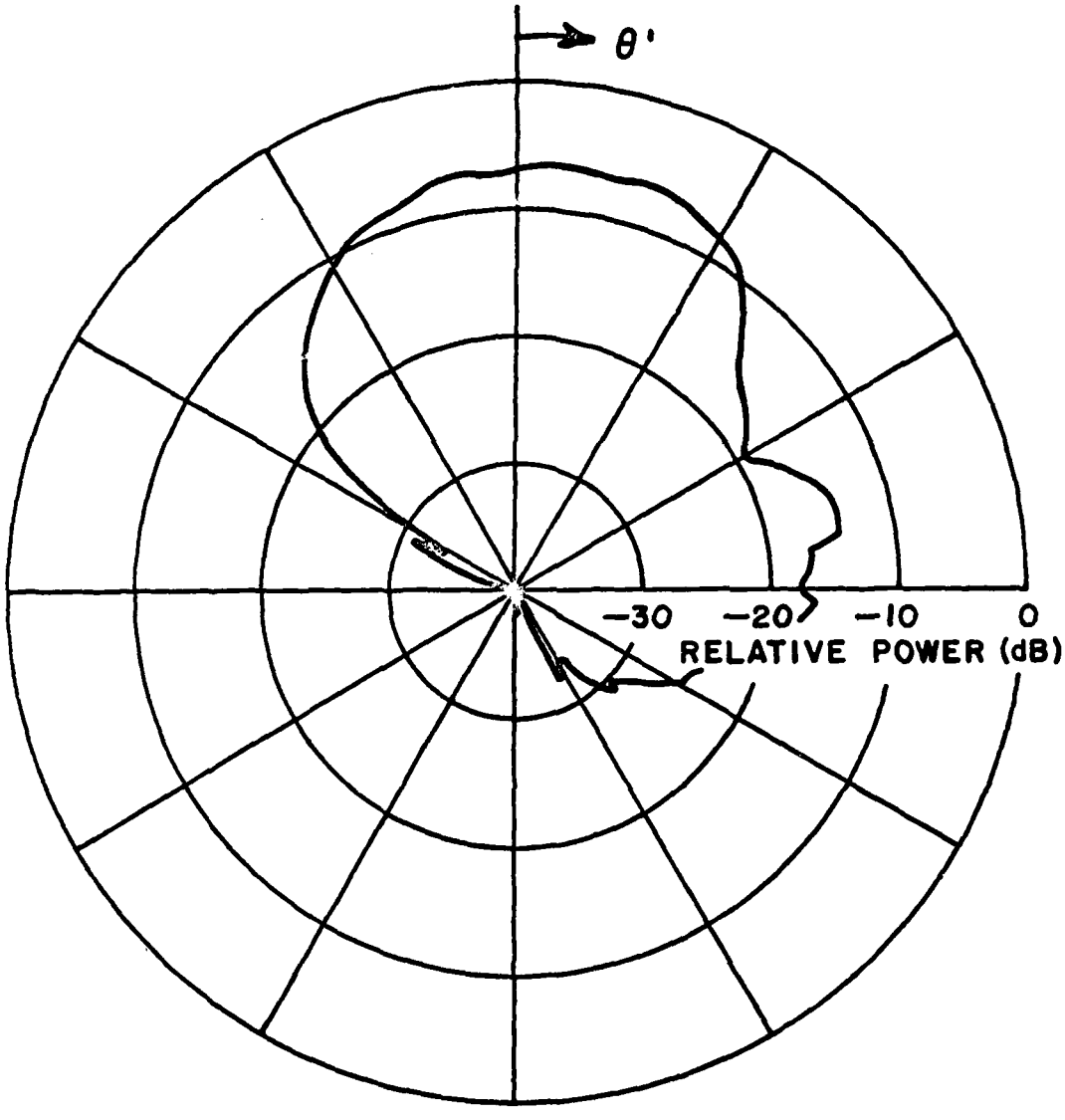


Fig. 63c. Directive gain pattern for optimum two-element array design mounted on the wing of an F-4 model in the $\phi' = 60°$ plane.

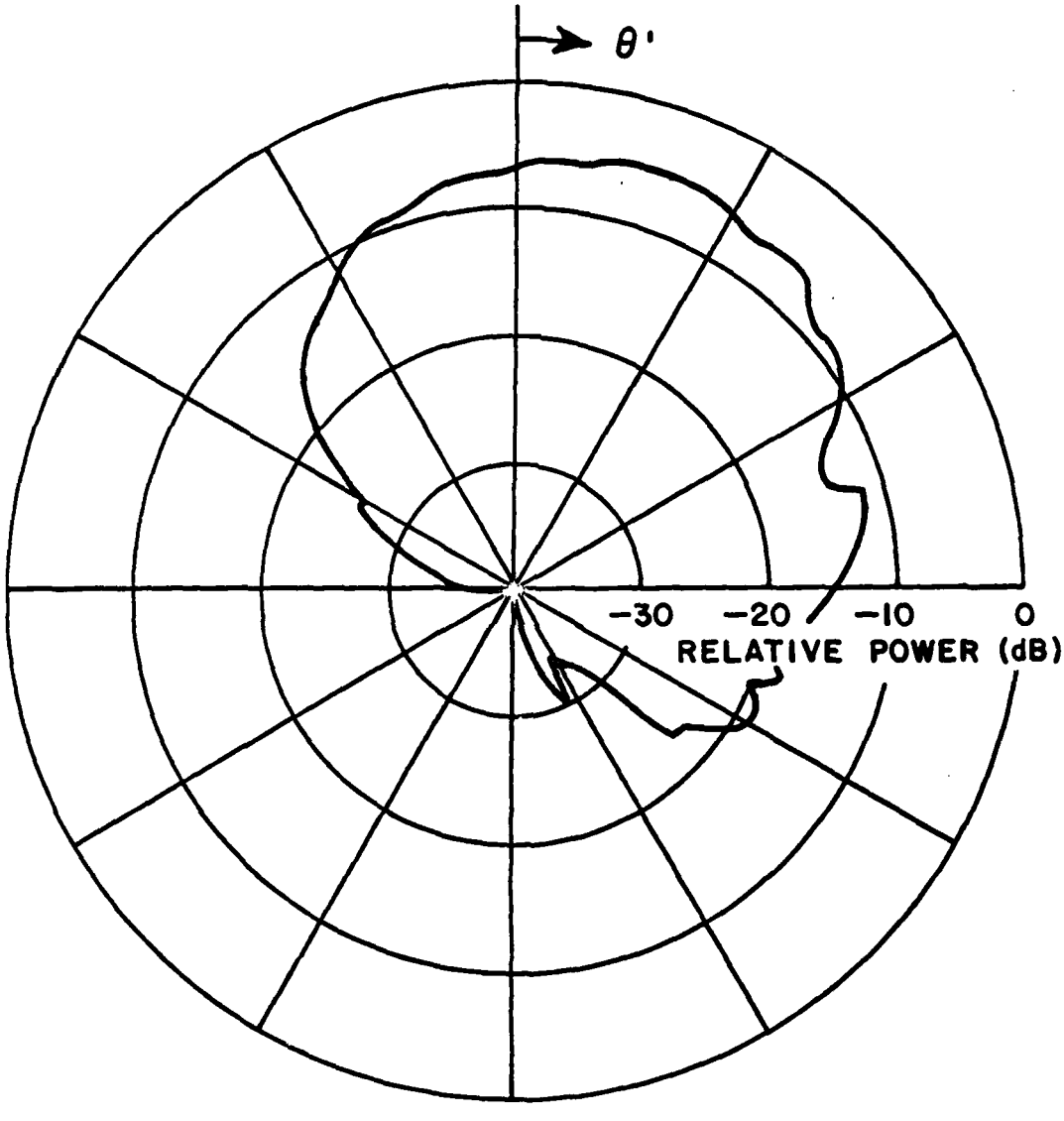


Fig. 63d. Directive gain pattern for optimum two-element array design mounted on the wing of an F-4 model in the $\phi' = 90°$ plane.

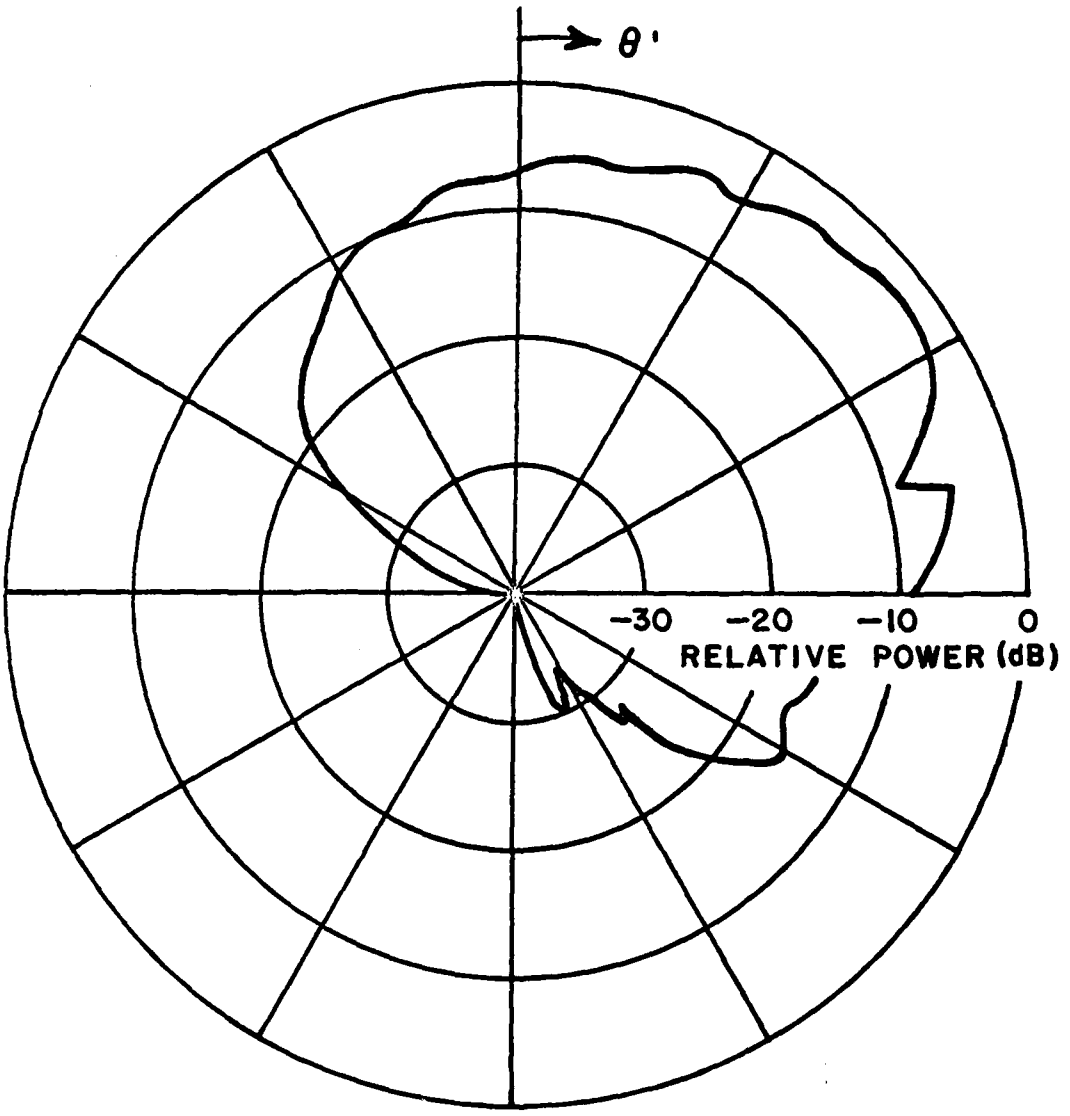


Fig. 63d. Directive gain pattern for optimum two-element array design mounted on the wing of an F-4 model in the $\phi' = 120°$ plane.

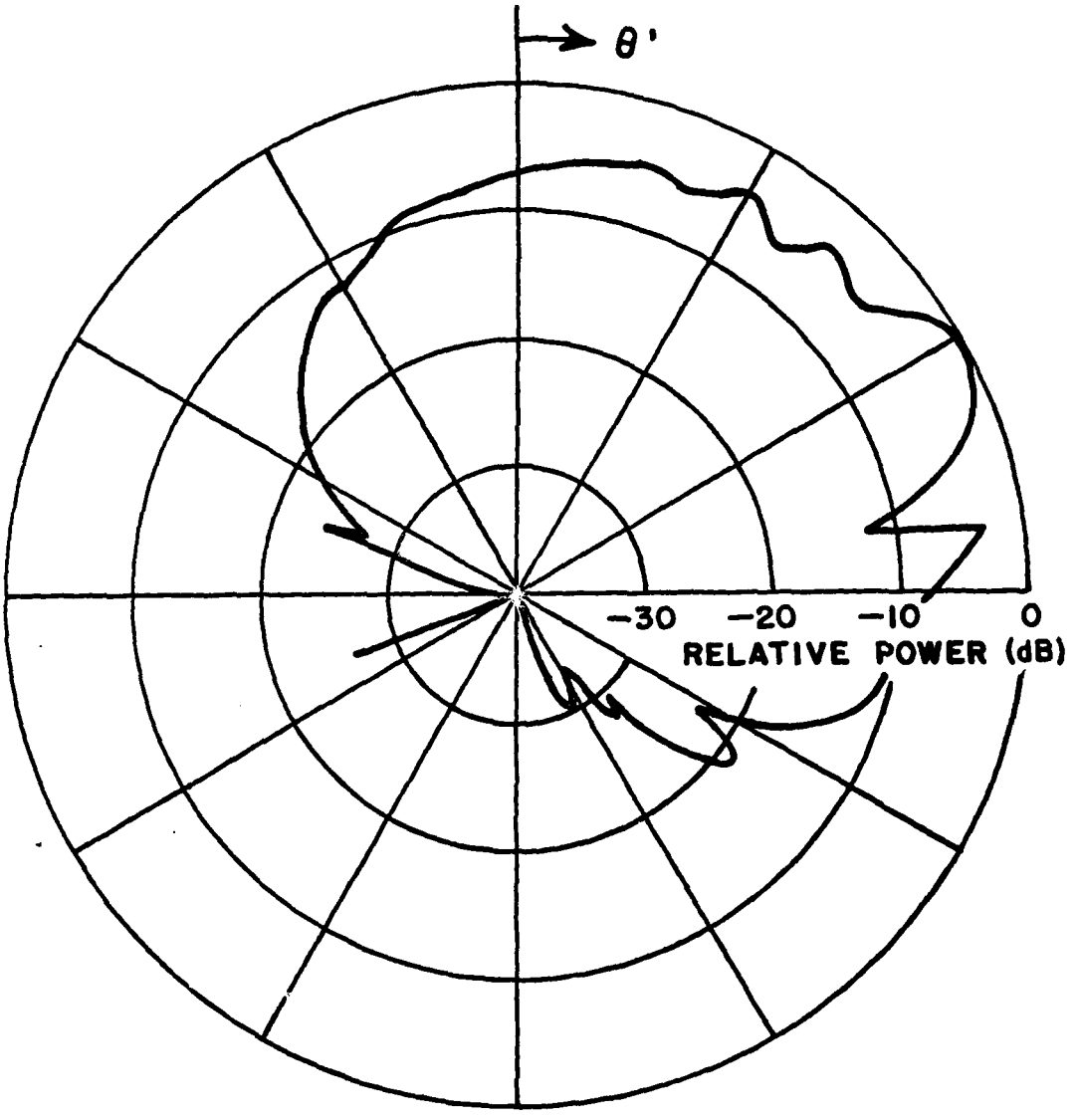


Fig. 63f. Directive gain pattern for optimum two-element array design mounted on the wing of an F-4 model in the $\phi' = 150°$ plane.

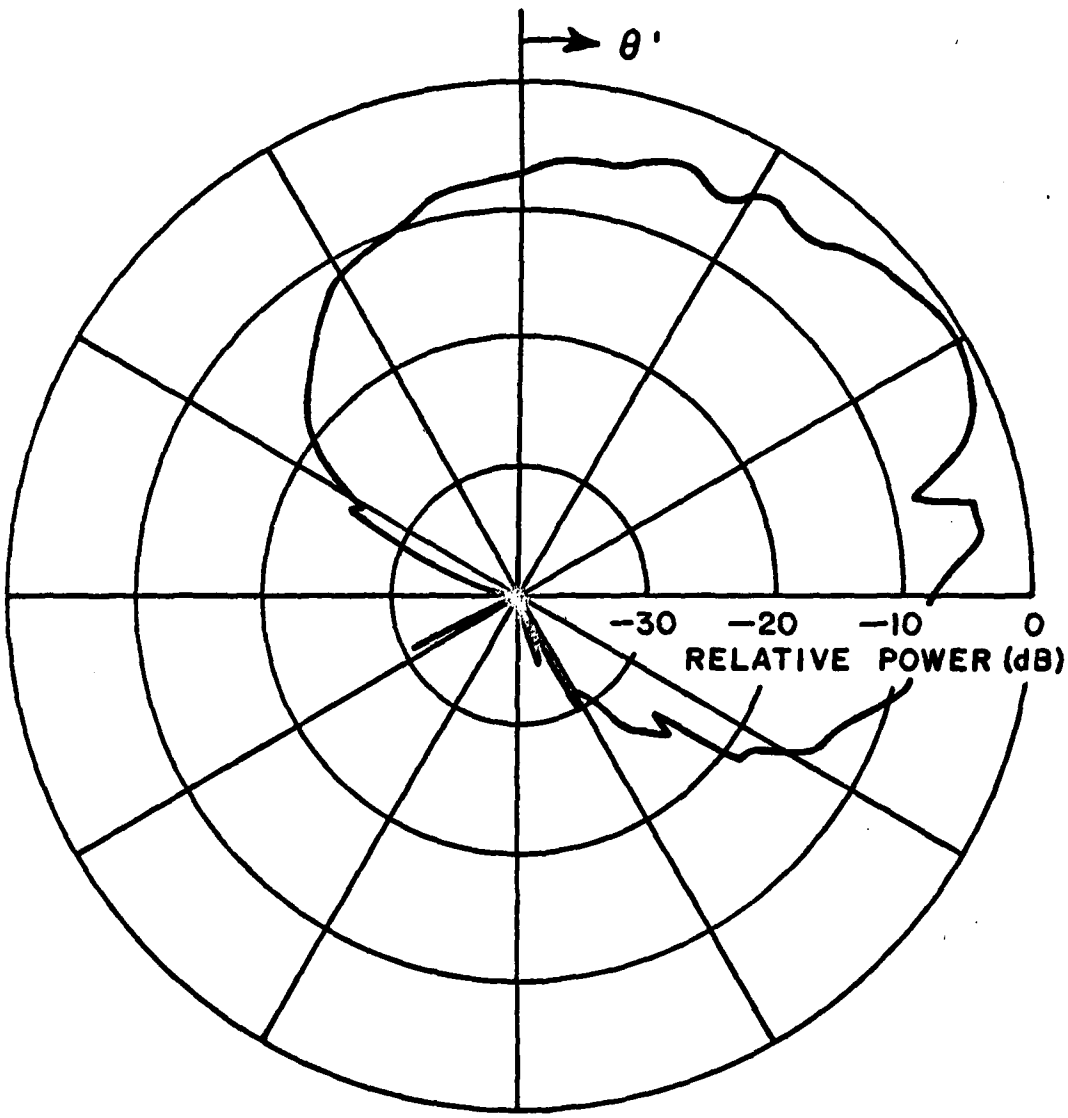


Fig. 64. Directive gain pattern in the main beam elevation plane $\phi' = 135°$.

appears best. To optimize the pattern in the azimuth plane, it was found that the cavity should be excited primarily with the first mode with a little of the third mode present.

A bent plate Geometrical Theory of Diffraction (GTD) computer program developed at the ElectroScience Laboratory (ESL) was initially used to best locate the antenna array on the wing of the F-4 aircraft. The computer-aided design techniques used can be applied to a wide variety of other aircraft as well. The bent plate model aids in determining the best orientation and position relative to the aircraft structure to give minimum scattering from the aircraft. The optimum pattern for this application is found when the array is aimed to the rear of the aircraft and at a 45° angle with respect to the axis of the fuselage. This places the maximum radiation direction in the center of the quadrant of interest. The array should be positioned away from the trailing edge of the wing to minimize the diffraction below the wing. The array should be placed close to the bend in the F-4 wing, however, to minimize the ripple in the pattern.

To test the validity of the approximations used in the bent plate model, measurements were conducted at the Naval Weapons Center (NWC) on a scale model of an F-4. The antenna was a single cavity backed slot mounted at five different locations. Radiation patterns were taken for four different pattern cuts. The measurements could not be made far enough away to eliminate near field effects for this aircraft, so that the far field calculated results and the near field measured results are not totally comparable. However, the comparison did point out that for antennas which strongly illuminate the fuselage, the flat plate model of the fuselage was not adequate.

The second phase of the contract was concerned with improvement in the numerical model of the aircraft. The new model consists of a finite elliptic cylinder to represent the fuselage and, if necessary, the stores and engines; whereas, flat plates are used to represent the wings, vertical and horizontal stablizers, wing flaps and stores. Measurements on a simple model which represented the structures that make up the theoretical model were taken and compared very well with calculated results in most regions of space. This tends to verify the approximations made in the model. The new calculated results compare more favorably with the NWC F-4 measurements, than did the results from the flat plate model; however, as before the results are not directly comparable.

Even though this new model is not fully developed, it appears to have a lot of potential as an aid to the antenna designer in designing wing mounted antenna systems. It is believed that this model will prove to be a versatile tool useful in designing many airborne antenna systems.

B. Recommendations

The present contract was concerned primarily with antennas mounted on the upper surfaces of the wings. The radiation pattern for an antenna mounted on the lower surface of a wing is affected by the presence of

stores and, in some aircraft, by the engines. The present contract has analyzed many of the separate mechanisms involved in the mathematical modelling of an antenna system below the wing; however, time did not permit the inclusion of these mechanisms into the model. It is proposed that these mechanisms be added to the model to increase its versatility. As these mechanisms are systematically added it will be necessary to continue to study the interaction between the parts of the structure (cylinder, flat plates, etc.) so that only the dominant diffraction terms are included.

The higher-order diffraction terms become more involved as the scattering structure becomes more complex. These terms will have to be analyzed and included as they become necessary. Further work should be done on some of the problem terms of the present contract such as the double diffraction term. The double diffraction term was studied during the present contract and proved to be useful in some applications. This term, however, did cause some additional problems in certain cases which could possibly be due to double diffraction corner effects.

With the capability in the model of mounting the antenna systems on the top or bottom of the wing structure, the representation for the fuselage should be further improved so that the model consists of a finite composite ellipse. This means that the fuselage would be composed of two half elliptic cylinders with the same radius in the common dimension but with different radii in their other dimension. This is illustrated in Fig. 54.

The scattering effects due to the presence of an endcap on a finite elliptic cylinder have been under investigation at the Electro-Science Laboratory. The presence of the elliptic end caps can produce caustics in certain regions. The problem has been circumvented by the use of the equivalent current method. If necessary, this method can be added to the fuselage model where needed. The equivalent current method is quite effective; however, it is time consuming numerically. A new GTD diffraction coefficient which is numerically efficient for the caustic effects due to the end cap would be very useful and should be considered as a worthwhile area of study in a future program.

As the finite elliptic cylinder model is improved, it can be used to examine the patterns for various aircraft configurations and computed results compared with a wide range of experimental results. Also, the computed results should be compared with additional experimental results taken on simplified aircraft models that correspond to the mathematical models. This confirmation is important as the more complex model is being developed. When the computer program is completed, a user's manual should be written. his would enhance the usefulness of the computer code by making it available to interested users.

The present contract has also raised a question concerning near field measurements such as aircraft models when measurements are taken. This raises the possibility of developing a near field computer program that can be used in conjunction with near field measurements. The near field computer program can be used to compare with near field experimental results; then, the far field computer program using essentially

the same theory as the near field solution can be used to predict the far field radiation pattern. The development of such a near field program should start with simple structures such as flat plates and cylinders. The program could then progress to more complex models such as aircraft structures as the techniques were improved.

REFERENCES

1. W. D. Burnside, C. L. Yu, and R. J. Marhefka, "Flush-Mounted Antennas Radiating on Aircraft Type Surfaces," Report 3001-5, July 1973, The Ohio State University ElectroScience Laboratory, Department of Electrical Engineering; prepared under Grant NGR 36-008-144 for National Aeronautics and Space Administration. (NASA-CR-2403)

2. P. H. Pathak, R. J. Marhefka, and W. D. Burnside, "High Frequency Scattering by Curved Surfaces," Report 3390-5, June 1974, The Ohio State University ElectroScience Laboratory, Department of Electrical Engineering; prepared under Contract N62269-72-C-0354 for Naval Air Development Center.

3. C. H. Walter, Traveling Wave Antennas, Dover Publications, Inc., New York, 1970, pp. 3-4 and pg. 116.

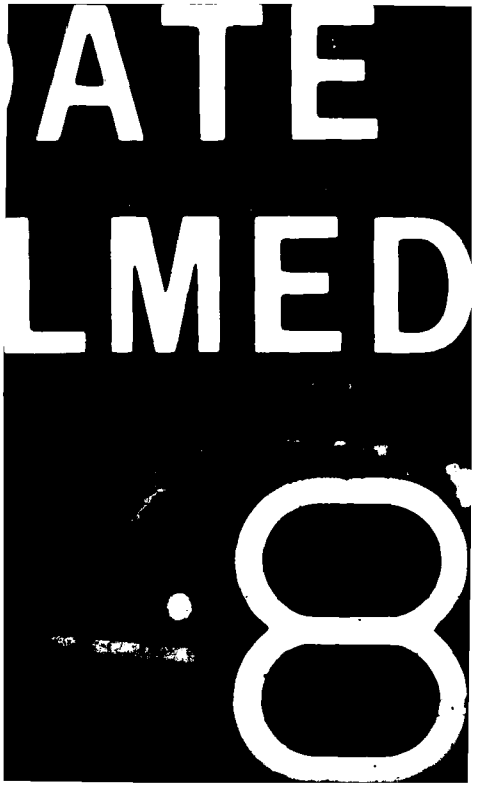
ATE
LMED
8